A novel QSGW+DMFT method for the study of strongly correlated materials

Pisanti, Paolo

Awarding institution:
King's College London

A novel QSGW+DMFT method for the study of strongly correlated materials

Paolo Pisanti

Department of Physics

School of Natural & Mathematical Science

King's College London

A thesis submitted for the degree of

Doctor of Philosophy

September 5, 2016

Declaration of authorship

I, Paolo Pisanti, declare that this Thesis, which I submit to King's College London in accordance with the requirements for the Degree of Doctor of Philosophy, composes the original work completed under the supervision of Prof. Mark van Schilfgaarde.
I certify that the work here presented was entirely done during my permanence as a PhD candidate at Kings College, from June 2012 to April 2016.
I declare that this Thesis is based entirely on my own original work. Where contributions from collaborators are used, the extent and quality of their assistance is clearly stated and acknowledged.
All the work presented here is original and was not previously submitted as an application for a degree or other qualification in any other institution.

Part of the work presented here was published or submitted for publication:

- **Non-local self-energies in metals and itinerant magnets: A focus on Fe and Ni.** L. Sponza, P. Pisanti, A. Vishina, D. Pashov, J. Vidal, C. Weber, G. Kotliar, M. van Schilfgaarde. *Submitted.*

Signed:

Date:

Acknowledgements

The very existence of this project of thesis relies on the intuition of my supervisor, Mark van Schilfgaarde. This intuition was two fold: on one hand, the ambitious prospect of reformulating a complex and inclusive theoretical model for the electronic structure of materials, and on the other, to build a bridge between two bright and skilful communities of researchers, whose mutual collaboration has always been complicated and lethargic. Together with pure Physics, Mark taught me the importance of this collaboration, which I believe is an essential feature of academic research. I want to genuinely thank him for that and for his precious guidance over all these years.

Not less crucial for the endurance of this project have been my collaborators and co-workers at King's College London. I want to start (in chronological order) with Cedric Weber, who opened the transcendent doors of Dynamical Mean Field Theory to an illiterate and lonely student and who has been incredibly patient throughout these years. The same I can say about Dimitar Pashov, as I am sure many of my colleagues agree on, he could have been the leading developer at Google but he preferred patiently assisting me with the analytical and numerical issues. Finally Lorenzo Sponza. He joined our group in a moment of stand of the project, and without his support, his guidance, his perseverance, we, I would never have made it to this point. A life-saver.

Outside of the walls of the Physics department there is a person who has been vital not only for my survival as a PhD student, but for the conservation of my integrity, my self-confidence, my lucidity, my happiness. The accomplishment of this thesis, and so many other things, would not have been possible without you Silvia.

“Support”, and “trust”, are words which yet do not capture entirely the feelings my parents were able to convey to me. My departure for the “new world” has been tough on them (as well as on me), but they are always been incredibly proud of me and trustworthy in my potential, often more than I ever was. Thank you guys.
Finally, without true friends you do not go anywhere, and I am lucky to have the most extraordinary ones. The ones I left (but only geographically), Pinis, Matt, Lor, Brix, Benny, Sacha, Stef, Silvia, Ale, and all the others, I miss you all. And the ones I found, Gio, Max, Giona, Lollo, Raffo, Elena, Cate, Silvia, Elena, Chiara, you made these three years (and this weather) brighter.

Abstract

In the past few years the quest for an accurate and inclusive theory in the field of electronic structure has led to the conjecture of combining of the most reliable methods available at the moment: GW approximation (GWA) and Dynamical Mean Field Theory (DMFT). The uncorrelated part of the system is treated within GWA, which yields parameters and inputs needed by DMFT, acting on the local subset of the full system responsible for the strong correlations in the material. In particular, the approach presented in this work of thesis is based on the Quasi-Particle self-consistent GW approximation (QSGW) method merged with DMFT. The reasons why we believe this combined approach to be promising are both practical (QSGW is state-of-the-art approach for electronic calculations) and fundamental (since both methods rely on a similar formalism and are somehow complementary).

We will present the motivations supporting a QSGW+DMFT scheme. The specifics of our implementation will be then provided, introducing its novel features and their capabilities. Finally, the first results obtained by means of this method will be presented and reviewed. In particular the materials under investigation have been La_2CuO_4, a cuprate compound displaying high-temperature superconductivity and the ferromagnetic Ni, a transition metal that was studied with a particular attention to its magnetic properties.

Contents

List of Figures

Introduction

Since its first formulation in the early twentieth century, the theory of electronic structure has undergone a remarkable evolution. Electronic structure refers the application of the principles of quantum mechanics to describe the properties of materials by means of the interactions between the electrons, for fixed configuration of nucleii.
This was first made possible thanks to the close collaboration between theory and experiments, the latter realized by means of state of the art techniques such as direct and inverse photo-emission, angle-resolved photo-emission spectroscopy and optical absorption. On the other hand, the development of electronic structure theory was two-fold: (i) through an upgrade of the analytical and theoretical methods, via a higher and higher measure of complexity and refinement, (ii) by means of the great improvements in the availability and speed of computer resources, now allowing for calculations of a number of degrees of freedom that was not even conceivable decades ago.
As of today, a deep interest in the condensed matter community grew towards the formulation of an *ab initio* and flexible electronic structure method, employing the best of today's technological advances and numerical techniques, allowing for the accurate description from first principles of any accessible compound on an equal footing. This work of thesis is meant to give a notable contribution to this quest.
There is a wide class of materials displaying exotic and unique properties open for uncountable outstanding technological applications, such as modern hardware components and nanotechnology, medical detectors (e.g. MRI and NMR), particle accelerators in nuclear physics, or even powerful superconducting electromagnets to be employed in *maglev* trains, to mention just a few. The materials

of interest in this sense are high-Tc superconductors, Mott insulators, Hund's metals, topological insulators. All of these compounds belong to the category of strongly correlated materials, the main object under investigation in this work.
The physics of these materials is rather complex but the underlying principle governing them is mainly determined by the correlations between electrons. Strong correlations usually interest very localized electrons (e.g. the ones in partially occupied d and f orbitals). Typically, due to the localization, the Coulomb interaction is less screened and cannot be neglected, therefore the electron correlations become dominant and this can bring the material to exhibit an "atomic like" behaviour. This distinctive character distinguishes these compounds from the weakly correlated materials, for which the electrons (typically inhabiting s and p shells) are very itinerant and the Coulomb interaction is so screened that the response of the system to it is much weaker.
With this picture in mind it is not surprising that the theoretical methods based on the independent-particle approximation (i.e. including the influence of electrons interactions at most by means of an effective mean field), such as Density Functional Theory, or even the more advanced Many-Body perturbation theory, despite being very effective for weakly correlated materials, break down when correlations become strong, in particular in their accounting for the interplay of localization and itinerancy of the electrons on the same footing. The resulting many-body effects have to be fully accounted for by means of alternative sophisticated non-perturbative methods.
Among these latter, the most reliable method has been the LDA+DMFT.
Dynamical Mean Field theory (DMFT) reduces the full many-body problem of the lattice to the one a single quantum *impurity*, treated calculating all orders of a given perturbative expansion in the effective Coulomb interaction, while the rest of the system is accounted as a non-interacting *bath* coupled *self-consistently* to the impurity. The DMFT formulation can be seen as a quantum generalization of the Weiss mean-field theory of the Ising Model, whose starting point is the one band Hubbard Hamiltonian [48]. Hence DMFT incorporates both the magnetic effects of the Statistical Mechanics framework together with the atomic physics (the treatment of the correlations between electrons at different lattice sites) of the Hubbard model. It was in fact originally formulated in the early 90s

for model Hamiltonians, whereas roughly 10 years later the LDA (Local Density Approximation to DFT) was used to account for the bath. With the definitive development of self-consistent LDA+DMFT [31, 62] a realistic electronic structure method was then fulfilled, its applications to strongly correlated materials have been remarkable, also thanks to the evolution of the impurity solver (key step in DMFT implementations), from the rudimentary FLEX up to today's state of the art Monte-Carlo algorithms [105]. A crucial step of LDA+DMFT lies in the integration of the two methods, and in particular the identification of the impurity: constructed by a projection or downfolding into a subspace of the entire Hilbert space on which the DMFT acts. One needs to introduce some mathematical operators responsible for the mapping between full space objects and their local space counterparts.

These multiple reasons stand as motivations to employ GW approximation in place of LDA. The GW-approximation originates a practical and reasonable shortcut to solve the Hedin's equations [40] consisting in getting rid of vertex corrections in the evaluation of the self-energy. It then lead the way to a full ab initio electronic structure method in the framework of Many-Body Perturbation Theory. The GW approaches make use of a dynamically screened Coulomb interaction W, which may be intuitively understood as the the system responding to a propagating charge in contrast to the interaction through be bare coulomb interaction v. The self-energy in this approach is non-local both in space and time. Two alternatives are typically chosen for the implementation of a GW method, the choice is about whether pursuing self-consistency or not, and it can determine the quality of the representation. Self-consistency ensures that the starting, noninteracting Green's function is optimally close to the interacting G. Without self-consistency, results depend on the starting point and are thus ambiguous. Results are also somewhat unpredictable even for weakly correlated systems (e.g. GW description, with LDA as the non-interacting starting point, of the band properties of InN or $CuInSe_2$ is poor). Another important advantage of this approximation is that it describes, within a single framework, without parameters or division into a subsystem, a wide range of materials. Fully self-consistent GW can remove the ambiguity in the starting point, but it has long been known that its description of spectral properties is poor, even in Jellium [47]. In transition metals, the spectral

properties are generally no better or less good than the LDA [11]. Quasi-particle self-consistent GW [98] (QSGW) was formulated to surmount these limitations. QSGW may be thought as an optimised version of GW, whose static (local in time) hermitian self-energy is extracted from the GW one by means of criterion of self-consistency, grounded of the concept of quasi-particle. The results of QSGW calculations are remarkably consistent, and overcome most limitations to GW for weakly and moderately correlated systems. Contrary to LDA and GW based on the LDA, QSGW band-gaps are systematically slightly overestimated [98], and this systematic overestimation can be connected to the underestimation of the screening due to the non-inclusion of electron-hole interactions through RPA.
We have now prepared the grounds for the principal claim of this work. We firmly believe that the most promising candidate for an ab initio, flexible and realistic electronic structure method for the investigation of both the most challenging strongly correlated materials and the less demanding weakly correlated ones, on an equal footing and with a high level of accuracy, is a QSGW+DMFT scheme. The reasons are the following. First, both GW and DMFT are Green's functions theories, the overlap contributions accounted by both schemes can be targeted, removing the cumbersome double-counting problem. Second, the effective screened interaction parameters of DMFT, namely the Hubbard interaction U and the Hund's coupling J can be computed by means of a cRPA procedure from first principles instead of picking them empirically. One could claim that such a procedure could be carried out also in LDA+DMFT, but this would pose an inconsistency with the fuzzy way the interaction is represented in LDA with respect to DMFT, whereas in GW the interaction is also computed at RPA level. A third, and most important remark, is based on non-locality. LDA+DMFT misses it completely, a GW+DMFT scheme would incorporate it at RPA level (meaning the diagrams included in the self-energy). There is reason to expect on physical grounds that the spatial non-locality is indeed carried almost entirely by the low order diagrams such as GW, while strong correlations are largely local and can adequately be treated in DMFT. A recent paper by Tomczak et al. [96] established that, at least for the Iron Pnictides and Chalcogenides family of superconductors in the Fermi liquid regime, the two dependencies can be fairly well separated, i.e. $\Sigma(\omega, \mathbf{q})$ can be well approximated by $\Sigma(\omega) + \Sigma(\mathbf{q})$. The validity

of GW+DMFT should in principle, rest only on the validity of this assumption. GW+DMFT was first proposed by Biermann et al. [12]. Since then, progress has been made [10, 95], but it has been slow because the full theory is very difficult to implement in practice. It is also not clear whether fully self-consistent GW+DMFT is an adequate description because of the problems with self-consistent GW we outlined above. For this reason, for the project of my PhD thesis a QSGW+DMFT formulation was considered preferable. Even though it does not suffer from the errors of fully self-consistent GW, it still needs to deal with different problems, the origin of which is that passing from the dynamical GW self-energy to the static QSGW one one loses the defined diagrammatic construction. This, as we will show, complicates the double-counting evaluation. Moreover, because such G is not fully conserving, there are other potential limitations, such as the reliability of the total energy or transport properties computed from G. The best way to address these open issues will be testing the new implementation on benchmark materials and carefully compare the results obtained with the alternative strategies. An open collaboration is therefore advised.
This work will present the basics steps towards the formulation and construction of a new QSGW+DMFT method.

This thesis will start with a broad introduction on the theoretical framework, it will be the object of Part I. The first chapter will be devoted to an introduction of the central features and characterization of weakly correlated and strongly correlated materials. The second chapter will be focused on the fundamental first-principle methods, organized and ranked in terms of the central object on which these theories pivot, in order to better clarify their methodology. First we will give an introduction of Density Functional Theory, concerning its formulation and evolution, its doubtless accomplishments and unavoidable limits. We will then present the underlying features of the Green's functions framework, culminating on GW approximation and derived methods, from the rudimentary *one-shot* GW to the fully self-consistent and quasi-particle self-consistent schemes.
The third chapter will be then devoted to DMFT, outlining its physical formulation, together with its successful applications, in particular within the LDA+DMFT scheme. We will then point out the motivation behind the limits and ambiguities of LDA+DMFT, and the advantage of a GW+DMFT model. This will conclude

part I.
Part II of this work will be focused to the details of the specific QSGW+DMFT method we have implemented. Among the most subtle points, the definition of the projection and embedding operators (allowing the mapping into and out of the correlated subset of DMFT) within the basis set of the QSGW scheme. We will also mention the open issues it still need to address and the improvements that are currently under development. An example of the latter is the determination of the double-counting correction, perhaps the most subtle point of such implementations and which is still an object open for debate.
Finally, part III will be dedicated to present the preliminary results we obtained by means of this scheme. The materials under investigation have been La_2CuO_4, a cuprate compound displaying high-temperature superconductivity (presented in chapter 6), and the ferromagnetic Ni, a transition metal that was studied with a particular attention to its magnetic properties (chapter 7).

Part I

Theoretical background: Electronic structure of correlated materials

Chapter 1

Digression on materials

1.1 Weakly correlated materials

The study of electronic structure, interacting electrons and nuclei, and of solids in general, is a remarkable task.
The physical properties of a solid state system are governed by the Hamiltonian for electrons (N_e in total) of mass m_e and nuclei (N_n in total) of mass M_I:

$$\mathscr{H} = -\frac{\hbar^2}{2m_e}\sum_{i}^{N_e}\nabla_i^2 - \hbar^2\sum_{I}^{N_n}\frac{\nabla_I^2}{2M_I} + \sum_{I,i}^{N_e}\frac{e^2 Z_I}{|\mathbf{r}_i - \mathbf{R}_I|} + \frac{1}{2}\sum_{i\neq j}^{N_e}\frac{e^2}{|\mathbf{r}_i - \mathbf{r}_j|} + E_{\text{ion}}, \quad (1.1)$$

where $\mathbf{r}_i, \mathbf{r}_I$ are respectively the coordinates of the given electron and nucleus, the first two terms describe the electronic and nuclear kinetic energies and the last three the Coulomb interactions between mutual particles, in particular E_{ion} is the potential term arising from the inter-nuclei Coulomb repulsion.
The fundamental problem in the field of electronic structure, i.e. finding the solution of the Schrödinger equation $\mathscr{H}|\Psi\rangle = E|\Psi\rangle$ for this Hamiltonian, with the many-body wave-function $|\Psi\rangle$ being dependent on a high number of particles (N_e electrons and N_n nuclei), is a practically impossible task even in modern implementations.
The first, intuitive approximation that one could think of, is to neglect the nuclear kinetic energy since $M_I \gg m_e$ and to decouple the dynamics of electrons from the one of nuclei, which can be considered still with respect to the motion of the

much faster electrons. This Born-Oppenheimer (or adiabatic) approximation is generally a good one [9]. Accordingly, the Hamiltonian to consider becomes:

$$\mathscr{H} = -\frac{\hbar^2}{2m_e}\sum_i^{N_e}\nabla_i^2 + \sum_i^{N_e} V_{\text{ext}}(\mathbf{r}_i) + \frac{1}{2}\sum_{i\neq j}^{N_e}\frac{e^2}{|\mathbf{r}_i - \mathbf{r}_j|}\,, \tag{1.2}$$

where

$$V_{\text{ext}}(\mathbf{r}_i) = \sum_I^{N_n}\frac{e^2 Z_I}{|\mathbf{r}_i - \mathbf{R}_I|}\,, \tag{1.3}$$

is the external potential created by the nuclei. The last term of this equation represents the Coulomb interaction of electrons, responsible for most many-body effects. When this component is relevant in the electron dynamics, it can lead to unique and interesting properties of the material, which include metal-insulator transitions, Mott insulating phase, unconventional superconductivity.
Nevertheless there is a wide range of cases for which this term can be safely cast into a one-body effective potential, in such a way to consider the electrons as uncorrelated apart from being subject to the Pauli exclusion principle. This is the basic assumption of the so called *non-interacting particles* models.
Within this framework the simplest assumption is to consider the electrons subject only to a periodic nuclei potential. As a consequence, the wavefunction of the particle (called Bloch electron in this context) can be written in terms of a component φ with the same periodicity of the crystal and a phase factor, in such a way that their corresponding wave-functions, called Bloch states, also gain a periodicity in the crystal:

$$\psi_{\mathbf{k}}(\mathbf{r}) = e^{i\mathbf{k}\cdot\mathbf{r}}\varphi_{\mathbf{k}}(\mathbf{r});\ \varphi_{\mathbf{k}}(\mathbf{r}+\mathbf{R}) = \varphi_{\mathbf{k}}(\mathbf{r}),$$

$\mathbf{k}$ being the reciprocal lattice vector. The Bloch states are named after Felix Bloch, who in 1928 in his PhD thesis introduced these functions as a main concept behind the formulation of his band theory: in the limit of a large crystal, for each wave-vector $\mathbf{k}$ there are multiple solutions ψ of the Schrödinger equation, and the Bloch states generate a discrete set of eigenvalues $\epsilon_{\mathbf{k},i}$ labelled by the so called band-index i. These eigenvalues, as a function of $\mathbf{k}$ and specifically on some specific symmetry lines of the lattice cell, form continuous functions (at least in

the limit of infinite bulk system) creating the band structure of the solid. Within the non-interacting particles model the bands are filled by the electrons of the solid by means of the Pauli exclusion principle, leading to the formation of core states, valence and conduction bands.

This brings us to the definition of the so-called *weakly correlated materials*(WCM), those for which this non-interacting particle picture remains valid, and the corresponding band-structure has fully physical meaning. This is typically true for materials with partially filled s- and p- bands since the electrons of these shells are very itinerant and their kinetic energy is strong enough to dominate the screened Coulomb repulsion between electrons. For these compounds (and in some cases and under some assumptions even in less simple ones), the band-structure description remains rather good, and the corresponding predictions can be reliably compared to experimental results of state-of-the-art techniques like the angle-resolved photo emission spectroscopy (ARPES), which relies on a single-particle excitation spectra. As a matter of fact a great deal of the accessible materials can be included under the classification of "weakly correlated", and the knowledge that we are able to describe their physics by means of this rather simple and schematic picture (the band-structure), and under a strong assumption like considering the electrons as substantially non-interacting, might even sound surprising for some.

A justification for this can be found in the concept of *quasi-particles* in Landau-Fermi liquid theory [73], which establishes a foundation for the independent-electron model. The quasi-particles are "dressed" particles, with a screening cloud surrounding them and accounting for the interactions in the system, which gives them a finite lifetime and renormalized spectral weight. Even in less trivial compounds, the band picture still holds in the low energy excitation spectra close to Fermi level by means of renormalization of the Coulomb interaction, resulting in a correction in the quasi-particles spectral weight and first appearance of minor satellites features at higher energies (but we will go back to this further on), as can be observed also in ARPES measurements [107].

The first part of next chapter will be devoted to the methods of reference on weakly correlated materials, and the order we picked is based on the fundamental variable chosen to address the problem. We will then start with the electronic

density, introducing the enormously successful and widely used DFT-based techniques. we will then include a reference to the most popular wave-functions methods, i.e. to the approaches laying the foundations of Solid States Physics (Hartree and Hartree-Fock methods), in order to lay the groundwork for to the state-of-the-art perturbative method of GW approximation and its developments (SCGW and QSGW), using the Green's function as a central variable, which more than any other has been successfully applied to a large class of materials with a good prediction on their band-structure and phase-space properties.

1.2 Strongly correlated materials

There is however still a considerable variety of compounds for which the methods just mentioned fail to provide a qualitative insight, and the band-structure representation in terms of Bloch states as well as the main concepts of Landau-Fermi theories cannot be applied any more (e.g. this is typically the case when the presence of satellites in the spectrum is predominant over the quasi-particle excitations). These materials often show phase-space properties, like metallic states or metal-insulator transitions, which cannot be explained in terms of the band theory and the electron count (e.g. like metallic properties in half-filled bands), and are instead significantly determined by the correlations between electrons.
We include under this broad definition the so-called *strongly correlated materials* (SCM), those for which the independent-particle picture and its extensions and corresponding derived approaches cannot be successfully applied, since the correlations and interplay between electrons cannot be neglected or underestimated.
Typically the materials with partially filled d- and f- shells show strong correlations, and the reason for this can be explained by the following argument (for further details see [29]). In the case of weakly correlated materials the electrons (usually belonging to s, p orbitals) tend to be highly itinerant and delocalized in the solid, schematically we can describe this process in a *wave-like* picture which leads to a well defined band theory. On the other hand, the d- and f- electrons have a limited spatial extent and end up to be more localized, the Coulomb repulsion is less screened and the correlations become relevant. This circumstance is rather better described in a *particle-like* picture whose extreme possible outcome

is the state where all the valence electrons are confined to the crystal lattice sites, as if the solid was composed by isolated atoms. In this scenario the mobility of electrons is suppressed and the material shows insulating properties. This is the origin of the behavior of the so-called Mott insulators [81], a class of materials animating a deep interest in the Electronic Structure community in the past decades, whose peculiar properties are way beyond the one-particle picture description and need to be addressed in terms of many-body theories.

The two extreme scenarios depicted above represent, in a didactic picture, the opposite limits of the ratio between the Coulomb interaction and the kinetic energy (that can be estimated from the bandwidth of the solid). A good theory has to be able to describe on the same footing the two opposite critical points as well as the more frequent intermediate states.

Nevertheless not all the physics of strongly correlated materials can be captured in terms of this simple scheme. Some unique properties are display even when the ratio between Coulomb interaction and bandwidth is rather small, and therefore other effects come into play, it is the case of Hund's coupling [22] or when magnetic effects are predominant[1]. It is well known that the methods mentioned before (DFT-related approaches and GW approximation) fail to reliably predict properties of such materials and to explain phenomena such as the Mott insulating state. On the contrary, the more recent Dynamical Mean Field Theory (DMFT), which will be introduced further on, has proved to be the most reliable method in the analysis of strong correlations.

In conclusion, after stressing that there is no unambiguous classification of strongly correlated materials apart from the general introduction just provided, we will mention some examples of them [29] (because of their specific properties and in retrospect of the failure of independent-particle models to reproduce them): transition metals and transition metal oxides (in particular $3d$ elements), doped cuprates, rare earth ($4f$) and actinides ($5f$) compounds.

[1] We will show a typical example in the chapter of results

Chapter 2

First principles approaches to Electronic Structure

2.1 Density as a central quantity: DFT

As mentioned before, the main complication impeding solutions of the Schrödinger equation of the Hamiltonian of eq.(1.2) comes from the pairwise electron interactions, which does not allow the N-body wave-function $\Psi(\mathbf{r}_1, ..., \mathbf{r}_N)$ to factor into products of one-body functions. This quantity brings with it a high number of degrees of freedom and, if it were accessible, all possible properties of the many-body system could be obtained from it. In common calculations the properties under analysis are very limited and specific though, usually related to ground state or one-particle excitations, like the equilibrium lattice parameter of a crystal, the ionization energy, or the electron affinity of a solid, and can be therefore obtained by means of more functions of fewer degrees of freedom accounting for the properties of the entire system as a whole.

Hohenberg and Kohn proved that the *electron density* can serve as a fundamental variable; it is sufficient in principle to completely determine the ground state of the system. The idea of using the density as the central variable in order to investigate the properties of the system first originated in the early works on quantum mechanics of L. H. Thomas [94] and E. Fermi [28] in 1927. In their formulation the energy components are directly linked to the density through the following

equations (respectively of Hartree energy and the energy related to an external potential):

$$E_{\mathrm{H}} = \frac{1}{2}\int d\mathbf{r}d\mathbf{r}'\frac{\rho(\mathbf{r})\rho(\mathbf{r}')}{|\mathbf{r}-\mathbf{r}'|},\ E_{\mathrm{ext}} = \int d\mathbf{r}\rho(\mathbf{r})v_{\mathrm{ext}}(\mathbf{r}), \tag{2.1}$$

whereas the kinetic Energy of an homogeneous gas of non-interacting electrons is expressed by the well-known Thomas-Fermi formula

$$T^{\mathrm{TF}} = a_s\int d\mathbf{r}\rho^{\frac{5}{3}}(\mathbf{r}),\ a_s = 3(3\pi^2)^{2/3}/10. \tag{2.2}$$

The breakthrough of P. Hohenberg and W. Kohn in 1964 [46] was to show rigorously that the ground-state density alone is enough to determine the total energy. Their renowned theorem yields the framework for basic Density Functional Theory (DFT).

2.1.1 Hohenberg-Kohn theorem

Considering the system of N-particles subject to an external background potential v_{ext}, the Hohenberg-Kohn theorem states:

- there is a one-to-one correspondence between the ground state density $\rho_0(\mathbf{r})$ and the background potential $v_{\mathrm{ext}}(\mathbf{r})$;
- all the properties of the interacting systems are completely determined through the knowledge of the ground state density $\rho_0(\mathbf{r})$;
- a given functional $E[\rho]$ can always be defined for any external potential v_{ext}. For any particular v_{ext}, the *exact* ground state energy is the global minimum of this functional, and the density that minimizes the functional is the exact ground state density: $E_0 = \min E[\rho] \equiv E[\rho_0]$.

The proofs of these theorems are essentially simple and bound to pure mathematical arguments, they are extensively explained in [73].
The straightforward conclusion to this theorem is writing all the components of the total energy in terms of a given density functional as it follows:

$$E[\rho] = F[\rho] + \int d\mathbf{r}\rho(\mathbf{r})v_{\mathrm{ext}}(\mathbf{r}), \tag{2.3}$$

where the *universal* functional $F[\rho]$ contains both the kinetic term as well as the potential energy of interacting electrons.
This is as far as the original formulation of [46] goes: by knowing the functional $F[\rho]$ one would be able to extrapolate the ground-state energy of any interacting many-body system. Nevertheless the exact expression of this functional can be just estimated by heavy computational methods, which spoils the elegance and simplicity of the method. We know from a fact $F[\rho]$ is highly non-analytic as it must, for example, describe the core states of an atom. By far the most problematic part is the kinetic energy part of $F[\rho]$.
This is where the work of Kohn and Sham is important.

2.1.2 Kohn-Sham ansatz

The approach of W.Kohn and L.J. Sham in 1965 [58] was to replace the original interacting many-body system, whose Schrödinger equation is very difficult to solve, with an *auxiliary system* of non-interacting particles, subject to an external one-body Kohn-Sham potential v_{KS}, provided that the ground state density for the auxiliary system is exactly equal to the one of the original many-body assembly.
We can then relate the ground state density to the one-particle wave-function ψ_i via

$$\rho(\mathbf{r}) \equiv \sum_{i=1}^{N} |\psi_i(\mathbf{r})|^2. \tag{2.4}$$

Introducing the auxiliary system into equation (2.3) we obtain

$$E[\rho] = T_{\mathrm{ni}}[\rho] + \int d\mathbf{r}\rho(\mathbf{r})v_{\mathrm{ext}}(\mathbf{r}) + E_{\mathrm{H}}[\rho] + E_{\mathrm{xc}}[\rho]\,, \tag{2.5}$$

where T_{ni} is the (trivial) kinetic energy of the non-interacting system, E_{H} is the Hartree component of the Coulomb energy (or self-interaction energy), equivalent to the first term of eq.(2.1), and E_{xc} is the so-called exchange-correlation energy. This last term is the key quantity in DFT approaches, accounting for the many-body effects in the system, it contains all the electron-electron interactions beyond the Hartree term, plus the difference between the true kinetic energy and the non-

interacting one, as it is clear by comparing eqs. (2.5) and (2.3):

$$E_{\mathrm{xc}}[\rho] = F[\rho] - T_{\mathrm{ni}}[\rho] - E_{\mathrm{H}}[\rho]. \tag{2.6}$$

From eq. (2.5) we can introduce the KS potential as

$$v_{\mathrm{KS}}[\rho](\mathbf{r}) = v_{\mathrm{ext}}(\mathbf{r}) + v_{\mathrm{H}}(\mathbf{r}) + v_{\mathrm{xc}}[\rho](\mathbf{r}), \tag{2.7}$$

where we have defined the exchange-correlation potential as the functional derivative of the corresponding energy:

$$v_{\mathrm{xc}}[\rho](\mathbf{r}) = \frac{\delta E_{\mathrm{xc}}[\rho]}{\delta \rho(\mathbf{r})}. \tag{2.8}$$

The problem is then reduced to the Schrödinger equation for the *single particle* Kohn-Sham eigensystem $|\phi_{n\mathbf{k}}\rangle, \epsilon_{n\mathbf{k}}$:

$$H = -\frac{\hbar^2}{2m_e}\nabla^2 + v_{\mathrm{KS}}[\rho](\mathbf{r}),\ H|\phi_{n\mathbf{k}}\rangle = \epsilon_{n\mathbf{k}}|\phi_{n\mathbf{k}}\rangle, \tag{2.9}$$

which can be solved iteratively with the following condition:

$$\rho(\mathbf{r}) = \sum_{\epsilon_{n\mathbf{k}} < \epsilon_F} |\phi_{n\mathbf{k}}(\mathbf{r})|^2 , \tag{2.10}$$

where the sum runs over all the states below the Fermi level.
I stress here that our analysis did not involve any approximation so far, this system of equations can be solved *exactly* for any many-body assembly of interacting particles, provided to know the explicit expression of v_{xc} (or equivalently E_{xc}). It is also important to remark that our KS eigenfunctions $|\phi_{n\mathbf{k}}\rangle$ are just auxiliary and do not have any direct physical meaning, apart from leading to the correct ground state density of our original system and therefore to the true ground state energy.
Unfortunately E_{xc} is unknown, an explicit form of this functional cannot be extracted and some approximation need to be introduced at this stage.

2.1.3 Exchange-correlation potentials

The first approximation for the exchange-correlation potential was suggested in the original paper of 1965 by Kohn and Sham [58], it is the so-called Local Density Approximation (LDA), it assumes

$$E_{\rm xc}^{\rm LDA}[\rho] = \int d\mathbf{r}\, \rho(\mathbf{r}) \epsilon_{\rm xc}^{LDA}(\rho(\mathbf{r})), \tag{2.11}$$

where $\epsilon_{\rm xc}^{LDA}(\rho(\mathbf{r}))$ is defined as exchange-correlation energy density of a homogeneous electron gas of density $\rho(\mathbf{r})$, which is uniform and well defined, and with the property of $\epsilon_{\rm xc}^{LDA}$ being a simple *local function*, not a functional, of $\rho(\mathbf{r})$.
This is the most popular and widely adopted among the approximations of the exchange-correlation potentials, and it will be the approximation on which we will refer to for the DFT calculations mentioned in this work of thesis further on.
LDA can be easily extended for spin-polarized calculations as Local Spin Density Approximation (LSDA) in systems where there is no homogeneous spin density, the entire KS formulation for the spin-polarized case is straightforward.
An alternative approximation that it is worth mentioning takes into account a possible inhomogeneity of the density, this is bypassed by performing a gradient expansion of the exchange-correlation energy density in terms of progressive derivatives of the reference density: $\rho(\mathbf{r}), \nabla\rho(\mathbf{r}), \cdots$. This is the case of the Generalized Gradient Approximation (GGA) [84]. Despite its credits and the remarkable results gained within GGA, it is not a fair statement to say that this approximation is universally safer and gives overall improvements on LDA. This is why it was not preferred to LDA in our DFT implementation.
Within this well-known approximations (LDA, GGA) for the exchange-correlation potential, the system of equations (2.9) and the corresponding minimization[1] of the ground-state energy functional can be solved exactly. One typically starts with an initial guess for the KS states and updates the solution iteratively by means of condition (2.10), until reaching convergence of a quantity of reference (typically the total energy). This is how practical DFT calculations are implemented. As mentioned before though, being just the by-products of the mini-

[1] the minimization can be performed with the standard method of Lagrange multipliers for handling the constraints in the search of a stationary point

mization scheme, the KS states $\phi_{n\mathbf{k}}$ refer to the auxiliary non-interacting particle system and thus they do not have a precise physical meaning, consequently the corresponding eigenvalues $\epsilon_{n\mathbf{k}}$ cannot be interpreted as exact ionization energies. Nevertheless, it is also true that the KS potentials yield the correct density and are designed to reproduce the highest occupied states. The practical consequence of this foundation is that in many DFT analysis on a wide class of materials the band-structure and spectral function resulting from the KS eigensystem usually resemble quite correctly the results of the corresponding photo-emission experiments. The corresponding DFT simulations can be then used not only to determine ground state energies but also to extract and to predict more general properties of the material under study, provided that extreme caution is taken in handling these results, keeping in mind the true character of the KS states and energies.

2.1.4 Basis set: augmented wave approaches

Once the approximation scheme for the exchange-correlation potential is set, one of the main differences among the wide variety of DFT implementations in the field of electronic structure regards the basis set chosen to represent the KS wavefunctions. As a matter of fact, this choice is not univocal and it turns out to be crucial in the cost and the accuracy of the calculation.

An approach that is worth mentioning is the *pseudo-potential* method, modelling the nuclei Coulomb potential with some designed tailored effective potential accounting for the core electrons to treat the valence electrons with. By removing the core electrons (not taking part in chemical bonds and whose rapidly varying wave functions and difficult to express in plane waves) the total number of electrons to account for is reduced, together with the number of plane-waves needed (which speeds up the calculation). On the other hand, when the core is more extended or the overlap with the valence states becomes larger, the description of the system gets worse.

Better accuracy than pseudo-potential approaches, especially related to the region close to the nucleus, can be obtained by means of the so-called *augmented wave* methods [1, 91]. This name is due to the fact that the space is partitioned

into muffin tin-like "augmentation spheres" centred at the nuclei coordinates and interstitial regions, as it is shown in Fig.2.1.

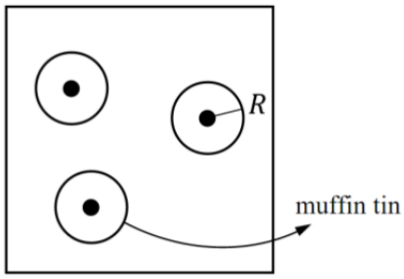

Figure 2.1: Simple scheme of space partitioning into muffin-tin (MT) spheres and interstitial regions in augmented approaches. Image from [97].

Two are the most popular and advanced augmented approaches developed: the *Linear Muffin Tin Orbital* (LMTO) method and the *Linear Augmented Plane Wave* (LAPW) method.
These approaches have in common the choice of solving the Schrödinger equation numerically *inside* the augmented spheres: the corresponding radial solutions and their energy derivative[1] are used in linear combination with spherical harmonics as the terms of expansion of the KS wave-functions, thanks to the fact that electrons close to the nuclei tend to replicate their behaviour in a free atom and therefore can be described by atomic-like functions.
Both approaches are said to be *all electron* and *full potential*, both being an improvement with respect to the pseudo-potential methods. The first means that all the electrons of the solid, both core and valence ones although with different weights, are accounted for in the calculation of the density, and the second refers to the notion that no approximation or modelling are taken for the external potential, which is fully included.
What differentiates LMTO from LAPW methods is instead the choice of the wave-function expansion at the interstitial regions. The LAPW basis consists of plane waves. These serve as envelopes augmented by partial waves inside augmentation spheres. In LMTO methods the envelopes functions have a more restricted

[1] this is what distinguishes LAPW from simple APW methods

form resulting the solution of the Helmholtz equation. The relative credits of each method over the other are extremely subtle and outline them is beyond the goal of this thesis. Our implementation contains both [60] but we will mainly deal with a variant of the LMTO basis set. Smoothed Hankel functions are defined, which are solutions of a generalized Helmholtz equation. These functions may be thought of as convolutions of Gaussian and ordinary Hankel functions that makes them regular at the origin and smooth everywhere. The extra degree of freedom allows for a finer adjustment of the functions with respect to ordinary LMTO's for a given rank of the Hamiltonian.

2.1.5 Credits and failures of DFT

The development of DFT methods has represented a breakthrough in the field of quantum chemistry and solid state physics. It achieved indisputable findings, among which the results on lattice parameters of simple crystals [52], the determination of ionization energies in molecules and the cohesive energy in solids.
Nevertheless it is well known that this method has limits.
A conceptual consideration to start: as mentioned before, the validity of the energy functional of DFT stands just for the ground-state, lacking a reliable reasonable prediction for the excited states, whereas most of the experiments like photo-emission, transport or optics use probes of excitation spectra. Although there are indeed several cases for which a reasonable prediction for the band-structure can be carried out, a well-known consequence of this restriction is to underestimate (sometimes severely) the fundamental gaps in many insulators and semiconductors.
In strongly correlated materials, however, DFT fails qualitatively. Because of the restricted degrees of freedom in the density (especially the lack of information about orbital character), DFT is unable to to capture on the same footing both the physics of the itinerant p- electrons and the more localized d- and f- ones, prominent feature of SCM. We have mentioned in the previous chapter of the tendency in electrons in SCM, in particular transition metals and their oxides, of shifting between itinerancy and localization, which in some cases brings the solid to exhibit phase-space transitions such as from metallic to insulating state. The

band-structure derived in DFT will always describe a metallic behaviour for this solids though, only based on considerations about the half-filling of KS bands. As a consequence, for Mott insulators the DFT spectra differs critically with the experimental results [51].
It is then crystal-clear how for this sort of solids, and for SCM in general, a more advanced treatment is required.

2.2 Wave-function as a central quantity

As mentioned before, the full knowledge of the properties of all the system components has necessarily to pass through the analysis of the many-body wave-function $\Psi(\mathbf{r}_1, \cdot, \mathbf{r}_N)$. The corresponding Schrödinger equation in terms of Ψ and of the full Hamiltonian is extremely hard to solve exactly, whereas it becomes solvable at a reasonable computational cost in simplified models like the independent particles approaches.
Before the development of DFT techniques, two main well-known wave function-based approaches based on independent particles model were developed: the *Hartree* and the Hartree-Fock approximation.

2.2.1 Hartree-Fock approximation

The Hartree approximation, following the treatment of [73], can be labelled as a *non-interacting* particle method, since the interaction is the one-body electrostatic interaction from all the electrons. As a consequence, the many-body wave-function Ψ can be expressed as just a product of single particle wave-functions ψ_i, with no inclusion of the Pauli exclusion principle, which corresponds to setting all the possible correlations between electrons to zero.
A step forward from this method is the so-called Hartree-Fock approximation (HFA): the Pauli exclusion principle is introduced in such a way that the total wave-function is defined as a Slater determinant Φ (anti-symmetrized product) of the single particles wave-functions.
The corresponding Hamiltonian again simplifies to an effective single-particle potential but now the potential explicitly depends on the single-particle state con-

sidered[1]:

$$H^i_{\mathrm{HF}}\psi_{i,\sigma}(\mathbf{r}) = \left[-\frac{\hbar^2}{2m_e}\nabla^2 + v^{i,\sigma}_{\mathrm{eff}}(\mathbf{r})\right]\psi_{i,\sigma}(\mathbf{r}); \tag{2.12}$$

where

$$v^{i,\sigma}_{\mathrm{eff}}(\mathbf{r}) = v_{\mathrm{ext}}(\mathbf{r}) + v_{\mathrm{H}}(\mathbf{r}) + v^{i,\sigma}_{\mathrm{x}}(\mathbf{r}), \tag{2.13}$$

the last term is the so-called exchange term:

$$v^{i,\sigma}_{\mathrm{x}}(\mathbf{r}) := -\left[\sum_j \int d\mathbf{r}'\psi_{j,\sigma*}(\mathbf{r}')\psi_{i,\sigma}(\mathbf{r}')\frac{1}{|\mathbf{r}-\mathbf{r}'|}\right]\frac{\psi_{j,\sigma}(\mathbf{r})}{\psi_{i,\sigma}(\mathbf{r})}, \tag{2.14}$$

its purpose is to lower the energy interaction for electrons of the same spin (since the wave-functions are orthogonal for different spin) by erasing the spurious self-interaction repulsive term in the Hartree component, equivalent to the first term in equation (2.1).

The outcome of the Hartree-Fock approximation is dual: first to neglect all correlations except the ones required by the Pauli exclusion principle and second to introduce the so-called exchange-hole interaction: the effect of lowering the interaction of every electron by means of a positive "exchange hole" surrounding it. The simple character of the interaction also means that the quality of the approximation is very limited: most of the correlations acting on the system are left out. By far the most important is to neglect the electrons' self-screening of the effective interaction between them. Omission of screening results in many severe errors. There is strong tendency to overestimate the tendency to the insulating state; thus bandgaps are generally severely overestimated. In metals the omission of screening leads to qualitatively wrong behaviour near the Fermi surface.

2.3 Green's function as a central quantity

Despite carrying less information than the wave-function, the one-particle Green's function G contains still more information than the density. It has evolved as a very useful fundamental variable used to address the analysis of a many-body system, thanks to its versatile properties. Not only it leads to the ground-state

[1] and this is an important distinction between HF theory and DFT.

energy of the system, but any single-particle observable can be expressed in terms of G. These two notions will not look enlightening to a careful reader, since they are a peculiarity of the electron density and DFT methods as well. The novelty comes from the fact that the density functional through which a generic observable can be expressed in DFT is generally unknown, whereas with the Greens functions methods the approximations are more explicit and transparent. Green's functions possess another important advantage: Green's function theory is explicitly designed for excited state properties. Through the knowledge of G the single-particle excitation spectrum of the system is directly accessible, as we will show.
The time-ordered one-particle Green's function is defined as

$$G(1,2) \coloneqq i\Theta(t_2 - t_1)\langle N|\psi^\dagger(2)\psi(1)|N\rangle - i\Theta(t_1 - t_2)\langle N|\psi(1)\psi^\dagger(2)|N\rangle \quad (2.15)$$

where Θ is the Heaviside step function and we used a short number notation for the time and radial coordinate and the spin state of the single particle $(n) \coloneqq (\mathbf{r}_n, t_n, \sigma_n)$. The physical interpretation of (2.15) is the following: either an electron with spin σ_2 is added at $(\mathbf{r}_2, t_2)$ to a N particle system and then an electron with spin σ_1 is removed at $(\mathbf{r}_1, t_1)$ or the same process involves a hole in opposite time configuration $t_1 < t_2$.
We can introduce an orthonormal basis in the Fock space of N states such that the definition of G can be cast in the form (setting $\tau = t_2 - t_1$):

$$\begin{aligned} G(\mathbf{r}_1, \mathbf{r}_2, \tau) = i\Theta(\tau) \sum_i \langle N|\psi^\dagger(2)|N-1, i\rangle\langle N-1, i|\psi(1)|N\rangle \\ - i\Theta(-\tau) \sum_i \langle N|\psi(1)|N+1, i\rangle\langle N+1, i|\psi^\dagger(2)|N\rangle. \end{aligned} \quad (2.16)$$

It is now useful to introduce the Heisenberg picture

$$\psi(1) = e^{i\mathscr{H}t_1}\psi(\mathbf{r}_1)e^{-i\mathscr{H}t_1}\,, \quad (2.17)$$

where we have omitted the spin index as we will do for the rest of the section, unless specified. In the Heisenberg representation eq. (2.16) reads

$$G(\mathbf{r}_1,\mathbf{r}_2,\tau) = i\Theta(\tau)\sum_i \langle N|\psi^\dagger(\mathbf{r}_2)|N-1,i\rangle\langle N-1,i|\psi(\mathbf{r}_1)|N\rangle e^{i(E_N-E_{N-1,i})\tau} \\ - i\Theta(-\tau)\sum_i \langle N|\psi(\mathbf{r}_1)|N+1,i\rangle\langle N+1,i|\psi^\dagger(\mathbf{r}_2)|N\rangle e^{-i(E_N-E_{N+1,i})\tau}. \tag{2.18}$$

Koopman's theorem allows us to interpret the arguments of the exponentials in the last equation as excitation energies. The physical intuition of this definition of the Green's function is effortless: the energy spent to excite the system from a ground state of N particles to the state $[N+1,i]$ (or $[N-i,i]$) with the injection of an electron (or hole) for $\tau<0$ (or $\tau>0$) is the addition energy $E_{N+1,i}-E_N$ (or removal energy $E_N-E_{N-1,i}$).
Fourier transforming eq.(2.18) results in the arguments of the exponentials being transferred to the denominator of a fraction entering the Lehmann representation of G:

$$G(\mathbf{r}_1,\mathbf{r}_2,\omega) = \sum_i \frac{f_i(\mathbf{r}_1)f_i^\star(\mathbf{r}_2)}{\omega-\epsilon_i+i\eta\,\mathrm{sign}(\epsilon_i-\mu)}\,, \tag{2.19}$$

where we have defined the Lehmann amplitudes f_i in terms of addition and removal energies (respectively above and below the chemical potential μ):

$$f_i(\mathbf{r}) \coloneqq \begin{cases} \langle N|\psi(\mathbf{r})|N+1,i\rangle & \text{if} \quad \epsilon_i = E_{N+1,i}-E_N \Leftrightarrow \epsilon_i>\mu \\ \langle N-1,i|\psi(\mathbf{r})|N\rangle & \text{if} \quad \epsilon_i = E_N-E_{N-1,i} \Leftrightarrow \epsilon_i<\mu \end{cases}. \tag{2.20}$$

The reason behind the $i\eta\mathrm{sign}(\epsilon_i-\mu)$ factor in eq.(2.19) is that performing analytically the Fourier transform one has to take care of the poles of G, which are fully real, shifting them by an infinitesimal factor η in the complex plane, below and above the real axis respectively for electrons and poles (due to their opposite signs of τ).
Let us introduce now the Green's function in the spectral representation

$$G(\mathbf{r}_1,\mathbf{r}_2,\omega) = \int_\infty^{-\infty} \frac{A(\mathbf{r}_1,\mathbf{r}_2,\omega')}{\omega-\omega'+i\eta\,\mathrm{sign}(\omega'-\mu)}d\omega', \tag{2.21}$$

the numerator of the integrand is the well-known *spectral function*, defined as

$$A(\mathbf{r}_1, \mathbf{r}_2, \omega) \coloneqq \frac{1}{\pi}|\Im[G(\mathbf{r}_1, \mathbf{r}_2, \omega)]| = \sum_i f_i(\mathbf{r}_1) f_i^\star(\mathbf{r}_2)\delta(\omega - \epsilon_i). \tag{2.22}$$

The last equality has been obtained from (2.19) by means of the Sokhatsky-Weierstrass theorem ($\mathscr{P}$ being the Cauchy principal value)

$$\lim_{\eta\to 0^+} \int_a^b \frac{f(x)}{x \pm i\eta}\, dx = \mp i\pi f(0) + \mathscr{P}\int_a^b \frac{f(x)}{x}\, dx,$$

and it embodies the meaning a of the spectral function, characterized by delta peaks in proximity of the poles of the Green's function. These poles can be directly linked to the single-particle excitations of the system, related to addition and removal of electrons, which is the object of study of respectively photo-emission and inverse photo-emission spectroscopy experiments.

2.3.1 Self-energy and Dyson equation

The dynamics of a N-particle problem in Green's function formalism can be introduced by means of the annihilation ψ and creation $\psi^\dagger$ field operators in the second quantization framework. The many-body Hamiltonian of (1.2) can be constructed through these operators and in the second quantized form it reads:

$$\hat{H} = \int d\mathbf{r}\, \psi^\dagger(\mathbf{r}) H_0(\mathbf{r})\psi(\mathbf{r}) + \frac{1}{2}\int d\mathbf{r}d\mathbf{r}'\, \psi^\dagger(\mathbf{r})\psi^\dagger(\mathbf{r}')v(\mathbf{r}-\mathbf{r}')\psi(\mathbf{r})\psi(\mathbf{r}'), \tag{2.23}$$

where $H_0 \coloneqq -\frac{\hbar^2}{2m_e}\nabla^2 + V_{\text{ext}}$ is the non-interacting one-body Hamiltonian. Introducing again the Heisenberg picture (2.17) we can re-extract the time-dependent wave-function $\psi(\mathbf{r}, t)$ in the last equation in order to express the second quantized Hamiltonian $\hat{H}$ in terms of the Green's function by means of (2.15). From the Schrödinger equation we then obtain the following equation of motion for G

$$\left[i\frac{\partial}{\partial t_1} - H_0(\mathbf{r}_1)\right] G(1,2) + i\int d3\, v(\mathbf{r}_1 - \mathbf{r}_3) G_2(1,3;2,3^+) = \delta(1,2), \tag{2.24}$$

where we notice that the Coulomb interaction v acts on a 2-particle Green's function G_2[1], the subscript $^+$ indicates an infinitesimally greater time $t^+ \sim t + \lambda$ with $\lambda \to 0$. This means that in order to get the one-particle Green's function you need to know the two-particle one, which is related to the 3-particle one, and so on, in an infinite hierarchy.
In order to overcome this difficulty, it is useful to introduce an external field U that will mimic the polarization induced in the medium in the propagation of one particle by the presence of others, with $U \to 0$, following the procedure of Schwinger [88]:

$$\frac{\delta G(1,2)}{\delta U(3,4)}\Big|_{U=0} = iL(1,2,3,4) = G_2(1,2;3,4) - G(1,2)G(3,4). \tag{2.25}$$

L is the two-particle correlation function, a 4-point object defining the difference between the propagation of the interacting (G_2) and non-interacting (GG) electron-hole pair, and it is directly obtained from the functional derivative with respect to the vanishing external perturbation field. As a remark of the importance of L, it is easy to show that setting $L = 0$ in (2.25) yields the Hartree approximation whereas $L = GG$ the Hartree-Fock approximation.
We can make use of relation (2.25) in eq. (2.24), keeping in mind that the term $iG(1,1) = -\rho(1)$ gives rise to the Hartree potential in the equation of motion, which becomes

$$\left[i\frac{\partial}{\partial t_1} - H_0(\mathbf{r}_1) - U(1) - V_{\mathrm{H}}(\mathbf{r}_1)\right] G(1,2) - i\int d3\, v(\mathbf{r}_1 - \mathbf{r}_3)\frac{\delta G(1,2)}{\delta U(3)} = \delta(1,2)\,. \tag{2.26}$$

It is now useful to introduce the self-energy with the following definition:

$$\Sigma(1,2) \coloneqq i\int d3d4\, v(\mathbf{r}_1 - \mathbf{r}_3)\frac{\delta G(1,4)}{\delta U(3)}G^{-1}(4,2) + V_{\mathrm{H}}(\mathbf{r}_1), \tag{2.27}$$

[1] $G_2(1,2;1',2')$ represents the transition from a N-particles state with electrons (holes) $1,2$ to the N-particles state with electrons (holes) $1',2'$.

or equivalently, in a more compact way, the one connecting the one- and two-particle Green's functions:

$$\int d3\,\Sigma(1,3)G(3,2) = -i\int d3\,v(\mathbf{r}_1-\mathbf{r}_3)G_2(1,3;2,3^+). \tag{2.28}$$

We can then, in a didactic way, reach the same conclusion either inserting eq.(2.28) in eq.(2.24), or alternatively eq.(2.27) in eq.(2.26) by explicitly omitting the term $U\simeq 0$ (condition of vanishing external field), in both cases we obtain

$$\left[i\frac{\partial}{\partial t_1} - H_0(\mathbf{r}_1)\right]G(1,2) - \int d3\,\Sigma(1,3)G(3,2) = \delta(1,2). \tag{2.29}$$

The last formula represents the well-known Dyson equation, another form of it which better clarifies the meaning of the self-energy can be extracted from the equation of motion for the non-interacting Green's function G_0:

$$\left[i\frac{\partial}{\partial t_1} - H_0(\mathbf{r}_1)\right]G_0(1,2) = \delta(1,2), \tag{2.30}$$

we can use this last equation as a definition of the operator G_0^{-1} that inserted in (2.29) gives

$$G_0^{-1}(1,2)G(1,2) - \int d3\,\Sigma(1,3)G(3,2) = \delta(1,2),$$

which re-arranging the terms can be recast in

$$\begin{aligned} G(1,2) &= G_0(1,2) + \int d3d4\,G_0(1,3)\Sigma(3,4)G_0(4,2) + \\ &+ \int d3d4d5d6\,G_0(1,3)\Sigma(3,4)G_0(4,5)\Sigma(5,6)G_0(6,2) + \cdots \end{aligned} \tag{2.31}$$

or, in a compact form, leaving the integration as implicit:

$$G = G_0 + G_0\Sigma G \quad \Leftrightarrow \quad \Sigma = G_0^{-1} - G^{-1}, \tag{2.32}$$

which is the most common expression for the Dyson equation.
It is important to focus on this last two equations giving an insight into the real meaning of the self-energy. Equation (2.32) clarifies how Σ represents the inter-

actions of the system, corresponding to the difference between the inverses of the interacting and non-interacting Green's functions, as depicted by the diagrams in Fig.2.2.

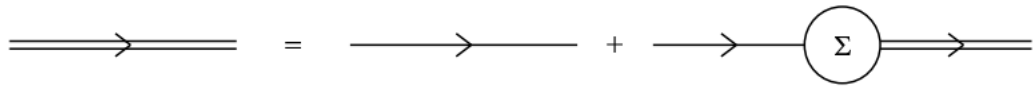

Figure 2.2: Diagrammatic representation of Dyson equation. The double line stands for the interacting Green's function and the single line for the non-interacting one.

Equation (2.31) makes a step forward in this direction: we can consider Σ as a polarization induced in the system to mediate the interactions. The non-interacting Green's function G_0 can represent an "undressed" particle propagating in the space, this induces a polarization with the particle becoming "dressed" by means of the self-energy, this polarization induces a change in its propagation which results in an additional polarization, and so on. This sketch is the idea behind the concept of *quasi-particle*, which will be introduced shortly.

2.3.2 Spectral function in many-body theory

We will now show how the concept of quasi-particles, first appeared in Landau-Fermi liquid theory, is entangled with the self-energy in the framework many-body theory.
From the second equation in (2.32) we can write

$$G = \frac{1}{G_0^{-1} - \Sigma} \quad ,$$

comparing this definition of G in terms of the self-energy to the one in terms of the spectral function (2.22) and expressing the term G_0^{-1} in the frequency space by means of (2.30), we obtain the matrix element

$$A_{ii}(\omega) := \langle i|A(\omega)|i\rangle = \frac{1}{\pi} \frac{|\Im[\Sigma_{ii}(\omega)]}{(\omega - \epsilon_i - \Re[\Sigma_{ii}(\omega)])^2 + (\Im[\Sigma_{ii}(\omega)])^2}. \tag{2.33}$$

This equation has a clear graphical understanding. In the non-interacting case the spectral function is resolved in sharp delta peaks in correspondence of the real poles $(\omega - \epsilon_i)$ of the Green's function G_0, these are simply single-particle excitations. Triggering the interactions by means of a non-zero self-energy results in shifting the original poles to the so-called *quasi-particle* peaks, whose corresponding energies are

$$E_{ii}^{\mathrm{QP}} = \epsilon_i + \Re[\Sigma_{ii}], \tag{2.34}$$

while the delta peaks get broadened by a factor of width equal to $\Im[\Sigma_{ii}]$ corresponding to the quasi-particle lifetime, which is finite. This effect is depicted in Fig.2.3.

The concept of quasi-particle is the result of describing the spectrum of a many-body system in terms of single-particle-like excitations. In the language of Landau theory, a quasi-particle is defined as a "dressed" single-particle with a polarization cloud surrounding it. As a consequence, we can see one quasi-particle eigenstate as a superposition of several single-particle eigenstates, with a finite lifetime due to the possibility of an eigenstate to decay into an other. The broad quasi-particle peaks approximately correspond to physical single-particles excitations as long as the correlations are small, in this case the difference between a true independent particle and a quasi-particle is minimal. Nevertheless when the deviation becomes strong the quasi-particle picture breaks down all together. A borderline example is the exciton, i.e. a particle-hole pair, emerging as a quasi-particle peak in the spectrum.

Any increasing broadening of the quasi-particle peak has to be necessarily accompanied, in order to preserve the spectral weight, by some feature in the tail of the spectrum, called *satellite*, visible of the left side of Fig.2.3. The simple physical explanation of this effect can be found in several phenomena, like plasmon excitations or, for example, in the screening effect following the propagation of our exciton in the interacting medium, and resulting in auxiliary many-particle effects. Satellites are a typical prominent feature of strong correlations in the solid, as they represent physical states that are beyond the concept of quasi-particles. The best way of weighting the effect of correlations and therefore the appearance

of satellites is looking at the so-called renormalization factor:

$$Z_i := \left[1 - \frac{\partial \Sigma_{ii}(\omega)}{\partial \omega}\Big|_{\omega=E_i}\right]^{-1}. \tag{2.35}$$

The renormalization factor is generally less than one, but approaches unity in absence of correlations, when the self-energy correction is vanishing. In presence of weak correlations but within a rather small imaginary part of Σ, the Z factor, representing the quasi-particle weight, gets smaller (the lower Z the more correlated the system), the spectral function gets broadened.
When instead the renormalization factor gets larger than one there is a breakdown of the quasi-particle picture, this description is no longer possible, it is the case when satellite features dominate.

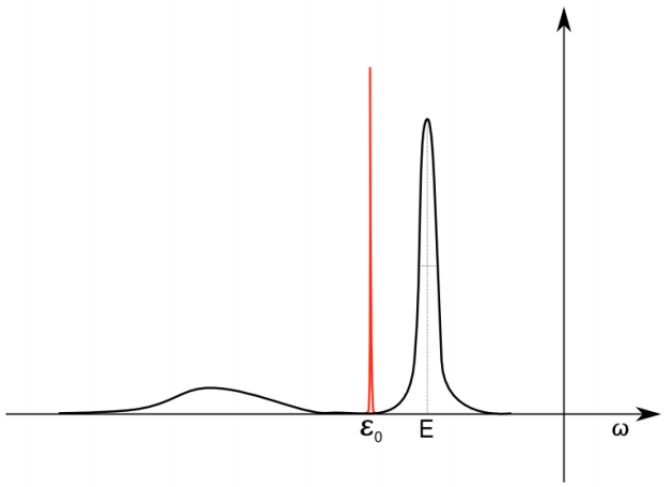

Figure 2.3: Single-particle shart delta peaks (centered in ϵ_0) vs broadened quasi-particle peaks (shifted in $E = \epsilon_0 + \Re[\Sigma]$) and appearance of satellites in the tail of the spectrum. Image from [92].

2.3.3 Self-energy as exchange-correlation

It is now instructive to decompose the self-energy into its non-interacting particles contributions, that is, the first order terms in powers of v. Looking at the right-hand side of (2.28) we take into account the "trivial" contributions to the two-

particle Green's function $G_2(1,2,3,3^+)$: i.e. the states where the initial particles are either unperturbed or they simply exchange place into the final particles. This corresponds to particle 2 either being identical to 1 or 3 (producing a delta function times the one-particle Green's function in place of G_2). These two terms bring the following contribution to the self-energy in (2.28):

$$\Sigma_{\rm HF}(1,2) = -i\delta(1,2)\int d3\, v(\mathbf{r}_1 - \mathbf{r}_3)G(3,3^+) + iv(1,2)G(1,2). \tag{2.36}$$

This is the so-called Hartree-Fock self-energy, represented in the Feynman diagrams of Fig.2.4. The first term, local in space, is the Hartree self-energy, corresponding to the Hartree potential $V_{\rm H}$ giving rise to $E_{\rm H}$ in (2.1). The second term is the Fock, or exchange self-energy $\Sigma_{\rm x}$, giving rise to (2.14).
We have then showed how keeping only the first order contributions to Σ consists in the Hartree-Fock approximation. From now on we will adopt the standard procedure to include just the contributions beyond Hartree in the self-energy $\tilde{\Sigma} = \Sigma - V_{\rm H}$, in such a way that the interactions it describes are related to exchange-correlation interactions only, with $\Sigma_{\rm x}$ as the first order term.

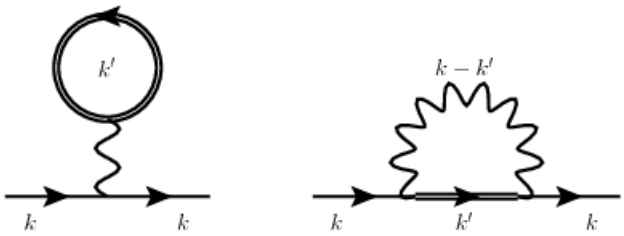

Figure 2.4: Hartree (first term) and Fock (second term) contributions to the self-energy. Image from [85].

Is is therefore natural to relate the self-energy, quantity defined in quasi-particle approaches, to the exchange-correlation potential of DFT [33]. This resemblance becomes more explicit by writing the so-called quasi-particle equation, which can be extracted by (2.30) in frequency space, expressing the non-interacting Green's function as the inverse of the operator $\omega - H_0$. One can derive a corresponding Schrödinger equation for this operator and the self-energy, and using again (2.32), in terms of the quasi-particle eigenfunctions $\phi^{\rm QP} := \phi(\mathbf{r}, \epsilon^{\rm QP} =$

ω):

$$\left[\frac{1}{2}\nabla^2 + V_{\text{ext}}(\mathbf{r}) + V_{\text{H}}(\mathbf{r})\right]\phi(\mathbf{r},\epsilon_{\text{QP}}) + \int d\mathbf{r}'\Sigma(\mathbf{r},\mathbf{r}',\epsilon_{\text{QP}})\phi(\mathbf{r}',\epsilon_{\text{QP}}) = \epsilon^{\text{QP}}\phi(\mathbf{r},\epsilon^{\text{QP}}), \tag{2.37}$$

keeping in mind that the left and right eigenvalues of this expression are not equal being the self-energy not Hermitian[1].

Comparing eq.(2.37) to eqs.(2.7,2.9) one notices that, in the different frameworks respectively of non-interacting particles eigensystem and quasi-particle many-body eigenfunctions, the exchange-correlation potential $V_{\text{xc}}[\rho](\mathbf{r})$ and the self-energy $\Sigma(\mathbf{r},\mathbf{r}',\epsilon)$ are counterparts, even if with an important difference. As it has been extensively stressed before, the eigenfunctions of the KS system do not satisfy the Koopman's theorem, therefore the exchange-correlation potential V_{xc} and the corresponding eigenvalues are not well defined physical quantities, and the differences between KS states cannot be rightfully interpreted as excitation energies. In the framework of Green's function theory the Koopman's theorem is instead satisfied, and the eigensystem of the QP equation has indeed a full physical justification, the self-energy directly yields the spectral function (a physical observable) and the eigenvalues the one-particle excitation energies (as long as the correlations are small). With this important clarification in mind, the association between V_{xc} and Σ is commonly made in the electronic structure community. We have already stressed how in DFT the explicit form of V_{xc} is unknown and one needs to find some approximation for it, like LDA, which although being very effective does not allow to distinguish contributions of different order in terms of interactions. As we have seen regarding the Hartree-Fock Σ, and we will see later for Hedin equations, by means of the self-energy it is possible to overcome this conceptual limit.

2.3.4 Hedin's equations

In order to introduce the GW approximation, one must start from the closed set of Hedin's equations, providing the exact solution for a many-body problem of

[1] The correct procedure at this stage would be an analytic continuation in the complex plane but it is our intention only to present the QP equation in order to make a resemblance with the DFT formulation.

interacting fermions. The explicit derivation of Hedin's equations is a result of Schwinger derivative technique [88] within the framework of many-body perturbation theory. Namely, in order to decouple the hierarchy of equations for the Green's function, a time-dependent vanishing external potential is introduced and the derivative with respect to this function allows to get rid of two-particles G_2 in the definition of G, similarly to the introduction of Σ. The main intuition of Hedin [40] was that in complex systems the interaction effects beyond the Hartree-Fock approximation are related to the screening of the Coulomb interactions due to the charged particles, screening expressed by the dielectric constant in the medium ϵ. This brings a dynamical correlation which is short-range rather than long-range like v. It is then necessary to set the problem in terms of the *screened* Coulomb interaction $W = \epsilon^{-1}v$, as well as the interacting Green's function G, as in Hedin's five set of equations (to be solved self-consistently):

$$G(1,2) = G_0(1,2) + \int d(34) G_0(1,3)\Sigma(3,4)G(4,2) \tag{2.38a}$$

$$\Gamma(1,2,3) = \delta(1,2)\delta(1,3) + \int d(4567)\frac{\delta\Sigma(1,2)}{\delta G(4,5)}G(4,6)G(7,5)\Gamma(6,7,3) \tag{2.38b}$$

$$\widetilde{P}(1,2) = -i\int d(34) G(1,3)\Gamma(3,4,2)G(4,1^+) \tag{2.38c}$$

$$W(1,2) = v(1,2) + \int d(34) v(1,3)\widetilde{P}(3,4)W(4,2) \tag{2.38d}$$

$$\Sigma(1,2) = i\int d(34) G(1,3^+)W(1,4)\Gamma(3,2,4). \tag{2.38e}$$

These equations can be easily obtained from (2.25-2.27) setting $V = V_{\mathrm{H}} + U$ as total potential applied and letting $U \to 0$. The function

$$\widetilde{P}(1,2) = \frac{\delta\rho(1)}{\delta V(2)}, \tag{2.39}$$

is the *irreducible* polarizability defined as the variation of the charge density ρ with respect to the total potential, the corresponding *reducible* polarizability is instead obtained as derivative with respect to the external potential U:

$$P(1,2) = \frac{\delta\rho(1)}{\delta U(2)},$$

and by looking at (2.25) this function can be identified with the two-particle correlation function for the same ingoing and outgoing particle: $L(1,2;1,2)$. The relation between reducible and irreducible polarizability can be expressed also through the definition of the dielectric function:

$$\epsilon^{-1} = 1 + vP, \tag{2.40}$$

and knowing that $\epsilon \coloneqq \delta U/\delta V$ one concludes $P = \epsilon^{-1}\widetilde{P} = \widetilde{P} + \widetilde{P}vP$. The function

$$\Gamma(1,2,3) = -\frac{\delta G^{-1}(1,2)}{\delta V(3)}, \tag{2.41}$$

is the *irreducible* vertex function, entering (2.38b), it describes all particle-hole and particle-particle interactions.
In eq.(2.38c) we evince that the irreducible polarizability $\widetilde{P} = -iGG\Gamma$ is related to the independent propagation of an electron and a hole (GG) which interact through Γ. Similarly, from (2.38e) one recognizes the propagation of particle (G) interacting with the rest of the system ($W\Gamma$).
The self-consistent cycle to solve Hedin's equation is represented in the pentagon of Fig.2.5.

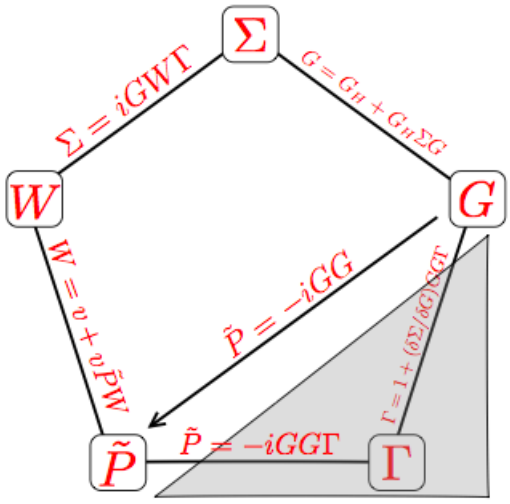

Figure 2.5: Hedin's close set pentagon of equations. Excluding the triangle in the corner corresponds to the GW approximation.

2.3.5 GW approximation

In practical implementations the iterative solution of Hedin's system of equations is numerically unworkable, the toughest step being the evaluation of the vertex correction. This is indeed a three-point object, and the physical reason for this is the following: if we consider a Fermi sea of electrons initially at equilibrium, removing an electron e^- , or equivalently creating a hole h^+ results in excitations which involve at least two particles (like e-h pairs). To get rid of the calculation of Γ, the natural approximation proposed by Hedin in [40] was to chose a trivial form for the irreducible vertex correction:

$$\Gamma(1,2,3) \sim \delta(1,2)\delta(1,3), \tag{2.42}$$

in such a way that the corresponding polarization field $\widetilde{P} \sim -iGG$ gets mediated by a particle-hole pair not interacting with each other. The self-energy, substituting in (2.38e), becomes

$$\Sigma(1,2) = iG(1,2)W(2,1), \tag{2.43}$$

giving the name to the so-called *GW approximation* (GWA), represented as avoiding the right bottom triangle of Fig.2.5, a short cut for the iterative solution of Hedin's pentagon. From the perspective of the simple schematic picture of the electron excited in the Fermi sea at rest, the GWA corresponds to neglect all the correlations related to the fermionic nature of the excited electron and to consider just the *classical* screened interaction that this particle creates.
The expression (2.43) implicitly yields a product in time of the screened Coulomb interaction and the Green's function. In practice, a convolution in frequency space in performed through the integral:

$$\begin{aligned}\Sigma(\mathbf{r},\mathbf{r}',\omega) = &\frac{i}{2\pi}\int d\omega e^{-i\delta\omega'} G(\mathbf{r},\mathbf{r}',\omega-\omega')v(\mathbf{r},\mathbf{r}') \\ &+ \frac{i}{2\pi}\int d\omega e^{-i\delta\omega'} G(\mathbf{r},\mathbf{r}',\omega-\omega')W_{\mathrm{p}}(\mathbf{r},\mathbf{r}',\omega'),\end{aligned} \tag{2.44}$$

where we have explicitly divided the screened Coulomb interaction into the static (bare) component and the dynamical correlated part $W = v + v\chi v \coloneqq v + W_{\mathrm{p}}$ (χ being the independent particle polarizability). As a consequence we extracted the well-known exchange term $\Sigma_{\mathrm{x}} = iGv$ of (2.36) from the correlated component $\Sigma_{\mathrm{c}} = iGW_{\mathrm{p}}$. This expression clearly elucidates the meaning of GW approximation as "screened Hartree-Fock". Comparing (2.44) and (2.36) we notice that we can obtain GWA from HFA simply substituting the bare Coulomb interaction v with the dynamically screened W. This is the main advantage of GW with respect to Hartree-Fock approximation, which it is known to make both qualitative and quantitative changes to the electronic structure predictions.
In Many-body Perturbation Theory (MBPT), as eq.(2.44) states, the self-energy is *non-local*, an important difference with respect to the LDA. Indeed, the locality of the LDA is both what gives it its simplicity and also is the source of many of its failures. As an example the locality of V_{xc} often results in underestimation of band-gaps which is overcome in GW (see Fig.2.7 further on). DMFT also has a non-local self-energy, the non-locality being restricted to the subspace in which DMFT operates (in other words it is local for each single or multiple designated sites).
The GW approximation yields the framework [7] for the state-of-the-art electronic structure techniques, accounted for in an overview in next section, offering remarkable improvements over DFT to predict the band-structure of moderately-correlated materials.

2.3.6 Practical implementation of GW approximation

Any GW method has to start from a trial non-interacting Hamiltonian

$$H_0 = -\frac{1}{2}\nabla^2 + V_{\mathrm{eff}}(\mathbf{r}, \mathbf{r}'), \tag{2.45}$$

usually a KS Hamiltonian, whose solution yields a system of eigenvalues and eigenfunctions $\{\epsilon_i, \phi_i(\mathbf{r})\}$ used to built the non-interacting Green's function

$$G_0(\mathbf{r}, \mathbf{r}', \omega) = [\omega - H_0]^{-1} = \sum_i \frac{\phi_i(\mathbf{r})\phi_i^\star(\mathbf{r})}{\omega - \epsilon_i \pm i\delta}. \tag{2.46}$$

A corresponding polarizability $\widetilde{P} = -iG_0G_0$, dielectric function $\epsilon^{-1} = 1 - v\widetilde{P}$ and screened interaction $W_0 = \epsilon^{-1}v$ are then computed, the latter usually by means of the time-dependent Hartree or Random Phase Approximation (RPA), which consists in mediating the particle interactions via a series of *independent* electron-hole pairs, as expressed in Fig.2.6. RPA yields a dynamically screened interaction $W(\mathbf{r}, \mathbf{r}', \omega)$, which, using (2.44) (with G_0 in place of G) gives back a GW self-energy $\Sigma(\mathbf{r}, \mathbf{r}', \omega)$. Finally this self-energy is directly use as a correction to the LDA Hamiltonian, and can be considered as a more accurate exchange-correlation potential. This is the procedure for one-shot G_0W_0 approaches, and also the first step for self-consistent GW formulations.

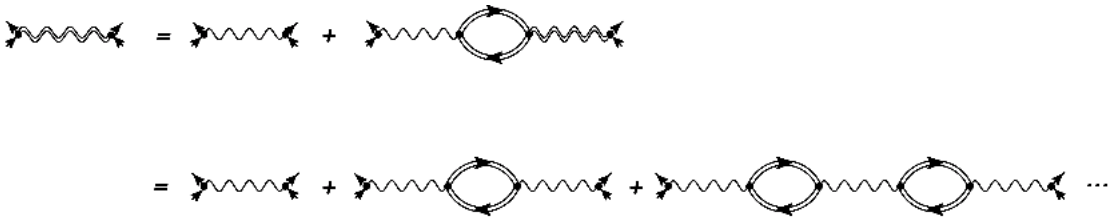

Figure 2.6: Diagram representing the RPA screening. The screened Coulomb interaction W (double curly line) is obtained by mediating the full v (single curly line) via iterative bubbles of electron-hole pairs (represented in terms of the double straight line of G). Note than there is no line inside the bubbles, electrons and holes are independent. Adding the interaction lines inside the bubbles would result in *ladder diagrams* kind of contributions. Image from [43].

2.3.6.1 G_0W_0 or 1-shot-GW

In G_0W_0 approaches, usually implemented with $G_0 = G^{\mathrm{LDA}}$ when the effective potential is usually a KS potential and the eigenvalues are the result of a converged LDA calculation, the interacting problem can be solved following the quasi-particle picture introduced in sec.2.3.3, and in particular the equation of motion (2.37). Even if the full dependency of $\Sigma(E^{\mathrm{QP}})$ with respect to quasi-particle energies is not known, one can avoid the analytic continuation from the complex plane on which this equation stands by introducing a first-order many-

body perturbation theory on the KS energies ϵ_i^{KS}:

$$E_i^{\mathrm{QP}} \simeq \epsilon_i^{\mathrm{KS}} + \langle \phi_i | Z_i [\Sigma(\epsilon_i^{\mathrm{KS}}) - V_{\mathrm{xc}}] | \phi_i \rangle, \tag{2.47}$$

where Z_i is the renormalization factor of (2.35) accounting for spectral weight renormalization and the broadening of quasi-particle peaks. It must be stressed that this picture still holds as long as applied on s, p systems and in general for moderately correlated materials. The satellite features characteristic of strongly correlated materials are instead not well accounted in GW and the quasi-particle picture fails.

This *ab initio* method, since its first implementation [49], has accomplished remarkable results in reproducing the experimental band-gaps and quasi-particles lifetimes of a wide class of materials, in particular semiconductors and insulators, overcoming the systematic underestimation of LDA predictions. A comparison between the G_0W_0 and LDA band-gaps for *sp* systems is depicted in Fig.2.7.

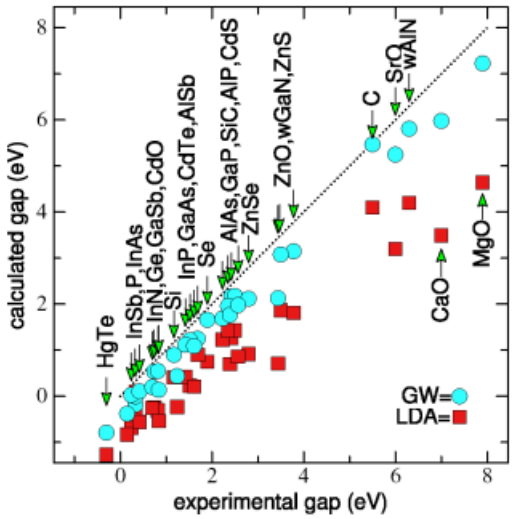

Figure 2.7: $G^{\mathrm{LDA}}W^{\mathrm{LDA}}$ vs LDA band-gaps of *sp* systems. The underestimation of LDA is decreased in GW (accurate within 0.1 eV). Image from [98].

2.3.6.2 Self-Consistent GW methods: an overview

Alternative to 1-shot GW approaches are the so-called self-consistent GW methods. The interacting Green's function obtained with a G_0W_0 self-energy is just used as a starting point $G^{(0)}$ used to re-build the screened interaction and the self-energy in such a way that a $G^{(1)}$ is derived, the operation is then reiterated until some convergence is reached. The principle behind this method is to construct an interacting problem which does not depend on the LDA starting point. The procedure and conditions through which self-consistency is built and the approximations or additional corrections applied on top of it, object of this brief overview, characterize the different scGW schemes.

Full and Partial scGW and extensions

Self-consistency in full scGW methods [64, 87] has been successfully developed in a rigorous formulation through the Luttinger-Ward functional $E_{\mathrm{LW}}[G]$ [72]. This functional is directly used to compute the total energy and its functional derivative with respect to G is set to zero as a condition to iterate self-consistency.

Regarding more advanced implementations, the explicit inclusion of low order vertex corrections in Σ has shown to improve the absolute positions of quasi-particle peaks in semiconductors [23] and to reproduce some multi-plasmon satellite features in alkali metals [8]. Nevertheless the results have often proved to be dependent on the model used for the vertex correction and most of all, it appears there is a compensation between self-consistency and vertex corrections[47], neglecting one of the two leads to discrepancies, and this is the main limit of full scGW schemes. For this reason, partial scGW approaches have been developed, in particular "GW_0 calculations" in which W_0 is computed just once through RPA and does not enter the self-consistent cycle whereas G does. An example [101] is the work of von Barth and Holm on Homogeneous Electron Gas (HEG), with a result of slightly increase the G_0W_0 occupied bandwidth.

Main approximations

It is worth mentioning the most common approximations adopted in scGW methods.

Most of the *ab initio* GW codes available at the moment make use of *pseudopotentials* (PP). This has the advantage of highly reducing the numerical cost

but at the price of not including the core states properly.
On the other hand, one of the most problematic obstacles in GW implementations consists in the non-locality, the energy-dependence and the non-Hermitianity of the self-energy. A reasonable approximation (initially proposed in [40]) which was fruitfully used in self-consistent schemes [14] is the COHSEX approximation. Namely, a static and Hermitian COHSEX self-energy is obtained as a sum of (i) the exchange self-energy of (2.36) but with a static screened interaction $W(\mathbf{r}, \mathbf{r}', \omega = 0)$ and (ii) a Coulomb-hole term describing the interaction energy between the quasi-particle and the potential due the Coulomb hole around the quasi-particle (for a more detailed introduction see [7]).
Another customary approximation adopted in these codes responds to the demanding computation of the screening $W(\omega)$ in eq.(2.44) for all frequencies, it is the *plasmon-pole* approximation [50]. This consist in approximating the imaginary part of W_{p} with delta peaks at specific weights. As a consequence the (Fourier transformed) dielectric matrix is approximated as

$$\epsilon^{-1}_{GG'}(\mathbf{q}, \omega) = \delta_{GG'} + \frac{\Omega^2_{GG'}(\mathbf{q})}{\omega^2 - \tilde{\omega}^2_{GG'}(\mathbf{q})}, \tag{2.48}$$

where $\tilde{\omega}_{GG'}(\mathbf{q}), \Omega_{GG'}(\mathbf{q})$ are respectively the plasmon energies and weights expressed as function of the wave-length $\mathbf{q}$.

2.3.6.3 QSGW

An overall conclusion about this overview of GW methods can be drawn: in general full scGW approaches, despite the high numerical cost, do not yield significant improvements over G_0W_0 calculations, and in some cases their results have cumbersome errors, related to the underestimation of the screening, unless these methods are combined with the additional expensive inclusion of vertex corrections.
On the other hand there is some clear evidence showing how 1-shot GW significantly fails in some cases, like the severe systematic underestimation of optical gaps in semiconductors [59] . From a more general perspective, the results of simulations are always very dependent on the LDA starting point, and in several

cases the LDA Hamiltonian H_0 is not a good enough approximation.
For this reason it is essential to exploit the self-consistent approaches in such a way to avoid the dependence from the starting point and on the same footing overcome the ambiguities we mentioned.
The quasi-particle self-consistent GW (QSGW) method, developed by Kotani, van Schilfgaarde and Faleev in 2006 [61, 98], is an *ab initio* perturbative full self-consistent approach. This method is set up in such a way to remove the dependence from the LDA starting point, overcoming the drawbacks of self-consistent schemes by means of the criterion on which self-consistency is determined. It is the approach we followed in this work of thesis.
The main principle behind the method is the following. Self-consistent GW approaches pivot on the mapping between the effective potential of the non-interacting problem, whose Hamiltonian is the one of eq.(2.45), and so-called GW potential $V_{\mathrm{GW}}(\omega) = V_{\mathrm{ext}} + V_{\mathrm{H}} + \Sigma(\omega)$ modelling the interacting problem. The novelty of this method consists in the fact that this mapping $V_{\mathrm{eff}} \to V_{\mathrm{GW}} \to V_{\mathrm{eff}} \cdots$ is grounded on Landau's concept of quasi-particle (QP).
We will summarize the main mathematical steps yielding the framework of this scheme, for more details see [61].
Starting from eq.(2.37), we can choose to take only the Hermitian part of the non-Hermitian operator Σ, defined as $\mathrm{Re}[\Sigma]$, in such a way to deal with fully real eigenvalues. The QP equation can be then recast in a compact form (where the $\mathbf{r}, \mathbf{r}'$ arguments will be omitted for simplicity):

$$\left[\frac{1}{2}\nabla^2 + V_{\mathrm{ext}} + V_{\mathrm{H}} + \mathrm{Re}[\Sigma(E_i)]\right] |\Phi_i\rangle = E_i |\Phi_i\rangle, \tag{2.49}$$

where we have used a shorter notation $\{\Phi_i, E_i\}$ for the eigensystem of the interacting problem described by the total Hamiltonian H, whose states will be referred to as "dressed QP". We used this definition in order to distinguish them from the "bare QP", objects of the non-interacting problem described by the one-particle Hamiltonian H_0, whose eigenvectors and eigenvalues are defined as $\{\Psi_i, \epsilon_i\}$. The physical connection between these two entities is the following: the dressed QP are indeed bare QP with a polarization cloud, formed by other bare QP, surrounding them. The bare QP evolve into the dressed QP when the in-

teraction $\Delta H = H - H_0$ is turned on adiabatically, as the perturbative method demands. In order for the perturbative theory to be effective, the Hamiltonian H_0 should not be any generic one, but the one for which ΔH is minimum. The measure, or norm, chosen in this method to determine and minimize ΔH, represents by all means the breakthrough of QSGW. This norm practically marks the difference between the dressed and bare QP states.
Supposing that the method is effective and the self-consistency is attained, $\{\Phi_i, E_i\} \sim \{\Psi_i, \epsilon_i\}$ at least around E_F. The bare QP set $\{\Psi_i, \epsilon_i\}$, being complete, can be used as a Hilbert space basis to expand the quantity

$$\mathrm{Re}[\Sigma(E_i)]|\Phi_i\rangle \sim \mathrm{Re}[\Sigma(\epsilon_i)]|\Psi_i\rangle = \sum_{ji} |\Psi_j\rangle \mathrm{Re}[\Sigma(\epsilon_i)]_{ji},$$

where the subscripts in ij represent the matrix elements between the states Ψ. We can then introduce a quantum operator R as

$$R \coloneqq \sum_{ij} |\Psi_j\rangle \mathrm{Re}[\Sigma(\epsilon_i)]_{ji} \langle\Psi_i|,$$

such that $R|\Psi_i\rangle = \mathrm{Re}[\Sigma(\epsilon_i)]|\Psi_i\rangle$, and then it can be inserted in (2.49) in place of $\mathrm{Re}[\Sigma(E_i)]$. This operator is not Hermitian though, we then must take the Hermitian part to define our QSGW self-energy according to

$$\Sigma_{\mathrm{QSGW}} = \frac{1}{2} \sum_{ji} |\Psi_i\rangle \left\{ \mathrm{Re}[\Sigma(\epsilon_i)]_{ij} + \mathrm{Re}[\Sigma(\epsilon_j)]_{ji} \right\} \langle\Psi_j|. \tag{2.50}$$

This static quantity, following our prescription of converging the bare and dressed QP states, can be taken as our new exchange-correlation potential V_{xc} entering the non-interacting Hamiltonian. Eq. (2.50) is then our reference point to complete the mapping $V_{\mathrm{eff}} \to V_{\mathrm{GW}} \to V_{\mathrm{eff}}$. QSGW is a perturbative treatment to determine H_0, V_{eff}, W and G self-consistently.
It is crucial to clarify the conceptual difference between this approach and the full scGW of last section. The latter is derived from Luttinger-Ward (or similar) functional $E[G]$, the mapping of self-consistency therefore involves the full Green's function $G \to G$. As a consequence, the screened interaction is obtained

as $\widetilde{P} = -iG \times G$, including intermediate states such as electron-hole excitations weighted by the square of the renormalization factor $Z \times Z$. These contributions are physically unclear since they are affected by the incoherent part of the spectra (like plasmonic satellites). Including vertex corrections results in a mutual cancellation of the effects of Z factor in G and this is reason behind the compensation between fully self-consistency and inclusion of vertex correction.
On the other hand QSGW methods overcome this difficulty by carrying out the expansion through G_0 (or H_0) instead of G, focusing on the QP contribution only. A very interesting *a priori* formal justification of the QP self-consistent equation of QSGW within the very framework of Luttinger-Ward theory can be found in [54].
The results of QSGW calculations [98], displayed in Fig.2.8, are remarkable. Contrarily to LDA and 1-shot GW predictions, QSGW band-gaps are systematically slightly overestimated, and this discrepancy can be easily targeted, being directly connected to the underestimation of the screening due to the non-inclusion of electron-hole interactions through RPA.

2.3.6.4 Limits of GW methods: strong correlations

Even QSGW is known to break down in the presence of strong correlations. Without additional ad-hoc corrections and extensions GW methods are not able to reproduce typical many-body effects like plasmon satellites or magnetic effects like spin fluctuations, and this is mostly due the missing diagrams in the RPA screening. A more-advanced many body theory is needed in these cases but nevertheless GW schemes (QSGW in particular) can be still used to treat the largest part of the system. Correlations are in fact known to be limited to a few degrees of freedom (e.g. d- f- orbitals near the Fermi level), for these a higher level of approximation has to be chosen. This requires a peculiar *partitioning* of the space, or equivalently the Hamiltonian, where a local, correlated subsystem is treated differently whereas the rest can be safely analysed at GW level. The details of this partitioning will be introduced in the next chapter.

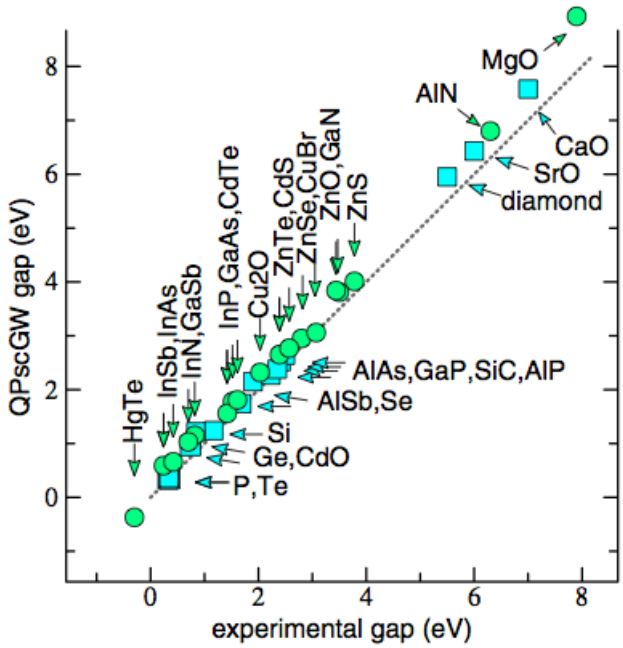

Figure 2.8: QSGW band-gaps of *sp* systems compared to experiments. The underestimation typical of LDA is reverted. The errors are small and systematic and could be further reduced by including e-h renormalization. Image from [98].

Chapter 3

Non-perturbative approaches for strong correlations

As mentioned in the first chapter, strongly correlated materials, displaying interesting exotic physical properties like high T_c superconductivity and Mott metal-insulator transitions, present a serious challenge for DFT methods as well as the most advanced GW approaches. The reason for this is the existence of several competing physical processes, in particular the interplay of localization and itinerancy of the electrons in the lattice or the quantum and spatial fluctuations, which cannot be adequately described by perturbative methods. A non-perturbative many-body theory treatment is required, at least to tackle the few degrees of freedom characterized by correlations.

3.1 Dynamical Mean Field Theory

Dynamical Mean Field Theory (DMFT) [30, 31, 62, 77], since its development in the early 90s, has proven to be the most effective model to study SCM. The idea is to substitute, or map, the full many-body problem of the lattice with a single quantum object with fewer degrees of freedom, called *impurity*, which dynamics is treated at many-body level, while the rest of the system is accounted as a non-interacting *bath* coupled *self-consistently* to the impurity.
DMFT can be seen as a quantum physics generalization of the Weiss mean-field

theory of the Ising Model in the framework of classical statistical mechanics. The expression "mean-field theory" applies to the Hartree-Fock approximation as well. Nevertheless in HF theory all the fluctuations (spatial and temporal) are frozen whereas DMFT freezes the spatial fluctuations but takes full account of the local quantum fluctuations (i.e. between the possible quantum states at a given time). Hence a *dynamical* mean-field theory.
In analogy with the Weiss mean-field theory, DMFT, despite being an approximation, becomes *exact* in the limit of infinite spacial dimensions ($d \to \infty$). DMFT is hence a controlled approximation for systems with large coordination numbers. In the following section we will briefly introduce Weiss mean-field theory in order to hold the ground for Dynamical Mean Field Theory.

The Ising model and the Weiss mean-field

In the context of classical statistical mechanics the Hamiltonian for the Ising model of a lattice of spins S_i reads as follows:

$$H = -J \sum_{\langle ij \rangle} S_i S_j - h \sum_i S_i, \tag{3.1}$$

where the external magnetic field is accounted with the energy h for the single spin whereas the spin-spin interaction, affecting just nearest neighbours sites ($\langle ij \rangle$), contributes to the ferromagnetic energy J. The interaction term introduces correlations between different spins and makes the system very hard to solve. Therefore we seek for an equivalent simple model describing the interactions of our system focusing on the magnetization on each lattice site obtained as a thermal average $m_i = \langle S_i \rangle$. In mean-field theory, the fluctuations of m_i around its average are assumed to be small. As an auxiliary system we can take an assembly of non-interacting spins embedded in an effective site-dependent field h_i^{eff} resulting in a Hamiltonian

$$H^{\text{eff}} = -\sum_i h_i^{\text{eff}} S_i. \tag{3.2}$$

The effective field is determined through the condition of leading to the original lattice magnetization, this requires $\beta h_i^{\text{eff}} = \tanh^{-1} m_i$, with β being the inverse temperature. The approximation proposed by Weiss, giving the name to the

mean-field chosen, is to take the effective field as the thermal average of the local field seen by the spin at a given site

$$h_i^{\text{eff}} \simeq h + J\sum_i \langle S_i\rangle = h + zJm, \tag{3.3}$$

where z is the coordination number and the magnetic order is assumed to be translational invariant ($m_i = m$). Such a choice of the mean field leads to the self-consistent equation for the magnetization:

$$m = \tanh(\beta h + z\beta J m). \tag{3.4}$$

We stress that the mapping from the interacting spin system to the non-interacting one in the effective field is not an approximation if addressed only to compute the local magnetization. It is when the Weiss mean-field is used to represent the neighbouring sites, in eq.(3.3), that the approximation takes place, even though this approximation becomes exact in the limit of $z \to \infty$. This is indeed intuitive to guess: as the number of neighbours becomes large they are safely included as an effective *bath* and the local fluctuations of the field can be neglected. Extending this underlying idea to the quantum framework is the main assumption of DMFT. The procedure of [29] will be taken as a guideline.

Quantum case: from Hubbard to Anderson model

In order to introduce the quantum variables we start from the single-band Hubbard model [48]:

$$\hat{H} = -\sum_{\langle ij\rangle,\sigma} t_{ij} c^\dagger_{\sigma i} c_{\sigma j} + U\sum_i n_{i\downarrow} n_{i\uparrow} + (\epsilon_0 - \mu)\sum_{i,\sigma} n_{i\sigma} \tag{3.5}$$

where the first term is the kinetic energy describing the hopping exclusively between nearest neighbours ($\langle ij\rangle$) through the destruction ($c_{\sigma j}$) and creation ($c^\dagger_{\sigma i}$) operators, the second term is the on-site interaction energy ($n_{i\sigma} = c^\dagger_{\sigma i} c_{\sigma i}$ the spin-dependent occupancy of the site), and we added a third term controlling the on-site filling through the chemical potential μ ($\epsilon_0 - \mu$ being the single-electron atomic level). The t_{ij} is a parameter controlling the hopping, whereas the Hub-

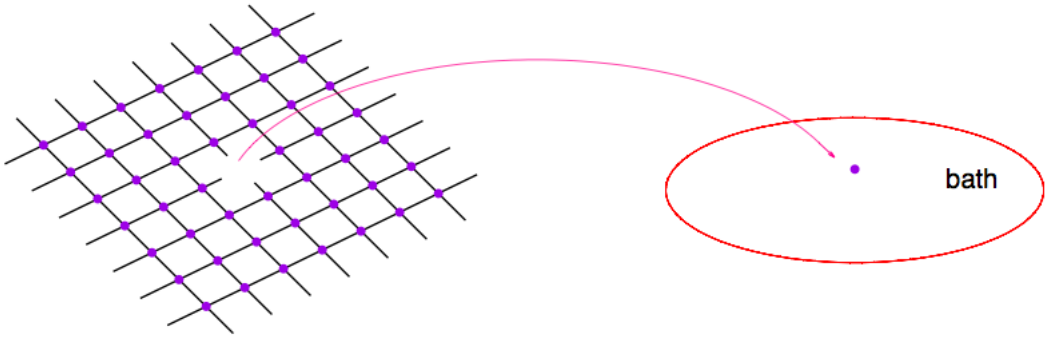

Figure 3.1: Schematic sketch of a mean field theory: the creation of an effective bath surrounding the single site extrapolated from the full lattice. The dynamics of this site, called impurity, can be represented in terms of the interaction of this site with the bath, which by itself is non-interacting. Image from [27].

bard parameter U defines the Coulomb energy cost for placing two electrons on the same site. An effect of screening has to be taken into account, hence this term is typically scaled with respect to the bare Coulomb interaction.
The quantity of reference in DMFT is the *local* on-site Green's function of the lattice

$$G_{ii}(\tau - \tau') \equiv -\langle T c_{\sigma i}(\tau) c^{\dagger}_{\sigma i}(\tau') \rangle. \tag{3.6}$$

This quantity is the quantum time-dependent counterpart of the local magnetization m_i in the classical framework of the Ising model. In analogy with the Weiss theory, the Green's function has to be embedded in a bath through the introduction of an effective mean-field reservoir which now is frequency-depended as the Green's function. This is the prescription of the Anderson Impurity Model [2], where a single interacting quantum *impurity* is coupled to an effective bath of non-interacting fermions via the following Hamiltonian

$$H_{\mathrm{AIM}} = H_{\mathrm{imp}} + H_{\mathrm{bath}} + H_{\mathrm{coup}}, \tag{3.7}$$

where we have defined, respectively, the components of the Hamiltonian relative to the impurity, the bath, and the coupling, as

$$H_{\text{imp}} = U n_{0\downarrow} n_{0\uparrow} + (\epsilon_0 - \mu) \sum_{\sigma} c_{\sigma}^{\dagger} c_{\sigma}; \tag{3.8a}$$

$$H_{\text{bath}} = \sum_{i,\sigma} \tilde{\epsilon}_i a_{i\sigma}^{\dagger} a_{i\sigma}; \tag{3.8b}$$

$$H_{\text{coup}} = \sum_{i,\sigma} V_i \left(a_{i\sigma}^{\dagger} c_{\sigma} + c_{\sigma}^{\dagger} a_{i\sigma} \right). \tag{3.8c}$$

The terms $a_{i\sigma}^{\dagger}, a_{i\sigma}$ represent the bath operators whereas the impurity operators $c_{\sigma}^{\dagger}$ (entering the corresponding Hamiltonian) are equivalent to the ones of the original lattice model. The superscript over $\tilde{\epsilon}_i$, describing the fictitious bath orbital energies, indicates that this is an effective parameter not to be confused with the single-particle energies of the original lattice model. The parameters $\tilde{\epsilon}_i$ together with the coupling constant V_i are chosen in such a way that the impurity model Green's function reproduces the original lattice Hubbard model one. The condition expressing this requirement is the quantum analogous of the expression of the Weiss mean field in terms of the magnetization. In the context of the Anderson Impurity Model it is embodied in the definition of the frequency-dependent *hybridization function*:

$$\Delta(i\omega_n) \coloneqq \sum_{l} \frac{V_l^2}{i\omega_n - \tilde{\epsilon}_l}, \tag{3.9}$$

where the $i\omega_n \coloneqq i\frac{(2n+1)\pi}{\beta}$ are complex Matsubara frequencies. The hybridization function is a key quantity in DMFT approaches, defining the coupling of the impurity with the surrounding bath in which is embedded. In order to extrapolate the dynamics of our problem we need to integrate out the bath degrees of freedom, this can be done in a straightforward manner by means of an effective action functional integral formalism [86]. The derivation of the effective action, together with a rigorous introduction of the hybridization function, is the object of Appendix A (see in particular eq. (32)). With the introduction of Grassmann

variables, the effective action for the impurity problem reads

$$S_{\text{eff}} = -\int_0^\beta d\tau \int_0^\beta d\tau' \sum_\sigma c_\sigma^\dagger(\tau)\mathscr{G}_0^{-1}(\tau-\tau')c_\sigma(\tau') + U\int_0^\beta d\tau n_\uparrow(\tau)n_\downarrow(\tau). \quad (3.10)$$

This action fully represents the dynamics of our single site impurity: $\mathscr{G}_0$ is the bare propagator of a fermion created (or extracted from the external bath) at time τ and destroyed (or put back in the bath) at time τ', whereas the second term represents the Coulomb interaction acting on two fermions with opposite spins occupying the same site. The propagator can be cast in the Matsubara spectral representation

$$\mathscr{G}_0^{-1}(i\omega_n) = i\omega_n + \mu - \epsilon_0 - \Delta(i\omega_n), \quad (3.11)$$

showing its connection with the hybridization function (again, see Appendix A for a derivation of the above formula). $\mathscr{G}_0$ is the quantum analogous of the classical Weiss mean-field of the Ising model, here with an energy (or frequency) dependence accounting for the local quantum fluctuations due to the coupling between the local impurity and the bath charges, distinctive feature of DMFT as well as further step on Weiss theory. It can be interpreted as the bare Green's function of the effective action S_{eff}, not to be confused with the non-interacting Green's function of the original lattice problem. Its relation with the interacting Green's function (or impurity Green's function) $G_{\text{imp}}(\tau-\tau') = -\langle Tc_\sigma(\tau)c_\sigma^\dagger(\tau')\rangle_{S_{\text{eff}}}$ is expressed through the *local* impurity self-energy Σ_{imp} by means of the following Dyson equation

$$\Sigma_{\text{imp}}(i\omega_n) = \mathscr{G}_0^{-1}(i\omega_n) - G_{\text{imp}}^{-1}(i\omega_n), \quad (3.12)$$

where the subscripts chosen are meant to stress that this equation regards the impurity as disentangled from the lattice.

In order to re-connect this effective auxiliary problem to the original Hubbard model, we introduce the *lattice* self-energy $\Sigma_{ij}(\tau-\tau')$ defined in terms of the full interacting Green's function $G_{ij}(\tau-\tau') = -\langle Tc_{\sigma i}(\tau)c_{\sigma j}^\dagger(\tau')\rangle$ (note that this

function is different from (3.6) because it is non-local) by means of

$$G(\mathbf{k}, i\omega_n) = \frac{1}{i\omega_n + \mu - \epsilon_0 - \epsilon_{\mathbf{k}} - \Sigma(\mathbf{k}, i\omega_n)}, \tag{3.13}$$

where we substituted the sites indices i, j with a momentum $\mathbf{k}$ dependence and we defined $\epsilon_{\mathbf{k}}$ as the Fourier transform of the hopping integrals t_{ij}.
Up to now, as long as addressed to the proper observable, the mapping we have devised is exact. The main assumption of DMFT, in analogy with eq.(3.3), consists in the following approximation: we neglect all the non-local components of Σ_{ij} in (3.13) and take its local component as the local impurity self-energy:

$$\Sigma_{i\neq j} \sim 0; \quad \Sigma(\mathbf{k}, \omega_n) = \Sigma_{\text{imp}}(i\omega_n), \tag{3.14}$$

approximation that, equivalently to the classical Ising model, becomes *exact* in the limit of infinite dimensions, as proved in [77]. This assumption requires the local lattice Green's function (3.13) to coincide with the impurity Green's function in (3.12)[1]:

$$G_{\text{imp}}(i\omega_n) = \frac{1}{N_{\mathbf{k}}} \sum_{\mathbf{k}} G(\mathbf{k}, i\omega_n), \tag{3.15}$$

leading to the self-consistency condition of DMFT:

$$G(i\omega_n) = \sum_{\mathbf{k}} \frac{1}{\Delta(i\omega_n) + G^{-1}(i\omega_n) - \epsilon_{\mathbf{k}}}. \tag{3.16}$$

Impurity solvers

The set of equations (3.16) has to be solved iteratively until the local lattice Green's function coincides with the impurity Green's function. The common procedure is to start from an initial guess on the hybridization function. This function is used as a starting input to study the many-body dynamics of the quantum impurity, this is a numerical procedure performed by means of the *impurity solver*, which yields an impurity self-energy Σ_{imp}. The other steps to complete the cycle are summarized in Fig.3.2.

[1] and thanks to this equation in what follows we can get rid of "imp" subscripts on $G_{\text{imp}} \sim G$ since there is no difference any more

Solving the quantum Anderson impurity problem is the key step in common DMFT implementations, whose reliability affects the cost of the solver. Several impurity solver have been developed in the past decades, from the earlier approximated schemes such as the Non-Crossing Approximation (NCA) [57], the Hubbard I approximation [48], or the Numerical Renormalization Group (NRG) [15] to more efficient numerical implementations like the Quantum Monte Carlo (QMC) method [30, 45] up to the most recent Continuous Time Quantum Monte Carlo (CTQMC) method [35, 105] (the one adopted in this work), which essentially provides an exact solution of the Anderson impurity model without statistical errors. More details on CTQMC will be provided further on.

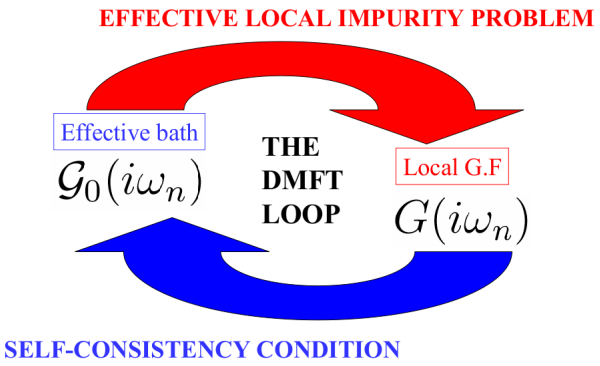

Figure 3.2: The simple idea behind the DMFT iterative self-consistent loop (from [29]). One starts from a guess on $\mathscr{G}_0$, (or equivalently on $\Delta(i\omega_n)$) and by means of an impurity solver extracts an impurity self-energy Σ_{imp}. This impurity self-energy is used, by means of the DMFT approximation (3.14), to derive the local lattice Green's function, which at convergence can be identified with the impurity Green's function G_{imp}. This function yields an updated Weiss field $\mathscr{G}_0$ through (3.11) and the loop is reiterated. Image from [29].

Asymptotic limits of DMFT

It is instructive to study the asymptotic limits in which DMFT becomes exact.

- **Non-interacting limit** $U = 0$. By solving the effective action in (3.10) we get $\mathscr{G}_0 = G$. By looking at the Dyson equation it follows that the self-energy

is null, which makes the DMFT approximation trivially satisfied. On the other hand eq.(3.16) reduces to the definition of the non-interacting lattice Green's function.

- **Atomic limit** $t_{ij} = 0$. A collection of independent atoms are on each site. The hybridization function $\Delta(i\omega_n)$ is therefore 0. The corresponding self-energy has to have only on-site components then, the DMFT approximation is again exact.

Applications of DMFT: Correlated materials and Mott transitions

The main difficulty of analysing correlated materials in a theoretical framework relies in the interplay between itinerancy and localization of the electrons, i.e. the competition between the kinetic energy, delocalising electrons and enabling more than one electron to occupy the same site (wave effect) and the Coulomb repulsion, which keeps electrons apart and acts to oppose double occupancy (particle effect). In strongly correlated materials these occurrences can coexist in the same material and a reliable model has to be able to capture the physics of both at the same time.
The Mott metal-insulator transition is a direct physical consequence of this particle-wave duality. The materials exhibiting this property, like vanadium oxide or nickel selenium sulphide, present a distinctive feature in the high temperature regimes of their phase diagrams, starting from different ordered states in the low temperature one, and this property can be directly connected to a change from a itinerant to a localized behaviour in the solid. From the point of view of the spectral function, following our treatment of sec.2.3.2, in this kind of transitions the weight of the quasi-particle peaks in the low energy part of the spectra is gradually transferred to the Hubbard satellites of the high energy region.
DMFT owes its success to the ability of accurately describing the features of both coherent and incoherent spectra on the same footing, contrarily to DFT and GW approaches.
As a remark, as well as a conspicuous test of the versatility of the method, one can analyse the evolution of the results of a DMFT calculation by varying the ratio between the correlation energy (or Coulomb repulsion) U and the band-width

W of non-interacting electrons. It is the work done in [63], in particular for a one-band Hubbard model (referred to eq.(3.5)) at zero temperature ($T = 0$) and half-filling ($n = 1$), and studying the spectral function $A(\omega)$ as the ratio U/W grows. The results are shown in Fig.3.3.

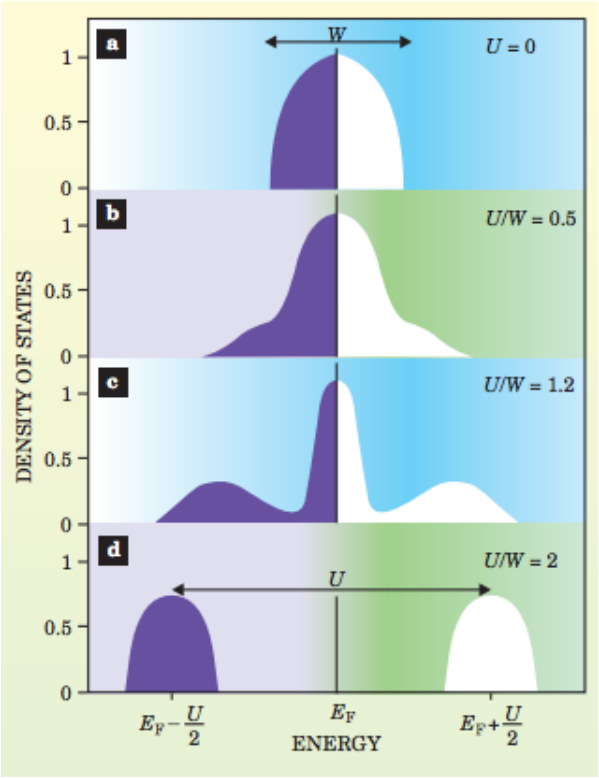

Figure 3.3: Density of states of electrons varying as a function of the ratio between Coulomb interaction and band-width U/W. A DMFT calculation on the Hubbard Hamiltonian for half filling ($n = 1$) and zero temperature $T = 0$ is performed. (a) is the independent-particle limit, (b) the weakly correlated region, (c) the strongly correlated system, (d) the Mott metal insulator transition.
Image from [63].

The upper panel (a) shows the non-interacting limit ($U = 0$), the spectral function is exactly the density of states (DOS) of band theory with the Fermi level right in the middle of the elliptical shape of the single-particle peak, predicting a metallic state. When turning on the correlations in the weakly interacting regime (b) there is a redistribution of spectral weight as in the Fermi liquid state, the

electrons can safely be described in terms of quasi-particles whose DOS still resembles that of the free electrons regime. When correlations become strong (c), a characteristic three-peaks structure appears in the spectrum: a narrow quasi-particle peak at low excitation energies coexist with the atomic-like Hubbard bands caused by local excitations and broadened by the hopping of the electrons in the atom. This is the typical peculiarity of strongly correlated materials, and being able to capture it represents the main accomplishment of DMFT . The Mott metal-insulator transition appears (d) when the correlations between electrons are strong enough to transfer all the spectral weight from the quasi-particle peaks (that vanish) to the two separate incoherent Hubbard bands. An insulator is produced.

3.1.1 LDA+DMFT

This analysis [63] on Mott insulators is an example of the first stage implementation of DMFT: by means of some model Hamiltonians (like the Hubbard one) acting on atomic-like correlated orbitals with specific parameters (the hopping term, the Coulomb interaction, the Hund's coupling) tailored for the system under consideration, the many-electron problem is treated within the self-consistent scheme of the DMFT equations. The results of this method reproduce the typical features of strong correlations, like the three-peaks structure in the intermediate region and the Mott insulating state at diverging U.
Nevertheless the model Hamiltonians are only loosely applicable to real materials mostly due to the parameter-dependence of the method, missing flexibility and reliability. Moreover, they completely lack accounting of non-local and long range interactions. In order to overcome these limitations an intuitive idea is to merge DMFT with realistic ab initio electronic structure methods such as DFT. A transitional step towards this goal is the formulation of the LDA+U method [5, 69]. In LDA+U, an ad hoc Hartree-Fock-like static interaction term U is explicitly added to the LDA Hamiltonian with the specific target of acting on a limited set of correlated orbitals in order to take account of local interactions. By means of this approach it was possible to reproduce the Mott insulating state of magnetically order transition metals [6] and rare-earth compounds. On the other

hand, by definition the LDA+U method is unable to treat the quasi-particle-like structure as well as the atomic-like Hubbard structure on the same footing. As a consequence LDA+U misses the strongly correlated metallic phase displayed by transition metal oxides at intermediate values of U or at a non-integer number of d, f electrons per site in such a way that the Mott insulator is doped and becomes metallic (this corresponds to the intermediate correlated region (c) of Fig.3.3). In order to adequately describe the many-body effects of strongly correlated materials the dynamical contributions of the local interactions cannot be neglected, and in this sense LDA+U can be considered as a static approximation to LDA+DMFT.

3.1.1.1 Definition and achievements

In the past decades LDA+DMFT [31, 62, 67] has been the most effective technique for modelling the physics of strongly correlated materials. The procedure is the following: the one-body part of the electronic Hamiltonian is treated at LDA level whereas a definite subset of correlated orbitals is treated with DMFT, in this manner the many-body effects, restricted to a small portion of the entire system, are fully taken into account by the numerics of the impurity solver.
The methodological advantages of this approach are conspicuous: by means of LDA one overcomes the limitations on real materials and the parameter dependence of model Hamiltonians with a realistic ab initio representation of the electronic structure. On the other hand the procedure of explicitly targeting the correlated orbitals degrees of freedom at DMFT level yields a great improvement over the approximation taken in using the Hartree-Fock static Coulomb repulsion as in LDA+U.
The crucial step in the implementation of the LDA+DMFT method relies in the explicit integration of the two schemes. The information about the entire system carried by LDA and embodied in the charge density has to be translated in the language of Green's function theory in order to carry on the DMFT numerical analysis. Practically, the course of action of this operation is twofold.
In the first place, the DMFT calculation has to be addressed to a limited set of correlated orbitals, therefore a mathematical tool has to be introduced in order

to represent the wave-function and all of the other variables of the entire system onto the degrees of freedom of this specific subset only. As it will be explained further on, the fulfilment of this task is not straightforward or free of ambiguities. Secondly, having two methods, each of them treating different orbitals of the system, brings an unavoidable consequence: some contributions in the properties of the materials are counted twice, beacause there is a portion of correlations that is already taken into account at DFT level by means of the exchange-correlation potential. Hence, a so called double-counting (DC) component has to be subtracted from the total energy of the system:

$$E_{\mathrm{TOT}} = E_{\mathrm{LDA}} + E_{\mathrm{DMFT}} - E_{\mathrm{DC}},$$

and since DFT is not suited to resolve the single orbitals of the system and LDA is not a well-controlled approximation, the estimation of this DC correction is indeed quite intricate.
Since its early development in the investigation of correlated paramagnetic compounds [4] the LDA+DMFT method proved to be a breakthrough in getting insights into the spectral and magnetic properties of a wide range of correlated materials, from transition metals to their oxides and rare earth compounds. Among these, the study of ferromagnetism in Fe together with the prediction of the satellite in Ni -6 eV (see Fig.3.4) as a Hubbard band in the majority-spin spectrum [68] or the analysis of Mott-Hubbard metal-insulator transition in V_2O_3 and the filling of the Mott-Hubbard gap at increasing temperature [42]. For a full review of LDA+DMFT accomplishments see [41, 62].

3.1.1.2 Limits and ambiguities of the method

Despite the great effectiveness on modelling strongly correlated materials this method suffers from ambiguities and limits that by now are widely recognized in the community.
The first concern is identifying mathematically the correlated orbitals object of the DMFT method, starting from the full space basis in which the Kohn-Sham eigenstates and eigenvalues of the converged DFT calculation are defined. This operation is complicated by the possible hybridization between the designated

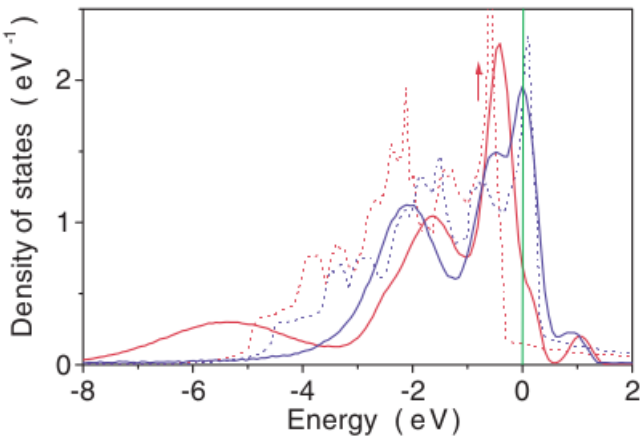

Figure 3.4: LDA+DMFT spin-resolved spectral function of Ni (solid lines) versus spin-polarized LDA (dotted lines). The majority spin channels are in red and the minority in blue. At -6 eV is clearly visible the satellite peak displayed by the majority spin channel. Image from [68].

correlated orbitals and the p orbitals, as it often occurs in oxides. When that is the case, a neat separation between the local atomic-like and the s, p-like physics is not allowed. The procedure of selecting the correlated orbitals either involves an operation of *downfolding* to a low energy model Hamiltonian, or a *projection* to a specific auxiliary complete basis set defining the Hilbert space of correlated orbitals, whose choice is somehow arbitrary. The difference between the two approaches is subtle and the relative credits object of debate, however the very choice of the basis set adopted plays an important role in accurately estimating the contribution of the correlated subset. Designing reliable mathematical tools to address this problem represents the main challenge of nowadays LDA+DMFT implementations.

A second concern regards what we can refer to as the "ab initio" nature of the full method. The constants entering the DMFT Anderson Hamiltonian, namely the Hubbard U and the Hund's coupling J, are originally introduced in the Hubbard model as effective parameters tuned by hand for the single orbital object of the study. If in the case of model Hamiltonians this picture is still reasonable, however in the analysis of real materials it gets rather naive. Focusing on the Hubbard U,

in solids this term takes the form of a general interaction parameter describing the interactions intra and inter sites and orbitals, and can be then considered an effective ad hoc counterpart of the screened Coulomb interaction W defined in the last chapter. Now, although formally U, J can be always determined from first-principles, as a matter of fact in common DMFT implementations these are usually tuned *ad hoc* for the material under study, and just recently the urge for a rigorous ab initio calculation of them have been addressed [100].
On a different note is the inclusion of the double-counting correction, which poses the main doubts towards the model. Several approaches have been proposed in the past years, among these the so-called *fully localized limit* has been widely used, under this assumption the DC energy reads:

$$E_{\mathrm{DC}} \coloneqq U(n_d - \frac{1}{2}) - J(\frac{n_d}{2} - \frac{1}{2}), \tag{3.17}$$

where the n_d is a parameter accounting for the occupation of the correlated subset and varying with respect to the material. Progress has been made in a more rigorous estimation of this factor (e.g. very recently in [37]), which however remains an evidence of a substantial discordance between the frameworks of the two theories.

3.2 Motivation for GW+DMFT: Need for a consistent framework

The case of the DC problem is indeed an exemplification of a wider and unavoidable limit of the LDA+DMFT formulation: not only do the two approaches have a different level of approximation and accuracy, but they are founded on different architectures and built around dissimilar central objects, namely the electron density and the Green's function. The two-points time-ordered function $G(1, 2)$ carries more information about the system than the degrees of freedom embodied in the one-point function $\rho(\mathbf{r})$. The choice of the electron density as the key object allowing to access the ground state properties of the system is the great advantage in terms of cost and simplicity of DFT, but with the clear drawback of

not being able to single out the different contributions from the multiple system components, such as the core from the valence states or the inner from the outer orbitals. Despite the great effort made towards a first-principles calculation of the Hubbard and Hund's parameters as well as the DC term, stronger and stronger is growing the suspicion that these open issues are intrinsic of the formulation itself.

Regardless on the ab initio character of the model, another problem arises from the fictitious character of the KS eigenfunctions and eigenvalues. As it has already been discussed at the end of Sec.2.1.3, the LDA results have a rigorous physical meaning if addressed only to extract ground state properties of the system, and not to excitation energies on which the photo-emission (or even inverse photo-emission) experiments such as ARPES are based. Comparing the LDA band-structure and density of states to the ARPES measurements is indeed partially justified strictly in presence of weak correlations only. Since the KS eigenstates are the starting point of any LDA+DMFT implementation, yielding the framework for the local correlated basis object of the DMFT loop, a sort of inconsistency comes into play.

It is to overcome these limits, as well as to refine the accuracy of the LDA+DMFT scheme, that a conjunction of DMFT with the GW approximation, or in other words a substitution of LDA with GWA in LDA+DMFT, in a so-called GW+DMFT method, was originally formulated by Biermann et al. [12].

As a first remark and as an intuitive motivation for this method, GW-based approaches are known to gain a significant improvement over LDA for an ab initio modelling on weakly correlated materials, in particular for what regards the band-structure of semiconductors (see Fig.2.7 as a reference). A considerable improvement in the starting point of a DMFT-based approach can severely affect the efficiency and the accuracy of the full calculation. The incentive towards the development of a GW+DMFT are however manifest if we focus on the fundamental aspects of the scheme.

Merging DMFT with GWA allows in the first place to work in the same framework of Green's function's theory, bypassing the difficulty of relating quantities expressed as density functionals with others being dependent on the Green's function instead. Furthermore, working in terms of the quasi-particle equation

(2.37), whose states and interactions, described in terms of the self-energy Σ, have a clear and univocal physical interpretation, allows to overcome the ambiguity of the fictitious KS eigenstates of the LDA framework when addressed to correlated orbitals.

The dynamically screened Coulomb interaction W calculated through RPA, distinctive feature of the GW methods, is of unique importance in the formulation of the GW+DMFT method. In the first place it replaces the bare Coulomb interaction v, which in the LDA starting point of any LDA+DMFT method is assumed to mediate the d-d and f-f interactions (as well as the interactions among all other orbitals) and it is known to generate convergence problems due to its long range action. Secondly, as we will clarify further on, the Hubbard constant U of the DMFT loop can be determined throughout the knowledge of W, by means of a partitioning of space in order to extract the component of W, called W_{rest}, relative to the degrees of freedom of the correlated subset (in a procedure similar to the analysis of [79]).

Finally, the double-counting problem can be rigorously addressed in GW+DMFT. The main advantage comes from substituting the exchange-correlation potential V_{xc} with the GW self-energy Σ. This function has a clear physical definition, it directly leads to the spectral function of the system, and it can be expanded through RPA diagrams in order to extract the contributions at different orders. More specifically, let us focus on the degrees of freedom of the correlated orbitals, which are treated at DMFT level by means of the fully local impurity self-energy. For what concern the GW contributions to these orbitals, one can in principle extract all the local components from the non-local self-energy in such a way to leave the field with no double counting components[1]:

$$\Sigma_{GW+DMFT}(\mathbf{k}, i\omega)_{LL'} \sim \Sigma^{\text{GW}}(\mathbf{k}, i\omega)_{LL'} - \sum_{\mathbf{k}} \Sigma^{\text{GW}}(\mathbf{k}, i\omega)_{LL'} + [\Sigma^{\text{imp}}(i\omega)]_{LL'},$$

where the subscripts LL' refer to the degrees of freedom of the correlated orbitals (typically the d- and f- shells).

In practice this operation is not completely trivial, however due to the non-

[1] the following equation is substantially equivalent to the one presented in the GW+DMFT formulation of [12].

locality of the GW self-energy and its flexibility, it is possible to extract and select its different components by means of a rigorous mathematical procedure, in such a way to approach the DC problem without the ambiguity of LDA-based approaches and in a first-principle fashion.
A GW+DMFT scheme is the object of this work of thesis and the next chapter will be devoted to give an detailed description of the method used. More specifically, We will present a novel QSGW+DMFT implementation for the study of strongly correlated materials.

Part II

My implementation: a QSGW+DMFT method

Chapter 4

Analytical implementation of the method

4.1 Connecting the full space to the correlated orbitals: Projectors

Any implementation involving DMFT merged with some electronic structure method (such as LDA or GW) has to face the conceptual challenge of identifying the local correlated subspace as the impurity of the problem. Speaking of "correlated orbitals", often referring to the d- and f- shells close to Fermi level, is physically justified just in an isolated atom or in any system with rotational symmetry. In complex molecules the d, f orbitals are in fact embedded in a medium composed of weakly correlated s, p orbitals, and in real materials there is often a significant overlap between different orbitals in such a way that the electrons are free to hop between one and another.

It is crucial to focus on the concept of *locality*. The main argument of DFT methods is that the exchange-correlation potential, describing the interaction between electrons, has a dependence with respect the charge density which is local in space, not changing much when moving along the material, a certainly reasonable assumption in weakly correlated materials. This is due to a strong screening of the Coulomb interaction that makes two electrons at different coordinates of the solid substantially uncorrelated. In strongly correlated materials this pic-

ture breaks down. Let us consider a generic oxide, and focus on its p-orbitals, a probing charged particle propagating in this region would experience a rather unperturbed charge density since the interaction between electrons is effectively screened. Hybridized with those orbitals are however regions where the propagation of a point charge will definitely affect and be affected by the surrounding electrons, which results in highly non-local interactions. It is customary to identify these regions with the correlated orbitals of DMFT, even if strictly speaking they do not correspond to the actual d, f orbitals of the isolated atoms. The assumption of full locality of the LDA exchange-correlation potential can be then replaced with a site-dependent locality of the DMFT impurity self-energy, where with "site" we mean the coordinates of the correlated subspaces.

Bearing this picture in mind, one needs to define an operation of *projection* and *embedding* capable of mapping the full space objects to the correlated orbitals subset and backwards.

Several definition of these operators as well as different techniques for the orbitals spanning the correlated subspace in LDA+DMFT and GW+DMFT methods have been proposed in the literature. Among these the maximally-localized Wannier orbitals have appealing mathematical properties and have been widely explored and efficiently employed in numerous cases [65, 74]. It is however convenient in our implementation to have basis functions which fully respect the symmetries of the problem and which are atom-centred, rather than bond-centred [39]. A very localized basis set is preferable for this scheme, for several reasons. In the first place the less localized the basis the more it contains of weakly correlated components (e.g. O-p states in MTO's). Too much population of the correlated subspace with uncorrelated parts conflicts with the physical interpretation of separation of bath and interacting subspace and it can then reduce the reliability of the method [36]. Moreover very localized basis functions have a much weaker energy-dependence, as a consequence with a very local projector it is possible to construct an effective interaction over a wide energy window, reducing the frequency-dependence of the effective interaction [19]. Finally very localized basis functions closely resemble atomic orbitals [19] and have a natural overlap with the correlated parts of the Hilbert space.

We adapted a procedure originally implemented in a DFT+DMFT formulation

within the LAPW basis [39] using the Wien2k package [13]. In this work the projection scheme is developed in the Full-Potential Linear Muffin-Tin Orbitals (FP-LMTO) basis of van Schilfgaarde and co-workers [76] and addressed to a QSGW+DMFT implementation.

Let us present the mathematical tools of this procedure: the projection operator $P^{LL'}_{ij\mathbf{k}}$ is a k-dependent 4-dimensional tensor mapping full space objects, expressed by the band and k-point label $\{i\mathbf{k}\}$, to the correlated subspace represented with the compact index $L \coloneqq \{\tau, R, \sigma, \ell, m\}$ which collects information on the atom of type τ at position R, the electron spin coordinate σ, and its angular momentum components ℓ and m.

In particular the lattice Green's function $G_{ij\mathbf{k}}$ can be mapped to its local correlated components $G^{\mathrm{loc}}_{LL'}$ by means of the *projection* operator:

$$G^{\mathrm{loc}}_{LL'} = \sum_{\mathbf{k},ij} P^{LL'}_{ij\mathbf{k}}\, G_{ij\mathbf{k}}\,. \tag{4.1}$$

On the other hand the impurity self-energy of DMFT, defined in the local subset, can be *embedded* onto a full space quantity by means of the operator $\hat{E}$:

$$\Sigma^{\mathrm{imp}}_{ij\mathbf{k}} = \sum_{LL'} E^{LL'}_{ij\mathbf{k}}\, \Sigma^{\mathrm{imp}}_{LL'}\,, \tag{4.2}$$

where the above sum is confined to the correlated subspace.

Several choices of the projection $\hat{P}$ and embedding $\hat{E}$ operators have been proposed in the literature, the arbitrariness of these choices poses a challenge. As pointed out in [39], the operators should be derived under the condition of satisfying some basic analytical and physical properties. Among the latter, of primary importance it is the conservation of spectral weight and the preservation of causality in DMFT equations. The first condition requires the local projected DOS to match the LDA-based (or GW-based) partial DOS for the chosen angular momentum. The second condition embodies the mathematical requirement for the impurity self-energy defined on a Matsubara mesh of frequencies to be non-positive: $\mathrm{Im}\,\Sigma_{\mathrm{imp}} \leq 0$.

Some of the analytical requirements originate from the mathematical relations between projection and embedding. The local correlated subset ideally defines a

Hilbert space which by definition is included in (or corresponds to) the Hilbert space representing the entire system. An operation of projection unavoidably implies a loss of information about the full system's properties. Therefore, a projection followed by an embedding will not result in the starting function: $\hat{E}\cdot\hat{P} \neq I$. The outcome is different for what regards the inverse operation, when embedding from the local to the full space and then projecting again no information about the local space is lost: $\hat{P}\cdot\hat{E} = I$.
In order to address these mathematical requirements, together with the condition of conservation of causality, it is convenient to take the projection operator in a separable form: $P^{LL'}_{ij\mathbf{k}} = U^{L}_{i\mathbf{k}} U^{L'\dagger}_{j\mathbf{k}}$, in such a way that eqs. (4.1,4.2) arrange as follows:

$$G^{\mathrm{loc}}_{LL'} = \sum_{\mathbf{k},ij} U^{L}_{i\mathbf{k}}\, G_{ij\mathbf{k}}\, U^{L'\dagger}_{j\mathbf{k}}, \tag{4.3a}$$

$$\Sigma^{\mathrm{imp}}_{ij\mathbf{k}} = \sum_{LL'} U^{L\dagger}_{i\mathbf{k}} \Sigma^{\mathrm{imp}}_{LL'} U^{L'}_{j\mathbf{k}}. \tag{4.3b}$$

The last of the previous set of equations shows how the embedding operation can be expressed by the same matrices defining the projection. This makes the relation between projection and embedding straightforward, even though this is not a general requirement of the theory. One could prove that any general projection operator cast in a separable form such as eqs.(4.3) automatically satisfies causality. See [39] for an analytic proof of this statement.

4.1.1 Projector within FP-LMTO basis

The explicit expression of the projection operator, and specifically of the U matrices, is related to the basis set chosen. In the original formulation of [39] the authors make use of the LAPW basis of the Wien2k package, and the full basis set is expressed in terms of Kohn-Sham states defining the LDA starting point. In this work the projection operation is extended to the QSGW quasi-particle eigenfunctions in the Full-Potential Linear Muffin-Tin Orbitals (FP-LMTO) set.

4.1.1.1 Introduction of the FP-LMTO basis

Making use of [61, 76] as a reference, and recalling sec.2.1.4 for an introduction of augmented wave methods, the eigenfunctions of our problem are expanded in linear combinations of linearized muffin-tin orbitals (LMTOs) $\chi^{\mathbf{k}}_{R\ell n}(\mathbf{r})$ with wave-vector $\mathbf{k}$ summed over Bloch states:

$$\psi_{i\mathbf{k}}(\mathbf{r}) = \sum_{Rln} z^{\mathbf{k}}_{R\ell n,i}\, \chi^{\mathbf{k}}_{R\ell n}(\mathbf{r}), \tag{4.4}$$

where the coefficient $z^{\mathbf{k}}_{R\ell n,i}$ are the QP eigenvectors, R identifies the site where the MTO is centred within the primitive cell and ℓ the angular momentum of the site. There can be multiple orbitals per $R\ell$ which are labelled by n. Inside the MT sphere the radial dependence of χ is captured by the combination of radial functions $\{\varphi^u_{R\ell}\}$. The meaning of the index u is the following: for $u = 1$ the function refers to $\varphi_{R\ell}$, radial solution of the Schrödinger equation inside the MTO at some fixed energy ϵ_ν, for $u = 2$ to its energy derivative $\dot{\varphi}_{R\ell}$, for $u = 2$ to its local orbitals $\varphi^z_{R\ell}$, which are solutions of the radial wave equation at energies well above or well below ϵ_ν. Outside of the MT, in the interstitial regions, the eigenfunction is represented by linear combinations of envelope functions consisting of smooth Hankel functions, which can be expanded in terms of plane waves. By means of this augmentation of space the eigenfunction in eq.(4.4) takes the following form:

$$\psi_{i\mathbf{k}}(\mathbf{r}) = \sum_{Ru} \mathcal{A}^{Lu}_{i\mathbf{k}} \varphi^{u\mathbf{k}}_{R\ell} + \sum_{\mathbf{G}} \beta^{\mathbf{k}i}_{\mathbf{G}} P^{\mathbf{k}}_{\mathbf{G}}(\mathbf{r}), \tag{4.5}$$

where the interstitial plane wave $P^{\mathbf{k}}_{\mathbf{G}}(\mathbf{r})$ is null inside the MT and equal to $e^{i(\mathbf{k}+\mathbf{G})\cdot\mathbf{r}}$ elsewhere, whereas the $\varphi^{u\mathbf{k}}_{R\ell}$ are intended as Bloch sums of $\varphi^u_{R\ell}$.

4.1.1.2 Definition and properties of U

Within the FP-LMTO basis the projection matrices read as follows

$$U^L_{i\mathbf{k}} = \sum_u \mathcal{A}^{Lu}_{i\mathbf{k}} \Phi^{u0}_{R\ell}\, S_{iL}, \quad \text{with} \quad S_{iL} = \sqrt{\frac{\sum_{uu'} \mathcal{A}^{Lu}_{i\mathbf{k}} \mathcal{A}^{Lu'*}_{i\mathbf{k}}\, \Phi^{uu'}_{R\ell}}{\sum_{uu'} \mathcal{A}^{Lu}_{i\mathbf{k}} \mathcal{A}^{Lu'*}_{i\mathbf{k}}\, \Phi^{u0}_{R\ell} \Phi^{0u'}_{R\ell}}}, \tag{4.6}$$

The index $L \coloneqq \{\tau, R, \sigma, \ell, m\}$ refers here to a correlated atom of type τ whose site R is the center of a corresponding MT, its electron spin coordinate being σ, and its angular momentum components ℓ and m. The band index i runs inside a specific energy window used to define the projection operation. The coefficients $\mathcal{A}^{Lu}_{i\mathbf{k}}$ account for localization inside the sphere, while $\Phi^{uu'}_{R\ell}$ gives an estimate of correlations relative to the specific orbital component ℓ. More specifically the coefficients $\mathcal{A}^{Lu}_{i\mathbf{k}}$, defined in eq.(4.5), are linear combinations of spherical harmonics $Y_{\ell m}$ and the QSGW quasi-particle eigenvectors $z^{\mathbf{k}}_{R\ell n,i}$ appearing in eq.(4.4), the $\mathcal{A}^{Lu}_{i\mathbf{k}}$ are derived by requiring the functions at the interstitial to match the radial functions at the MT boundaries. The terms $\Phi^{u}_{R\ell}$ are radial integral of the kind $\langle\varphi^{u}_{R\ell}|\varphi_{R\ell}\rangle$ where the $\varphi^{u}_{R\ell}$ are the group of radial functions of eq.(4.5). The coefficients S_{iL} are renormalizing factors correcting missing spectral weight.
The projection operator in (4.6) satisfies in fact both causality (by definition), and conservation of spectral weight, leading to the correct partial DOS. The cost of the renormalizing factors S_{iL} is dual [39]: in the first place the projector of (4.6) is not a proper projection operator in the sense of linear algebra since it does not strictly satisfy $P^2 = P$, and second, P is not fully local since the S_{iL} factors are weakly momentum-dependent.
In order to avoid a loss of spectral weight, any kind of transformation matrices has to satisfy the following orthonormality condition:

$$\sum_{i\mathbf{k}} U^{L}_{i\mathbf{k}} U^{L'\dagger}_{i\mathbf{k}} = \delta_{LL'}, \tag{4.7}$$

which in the language of standard quantum mechanics represents the resolution of the identity of the projection operators and it is a direct consequence of the completeness of the full Hilbert space basis.
As a matter of fact the projection operator in (4.6) fails to satisfy condition (4.7), which has to be superimposed on the matrices by means of an overlap operator:

$$O_{LL'} \coloneqq \sum_{i\mathbf{k}} U^{L}_{i\mathbf{k}} U^{L'\dagger}_{i\mathbf{k}} \;:\; U^{L}_{i\mathbf{k}} = O^{\frac{1}{2}}_{LL'} U^{L'}_{i\mathbf{k}}. \tag{4.8}$$

After this renormalization of the U matrices, the orthonormality condition expressed by (4.7) is automatically satisfied.

The orthonormality condition is also a requirement for the relation of identity between projection and embedding to stand:

$$\hat{P} \cdot \hat{E} = I \,. \tag{4.9}$$

A small digression on this subject is due. In order to prove analytically that an orthonormal projector always satisfies (4.9) a somewhat stronger orthonormality condition is required, through a k-dependent overlap matrix:

$$O_{LL',\mathbf{k}} \coloneqq \sum_i U^L_{i\mathbf{k}} U^{L'\dagger}_{i\mathbf{k}} \;:\; U^L_{i\mathbf{k}} = O^{\frac{1}{2}}_{LL',\mathbf{k}} U^{L'}_{i\mathbf{k}} \quad \text{such as} \quad \sum_i U^L_{i\mathbf{k}} U^{L'\dagger}_{i\mathbf{k}} = \delta_{LL'},\,.$$

By means of this condition, the automatic validity of (4.9) can be proved:

$$\begin{aligned}
\hat{P} \cdot [\hat{E} \cdot A^{\text{loc}}] &= \sum_{\mathbf{k},ij} U^L_{i\mathbf{k}} \left[\sum_{MM'} U^{M\dagger}_{i\mathbf{k}} A^{\text{loc}}_{MM'} U^{M'}_{j\mathbf{k}} \right] U^{L'\dagger}_{j\mathbf{k}} \\
&= \sum_{MM'} \sum_{\mathbf{k},ij} U^L_{i\mathbf{k}} U^{M\dagger}_{i\mathbf{k}} A^{\text{loc}}_{MM'} U^{M'}_{j\mathbf{k}} U^{L'\dagger}_{j\mathbf{k}} \\
&= \sum_{MM'} \sum_{\mathbf{k}} \sum_{i} U^L_{i\mathbf{k}} U^{M\dagger}_{i\mathbf{k}} A^{\text{loc}}_{MM'} \sum_{j} U^{M'}_{j\mathbf{k}} U^{L'\dagger}_{j\mathbf{k}} \\
&= \sum_{MM'} \delta_{LM} A^{\text{loc}}_{MM'} \delta_{L'M'} = A^{\text{loc}}_{LL'} \,,
\end{aligned}$$

where we exchanged the order of sums to make use of the k-wise normalization scheme. Such a procedure is legitimate but results in a non-local projection operation. As a matter of fact, despite the lack of an elegant analytic proof, condition (4.9) is satisfied numerically also for a local projector normalized such as in (4.7), and this is the choice we have made for our implementation.
On the other hand neither eq.(4.7) nor the k-wise orthonormality also imply $\hat{E} \cdot \hat{P} = I$, as it should be. This would require $\sum_L U^{L\dagger}_{i\mathbf{k}} U^L_{j\mathbf{k}} = \delta_{ij}$ which is not matched by our matrices.

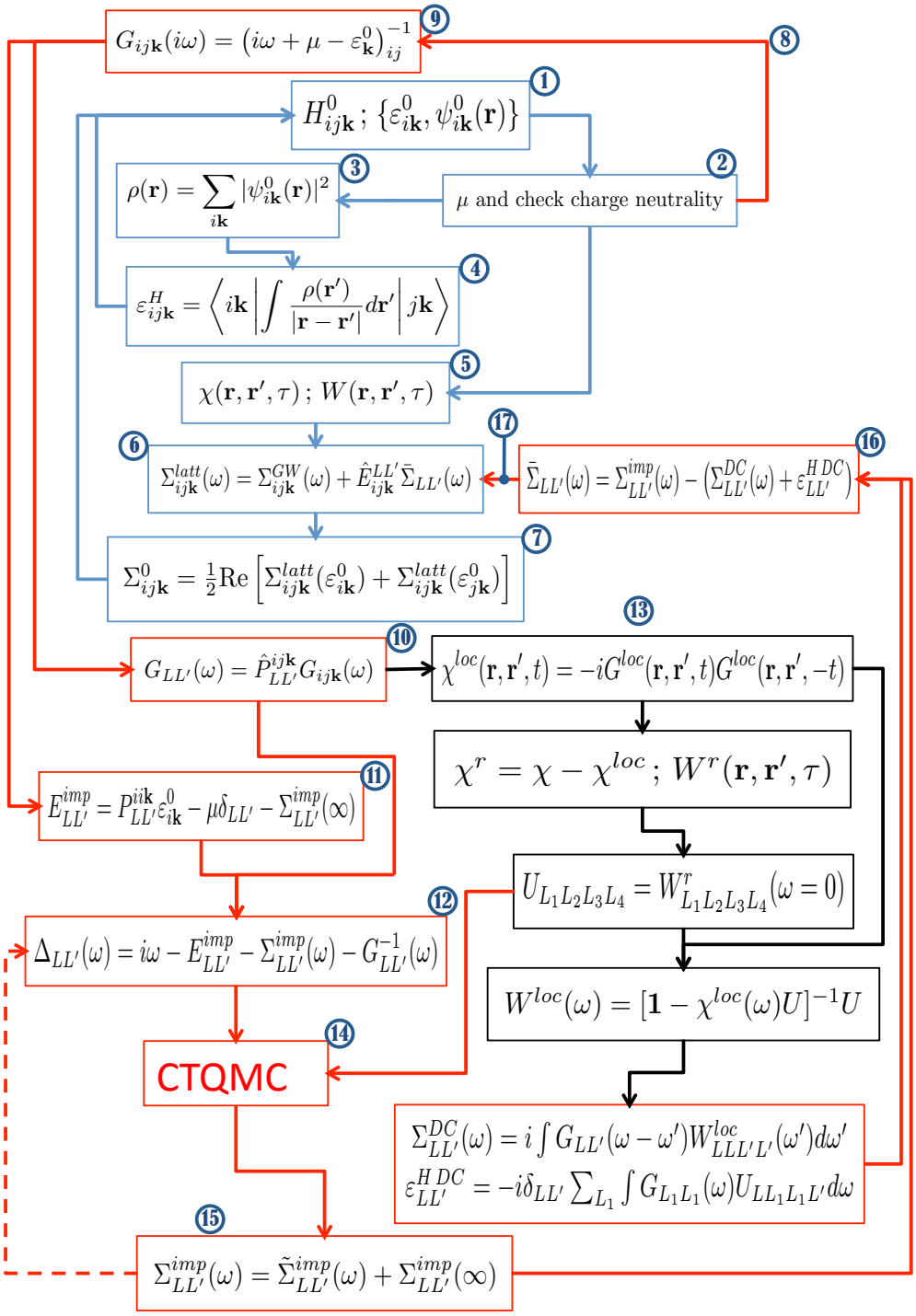

Figure 4.1: The full self-consistent QSGW+DMFT scheme. The red blocks represent the QSGW steps, the blue blocks the DMFT steps. The black blocks, covering an ab initio derivation of the Hubbard U, are not fully implemented yet.

4.2 Full self-consistent QSGW+DMFT scheme

Once the projection operators, building the bridge between full space objects (treated at QSGW level) and local correlated objects (treated at DMFT level), have been presented, we are finally able to depict an outline of the full self-consistent QSGW+DMFT scheme, the main goal of a project whose foundations are laid in this work of thesis. The full cycle is represented in the block diagram of Fig.4.1. The blue boxes indicate the steps of the QSGW loop, the red boxes the ones of the DMFT loop, and the black ones represent an ab initio derivation of the Hubbard U, singled out since their implementation is still a work in progress. We will now present the main stages of this procedure, referring on sections 2.3 and 3.1 for an introduction on the quantities into play belonging respectively to the GW and DMFT framework .

1. **Static (non-local) Hamiltonian:** The starting point is a static non-local Hamiltonian $H^0_{ij\mathbf{k}} = \langle i\mathbf{k}|H^0(\mathbf{r},\mathbf{r}')|j\mathbf{k}\rangle$ which can be diagonalized to return a set of eigenvalues $\varepsilon^0_{i\mathbf{k}}$ and eigenfunctions $\psi^0_{i\mathbf{k}}$. $H^0_{ij\mathbf{k}}$ can be a DFT Hamiltonian (intended as a first guess of the QSGW cycle) or it can be obtained from a full QSGW calculation.

2. **Chemical Potential:** In order to ensure neutrality in the system in every step of the calculation, the Fermi energy has to be correctly placed. The chemical potential is then computed from the set of eigenvalues $\varepsilon^0_{i\mathbf{k}}$. This step is extremely important at the end of the first iteration of the full cycle, when the full Green's function is updated with the local impurity self-energy. The adjustment is made under the condition of matching the chemical potential computed from the local Green's function with the one of the full lattice problem (sec. 4.4.3 will present the details of this procedure). After this step in principle one has all the information to enter the DMFT loop, otherwise a better convergence of the QSGW loop can be sought (the object of the next steps).

3. **Density:** The density $\rho(\mathbf{r})$ of the full system is computed from the eigen-

functions $\psi^0_{i\mathbf{k}}(\mathbf{r})$ by means of

$$\rho(\mathbf{r}) = \sum_{i\mathbf{k}} \left|\psi^0_{i\mathbf{k}}(\mathbf{r})\right|^2 .$$

4. **Hartree potential:** From the density one computes the Hartree energy,

$$\varepsilon^H_{ij\mathbf{k}} = \langle i\mathbf{k}| \int \frac{\rho(\mathbf{r}')}{|\mathbf{r}-\mathbf{r}'|} d\mathbf{r}' |j\mathbf{k}\rangle \,. \tag{4.10}$$

5. **Polarizability and Screened Coulomb interaction:** The irreducible Polarizability χ and the screened Coulomb interaction W of the lattice are evaluated under the random phase approximation (RPA),

$$\chi(\mathbf{r},\mathbf{r}',t) = -iG(\mathbf{r},\mathbf{r}',t)G(\mathbf{r}',\mathbf{r},-t)\,, \tag{4.11}$$

$$W(\mathbf{r},\mathbf{r}',t) = \int \left(\delta(\mathbf{r}-\mathbf{r}_1) - \int \frac{\chi(\mathbf{r}_2,\mathbf{r}_1,t)}{|\mathbf{r}-\mathbf{r}_2|} d\mathbf{r}_2\right)^{-1} \frac{1}{|\mathbf{r}_1-\mathbf{r}'|} d\mathbf{r}_1 \,. \tag{4.12}$$

6. **Lattice dynamical self-energy:** The dynamical self-energy of the lattice reads

$$\Sigma^{\text{latt}}_{ij\mathbf{k}}(\omega) = \Sigma^{GW}_{ij\mathbf{k}}(\omega) + \sum_{LL'} U^{L\dagger}_{i\mathbf{k}} \bar{\Sigma}_{LL'}(\omega) U^{L'}_{j\mathbf{k}} \,, \tag{4.13}$$

where $\Sigma^{GW}_{ij\mathbf{k}}(\omega)$ is the common GW self-energy calculated according to (2.44). The correction $\bar{\Sigma}_{LL'}$ is a local quantity originating from the DMFT loop and undergoes an operation of embedding using eq.(4.3b), it accounts for all diagrams beyond GW for the local correlated subset. It is obviously set to zero before the execution of the first DMFT cycle.

7. **Lattice static QSGW self-energy:** The dynamical lattice self-energy is quasi-particlized in the static QSGW self-energy using eq.(2.50):

$$\Sigma^0_{ij\mathbf{k}} = \frac{1}{2}\text{Re}\left[\Sigma^{\text{latt}}_{ij\mathbf{k}}(\varepsilon^0_{i\mathbf{k}}) + \Sigma^{\text{latt}}_{ij\mathbf{k}}(\varepsilon^0_{j\mathbf{k}})\right] \,, \tag{4.14}$$

which can be assumed as a static potential (equivalent to the exchange-correlation one) for an independent particle problem.

8. **End of QSGW loop:** The QSGW self-energy, together with the Hartree potential, can be employed to update the static hermitian non-local Hamiltonian $H^0_{ij\mathbf{k}}$ (going than back to step 1). The steps from 1 to 8 can be reiterated without passing through the DMFT loop until convergence. When the latter is reached, we can enter the DMFT loop.

9. **Lattice Green's function:** First step of the DMFT loop. The full lattice Green's function (which is adopted to update the GW self-energy at each stage of the QSGW loop) can be defined on a grid of Matsubara imaginary frequencies[1] $i\omega_n = i\pi(2n+1)/\beta$, β being the inverse temperature, such as

$$G_{ij\mathbf{k}}(\omega_n) = \left(i\omega_n + \mu - \varepsilon^0_{\mathbf{k}}\right)^{-1}_{ij} = \left(i\omega_n + \mu - \varepsilon^H_{\mathbf{k}} - \Sigma^0_{\mathbf{k}}\right)^{-1}_{ij}, \tag{4.15}$$

extracting the eigenvalues from the diagonalization of the updated Hamiltonian $H^0_{ij\mathbf{k}}$ (step 1) and the chemical potential μ (step 2).

10. **Local Green's function:** A local correlated subset (say, the $3d$ orbitals of Cu in a copper oxide) L is then identified and the projector operators $U^L_{i\mathbf{k}}$ calculated and normalized according to (4.6,4.8). The local Green's function is calculated by means of these projection operators using eq.(4.3a):

$$G^{\mathrm{loc}}_{LL'}(\omega_n) = \sum_{\mathbf{k},ij} U^L_{i\mathbf{k}}\, G_{ij\mathbf{k}}(\omega_n)\, U^{L'\dagger}_{j\mathbf{k}}. \tag{4.16}$$

When the DMFT convergence is reached this function is identified with the impurity Green's function in the well-known DMFT self-consistent relation:

$$\begin{aligned}\sum_{\mathbf{k},ij} U^L_{i\mathbf{k}} \left[i\omega_n + \mu - \varepsilon^H_{\mathbf{k}} - \Sigma^0_{\mathbf{k}}\right]^{-1}_{ij} U^{L'\dagger}_{j\mathbf{k}} = \\ = \left[i\omega_n - E^{\mathrm{imp}} - \Sigma^{\mathrm{imp}}(\omega_n) - \Delta(\omega_n)\right]^{-1}_{LL'} .\end{aligned} \tag{4.17}$$

11. **Impurity level:** The impurity level is a quantity extracted from the high-energy expansion of the self-consistent condition (4.17), on the requirement that the hybridization function approaches zero in the high-frequency limit.

[1] We will now use the subscript n when referring to Matsubara frequencies ω_n in order to distinguish them from real ones ω.

In the full self-consistent scheme it reads:

$$E^{\text{imp}}_{LL'} = \sum_{i\mathbf{k}} U^{L}_{i\mathbf{k}} \varepsilon^{0}_{i\mathbf{k}} U^{L'\dagger}_{i\mathbf{k}} - \mu\delta_{LL'} - \Sigma^{\text{imp}}_{LL'}(\infty)\,. \tag{4.18}$$

See appendix B for a derivation of the impurity level in the high-frequency limit.

12. Hybridization function: The Hybridization function defines the coupling between bath and impurity in DMFT, it represents the mapping from the local Green's function onto the Weiss field of the Anderson impurity model. It can be extracted from the right hand side of (4.17) in terms of the local Green's function and the impurity level from steps 10 and 11 and the impurity self-energy resulting from the impurity solver (step 18):

$$\Delta_{LL'}(\omega_n) = i\omega_n - E^{\text{imp}}_{LL'} - \Sigma^{\text{imp}}_{LL'}(\omega_n) - {G^{\text{loc}}_{LL'}}^{-1}(\omega_n)\,. \tag{4.19}$$

At the first iteration Σ^{imp} is set to zero.

13. Ab initio derivation of Hubbard U: This step is outlined in the black boxes of Fig.4.1, presenting the derivation of the static and dynamical components of the Hubbard U using cRPA. As mentioned already, it is still a work in progress of our implementation.
The starting point is the local irreducible polarizability χ^{loc}(local bubble diagrams) which can be extracted from the local Green's function G^{loc} (computed in step 10) by means of eq.(4.11). Consequently the polarizability of the rest of the system will be simply given within cRPA by $\chi^{\text{r}} = \chi - \chi^{\text{loc}}$ where χ is the quantity calculated in step 5. The screened Coulomb interaction W^{r}, which accounts for screening from the uncorrelated portion of the system, will be computed from χ^{r} by means of eq. (4.12). The cRPA formulation is commonly set in time τ and real space $\mathbf{r}$ basis, we preserved it when expressing eqs.(4.11,4.12) in order to lighten the notation and make the procedure easier to follow, even though there is no conceptual obstacle in carrying out these operations in any basis which is more convenient for us. To keep up with the chosen notation, in order to reconnect to the working

local basis a Fourier transformation and an integration with respect to the radial coordinates will allow to extract the screened frequency-dependent Coulomb interaction $U(\omega)$ from the time-dependent one:

$$U_{L_1L_2L_3L_4}(\omega) = \int \mathcal{F}^{\omega\ -1}_{L_1L_2L_3L_4}[W^r(\mathbf{r},\mathbf{r}',t)]d\mathbf{r}d\mathbf{r}'dt. \tag{4.20}$$

This dynamical screened interaction could be in principle used directly as a dynamical Hubbard $U(\omega)$ for the Anderson Impurity Model. This has in fact recently been accomplished [16, 17]. Such a method requires a Monte-Carlo solver capable of handling dynamical interactions, an algorithm which has been recently developed [106], but not in CTQMC solver developed by Haule, that we use here. Our implementation make use of the Continuous-Time Quantum Monte Carlo solver that handles static Hubbard interactions at all orders. The energy-dependence of U is strongly sensitive to the choice of projector, here we follow Haule's prescription and build the projector in a wide energy window. This strongly reduces the ω dependence of U [19], while introducing a different kind of error. In particular, because of the wide energy window, partial waves from tails of other orbitals (call them for simplicity p orbitals) are also removed from the screening, and should be included as part of the subspace to be treated in a many-body manner, with effective interactions U_{pd} and U_{pp}. However, these partial waves are not strongly correlated, and dealing with them at Hartree-Fock level is sufficient [36]. It is then necessary to calculate a static limit of $U(\omega)$.
Assuming a static interaction, our ab initio Hubbard U can be extracted from the static limit of eq.(4.20):

$$U_{L_1L_2L_3L_4} = W^r_{L_1L_2L_3L_4}(\omega=0) = \int \mathcal{F}^{0\ -1}_{L_1L_2L_3L_4}[W^r(\mathbf{r},\mathbf{r}',t)]d\mathbf{r}d\mathbf{r}'dt\ . \tag{4.21}$$

As an alternative, the Hubbard U parameter (together with the Hund's coupling J) can be chosen ad hoc for any material based on previous studies in the literature.

14. Impurity Solver: The (static) Hubbard interaction (4.21), the hybridization function (4.19), and the impurity energy (4.18) are the required input

to solve the Anderson impurity problem in the Continuous Time Quantum Monte Carlo (CTQMC) solver. As a result, a local dynamical impurity self-energy $\Sigma^{\text{imp}}_{LL'}(\omega_n)$ is generated. More specifically the Monte-Carlo data gives an accurate estimate of the low-frequency regions of the self-energy whereas it is known to being very noisy in the high-frequency regime. It is however crucial that Σ approaches its Hartree-Fock value for high-frequencies. With this goal, the high-energy tails are analytically corrected and concatenated with the Monte-Carlo sampling according to boundary conditions on value and slope. Details on the solver will be provided in the next chapter.

15. **Impurity self-energy:** The main output of the impurity solver is the local dynamical impurity self-energy (defined on the same mesh of Matsubara frequency of step 9,10 and 12):

$$\Sigma^{\text{imp}}_{LL'}(\omega_n) = \widetilde{\Sigma}^{\text{imp}}_{LL'}(\omega_n) + \Sigma^{\text{imp}}_{LL'}(\infty)\,. \tag{4.22}$$

We chose to explicitly split the frequency-dependent self-energy $\widetilde{\Sigma}^{\text{imp}}$ from its asymptotic limit $\Sigma^{\text{imp}}(\omega_n \to \infty)$ since this value is defined to be real and it can be directly used in the definition of the impurity level (see appendix B for details). This convention matches the definition of the impurity level (4.18) and the hybridization function (4.19).

16. **Accounting for Double-counting:** A DC correction has to be subtracted from the impurity self-energy before this quantity can be used to update the GW self-energy in eq. (4.13). The correction to the lattice self-energy coming from the impurity solver is meant to include all the local diagrams beyond the GW ones and nothing more. Consequently the DC term has to account for all the local GW diagrams and the local Hartree term.
The derivation of this DC correction can follow multiple choices subject to different degrees of approximation. An account of these choices will be extensively presented in sec. 4.4. For now we will refer to this term as $\Sigma^{\text{DC}}(\omega_n)$, whose frequency-dependence can be set to zero in some cases (depending on the choice). The correct impurity self-energy will be indicated

as

$$\bar{\Sigma}_{LL'}(\omega_n) = \Sigma^{\text{imp}}_{LL'}(\omega_n) - \Sigma^{DC}_{LL'}(\omega_n)\,, \tag{4.23}$$

and this is the quantity introduced in (4.13).

17. Analytic continuation: The introduction of Matsubara frequency in the DMFT stage is convenient when dealing with the real poles of the impurity Green's function and it is a necessary requirement of the CTQMC solver. The CTQMC provides in fact the Green's function at thermal equilibrium and the use of imaginary time is necessary to deal with thermal excitations (e.g. when involving spin fluctuations). The dynamical functions belonging to the QSGW loop, accounting for the full lattice, are however defined on the real frequency axis. When building a bridge between the two environments, i.e. when using the impurity self-energy to update the lattice one, we have to make use of an analytic continuation method in order to extract real-axis quantities from the Matsubara ones. Two methods are included in our implementation: the well known Maximum Entropy Method (MEM) [34] and the Stochastic Optimization Method (SOM) of A.S. Mishchenko [78]. In the MEM the most probable true solution $A(\omega)$ is selected among many possible particular solutions by assuming *a priori* the true solution to be close to a predefined function $D(\omega)$ called default model. In the SOM no a priori assumption is made about the solution but the true solution is obtained as an average of particular solutions A weighted by a so-called "likelihood" function.

18. Closing the DMFT loop: In order to achieve a finer result the DMFT loop can be repeated. This will require updating the local Green's function and the hybridization function with the impurity self-energy and re-iterating the procedure until convergence. This operation follows slightly different equations than the ones presented so far, they will be the object of next section. Once the DMFT loop is converged, the full self-consistent QSGW+DMFT loop can be closed. The impurity self-energy has to be analytically continued to the real axis and used to generate a new lattice self-energy (4.13) (step 6) and consequently a new static self-energy (4.14)

(step 7) that now accounts for a more accurate description of the local subset. A new Hamiltonian can be diagonalised (step 1) and the new chemical potential (step 2) can be correctly located. A new lattice Green's function with an updated impurity part can be projected into a local component and the DMFT loop can be reiterated (step 9) until a convergence is reached.

4.3 One-shot QSGW+DMFT scheme

The full self-consistent QSGW+DMFT cycle presented in the previous section is doubtlessly the most rigorous and accurate method to describe the electronic structure of composite strongly correlated materials as well as compound exhibiting unique magnetic properties. The cost in term of time and CPU resources of such an implementation is however considerable. Two are the main costly steps, belonging respectively to the QSGW and the DMFT loop. The first is the calculation at all energies of the GW self-energy that allows the quasi-particlization of the QSGW one, in particular during the construction of the polarizability. The second is the Monte-Carlo sampling of the impurity solver. Another hurdle comes from the analytic continuation method (the step 17 of the previous section). This operation, which has to be repeated for each stage of the full self-consistent loop, is often not trivial as well as computationally expensive.
For this reason we present in this section a simplified scheme, which we refer to as "one-shot QSGW+DMFT loop", whose cost is extensively reduced without, we trust, losing much in terms of accuracy. The idea is the following: being confident that the results of the converged QSGW cycle correctly account for the weakly correlated components (*sp*-physics), which are the predominant contributions to the electronic structure of the material, one seeks for a correction for the degrees of freedom of the local correlated subset only, which will be provided by an extensive DMFT loop. With "extensive" we mean that the DMFT step can be repeated several times (as it is customary in common DMFT implementations) refining the final results by re-updating the local Green's function and consequently the impurity self-energy until some convergence is reached. The final converged impurity self-energy is then directly employed to update the QSGW lattice Green's function in order to produce sensible results (such as the spectral function and

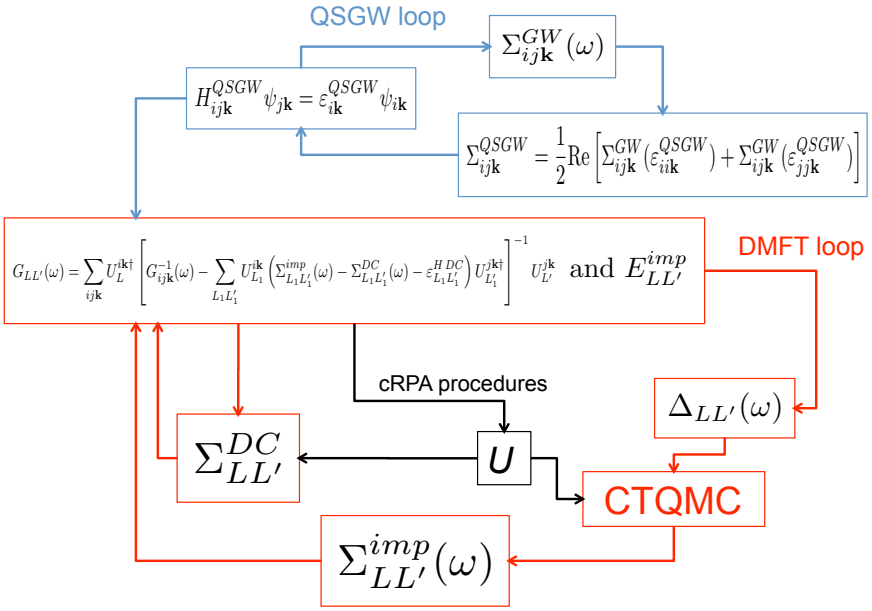

Figure 4.2: The one-shot QSGW+DMFT scheme. In this loop a converged QSGW calculation (blue blocks) provides the inputs to converge a DMFT loop (red blocks).

the band-structure of the material), without updating the QSGW Hamiltonian and re-entering the QSGW loop. As mentioned before, this reiterated extensive DMFT loop can be rightfully implemented also in the self-consistent scheme, however it involves slightly different equations that will be presented in details in this section.

The one-shot method lacks the self-consistency of the full loop, even though keeping in mind that the two approaches focus on distinguishable subspaces (responding to a different physics), the independent convergence of the two cycles can be considerate adequate enough at least for some materials. In addition to save time and resources in terms of numerical cost, another advantage of such implementation would come from avoiding several iterations of the analytic continuation procedure, which in the one-shot scheme is used only once in order to extract real-axis dynamical properties from the DMFT output. The one-shot QSGW+DMFT loop is outlined in Fig. 4.2.

Let us enter into the detail of the quantities into play in this scheme and the differences with the full one. The impurity self-energy does not enter the QSGW

loop as in eq. (4.13), once the QSGW iteration is converged the corresponding self-energy and Hamiltonian remain unchanged. In other words, referring to the steps of the full self-consistent loop of the previous section, in the one-shot loop the step 8 is then equivalent to step 1. We then enter the DMFT loop (red blocks of Fig. 4.2). At the first iteration of this cycle the impurity self-energy is null and the calculation follows the same steps (from 9 to 16) and equations as in the full scheme until an impurity self-energy is produced. At this point the second iteration of the DMFT loop starts: the impurity self-energy is now just employed to update the lattice Green's function (central block of Fig. 4.2), which corresponds to a jump from step 16 to step 9. This operation does not involve analytic continuation since both functions are defined on the imaginary axis. The lattice Green's function is updated as follows:

$$\begin{aligned} G_{ij\mathbf{k}}(\omega_n) &= \left(\left[i\omega_n + \mu - \varepsilon_{i\mathbf{k}}^{QSGW} \right] \delta_{ij} - \bar{\Sigma}_{ij\mathbf{k}}(\omega_n) \right)^{-1} \\ &= \left(G_{i\mathbf{k}}^{-1}(\omega_n)\delta_{ij} - \sum_{LL'} U_L^{i\mathbf{k}\dagger} \left[\Sigma_{LL'}^{\text{imp}}(\omega_n) - \Sigma_{LL'}^{DC}(\omega_n) \right] U_{L'}^{j\mathbf{k}} \right)^{-1}, \end{aligned} \tag{4.24}$$

expression that replaces eq. (4.15) in the step 9 of the full loop. In order to avoid confusion, we referred to $\varepsilon_{i\mathbf{k}}^{\text{QSGW}}$ as the eigenvalue of the QSGW Hamiltonian (see top left block of Fig. 4.2), which in this scheme is "frozen" since it is not updated after the QSGW loop is converged. This term is diagonal in the band index since the corresponding Schrödinger equation is diagonalized after the quasi-particlization of $\Sigma_{ij\mathbf{k}}^{\text{QSGW}}$. The reader will notice that the same embedding procedure applied to the impurity self-energy (scaled to the DC correction) which in eq. (4.13) was used to update the QSGW Hamiltonian is here employed to correct the lattice self-energy only in the definition of the Green's function. No quasi-particlization of the self-energy and diagonalization of the Hamiltonian follow the DMFT step, therefore after the first DMFT iteration the lattice self-energy (and consequently the Green's function) becomes non-diagonal. The lattice Green's function is then projected to its local counterpart equivalently to step 10 in eq. (4.16).

The impurity level (step 11) has a different definition with respect to the full scheme, the details of its derivation in the high-frequency limit for what regards

both schemes will be provided in appendix B. In the one-shot loop the impurity level reads

$$E^{\text{imp}}_{LL'} = \sum_{i\mathbf{k}} U^{i\mathbf{k}}_{L'} \varepsilon^{QSGW}_{i\mathbf{k}} U^{i\mathbf{k}\dagger}_{L'} - \Sigma^{DC}_{LL'}(\infty) - \mu\delta_{LL'} \ , \tag{4.25}$$

where $\Sigma^{DC}_{LL'}(\infty)$ is the DC correction in the high-frequency limit, which is trivially equal to $\Sigma^{DC}_{LL'}$ when this term is static. The DC correction of the one-shot scheme, appearing in eqs. (4.24) and (4.25), has a slightly different definition with respect to the full scheme, more details will be provided in the next section. After the impurity level is computed, the hybridization function is assembled according to eq. (4.19) (step 12) and a new impurity self-energy is obtained from the CTQMC impurity solver (steps 13-16). This DMFT loop can be reiterated until some convergence is reached and a converged $\Sigma^{\text{imp}}_{LL'}(\omega_n)$ is provided. At this point, an analytic continuation procedure as outlined in step 17 is required in order to extend impurity quantities to the real axis and to produce sensible results.
As a final remark it is worth to recapitulate that this entire extensive DMFT loop can be carried on also in the full self-consistent scheme (as mentioned in step 18) before updating the lattice self-energy. If in the full self-consistent loop this is a possible choice, in the one-shot scheme this procedure is instead necessary in order to achieve reasonable results.

4.4 Addressing the double-counting problem

One of the great advantages of GW+DMFT implementations is the specific and unambiguous definition of the double-counting correction when needed, and in some formulations even the possibility of avoiding DC contributions at all [12]. The reasons for this have already been outlined in sec. 3.2, regarding in the first place the two theories being set in up in the common framework on Green's functions theory and secondly the possibility to select the different contributions at different orders of a given perturbative expansion (since the GW self-energy is confined to RPA diagrams). In what follows we will present a scheme for a rigorous derivation of a dynamical DC term, which is still under implementation, as well as some practical alternatives in a form of a static approximation which have been tested and optimized.

4.4.1 Dynamical DC from static U

The main argument dictating the derivation of the DC term is the following: when updating the QSGW-based lattice self-energy $\Sigma^{\text{latt}}_{ij\mathbf{k}}$ with the local impurity self-energy $\Sigma^{\text{imp}}_{LL'}$ resulting from the solver, we want to retain all the work done by the QSGW loop, and add only local diagrams beyond GW. Therefore the local GW diagrams and the local Hartree contribution have to be subtracted from the impurity self-energy $\Sigma^{\text{imp}}_{LL'}$. It is then convenient to explicitly split the Hartree term, the static exchange term and the dynamical correlated term as we did in eq. (2.44) to express the GW self-energy, but in this case only working with the local Green's function and the Hubbard U (the screened interaction acting on the subsystem):

$$\varepsilon^{HDC}_{LL'} = -i\delta_{LL'} \sum_{L_1} \int G_{L_1L_1}(\omega) U_{LL_1L_1L'} d\omega \,, \tag{4.26a}$$

$$\Sigma^{DC}_{LL'}(\omega) = i \int G^{\text{loc}}_{LL'}(\omega - \omega') W^{\text{loc}}_{LLL'L'}(\omega') d\omega' \,, \tag{4.26b}$$

where for simplicity we have dropped the index n in ω_n to distinguish Matsubara frequencies from real ones since all the functions in (4.26) are defined on the imaginary axis. Eq. (4.26a) represents the local Hartree component, corresponding to the first term in (2.36), where the bare Coulomb interaction v has been substituted with the "effective" Hubbard interaction U which relates the electrons in the impurity and which is taken static in the formulae above. Eq. (4.26b) is instead the analogous of the exchange-correlation self-energy of (2.44), it incorporates both the static exchange term $\Sigma^{\text{loc}}_{\text{x}} \sim iGU$ and the dynamical correlated component $\Sigma^{\text{loc}}_{\text{c}} \sim iGW^{\text{loc}}_{\text{p}}$. The local component of the screen Coulomb interaction W^{loc} has been derived in analogy with the RPA expression of $W = (1 - v\chi)^{-1}v$, it reads[1]

$$W^{\text{loc}} := (1 - U\chi^{\text{loc}})^{-1}U = U + U\chi^{\text{loc}}(1 - U\chi^{\text{loc}})^{-1}U = U + W^{\text{loc}}_{\text{p}} \,, \tag{4.27}$$

where the local component of the irreducible polarizability χ^{loc}, which has been introduced in the step 13 of the full loop, has been used instead of the full one

[1] where to lighten the notation we have dropped the frequency-dependence of W^{loc} which in our implementation is entirely determined by χ^{loc}, which is dynamical.

entering (2.44). Since the Hubbard U is static in our implementation, both the expression in (4.26a) and the component in (4.26b) resulting from the U in the RHS of (4.27) are simple integrals over the frequency, therefore static. Conversely, the component in (4.26b) related to dynamical term $W_{\mathrm{p}}^{\mathrm{loc}}$ involves a convolution over frequencies and it is therefore energy-dependent[1].
It is worth stressing that eqs. (4.26) give a rigorous and unambiguous account of the dynamical DC correction as long as we are inside the full self-consistent loop, in such a way that the local GW diagrams can be extracted from the impurity self-energy (before the quasi-particlization of Σ) and then relating just dynamical quantities as in eq. (4.13). In the one-shot loop instead the DC correction entering eq. (4.24) does not have an analogous unambiguous definition and some approximation must be taken. Since only the one-shot loop has been extensively implemented and tested, the practical derivation of the dynamical DC of (4.26) is still a work in progress of our project.

4.4.2 Static approximations to DC

An intuitive static approximation for (4.26b) consists in taking the standard local projection of the QSGW self-energy (4.14) to the correlated subspace. A similar procedure can be then carried on for the Hartree term (4.26a) starting from (4.10). This would result in a local quantity by construction which can be directly related to the impurity self-energy and would bring by definition only the contributions from the RPA diagrams. The major drawback comes from the fact that QSGW substitutes the dynamical, non-hermitian Σ with an (optimally chosen) static, hermitian Σ^{QSGW} that cannot be expressed diagrammatically. Thus Σ^{QSGW} is not identical to the GW self-energy. This implies that there is no diagrammatic expansion allowing the unambiguous identification of doubled contributions. Our

[1] In the case of dynamical $U(\omega)$ obtained in cRPA, eq. (4.26a) would become a convolution and consequently $\epsilon^{H,DC}(\omega)$ would also depend on ω. Eq. (4.26b) would look the same but instead of $W^{\mathrm{loc}}(\omega')$ one should use the full $W(\omega')$

static DC reads

$$\varepsilon^{H\,DC}_{LL'} = \sum_{ij\mathbf{k}} U^{i\mathbf{k}\dagger}_{L'} \varepsilon^{H}_{ij\mathbf{k}} U^{j\mathbf{k}}_{L'} \tag{4.28a}$$

$$\widetilde{\Sigma}^{DC}_{LL'} \coloneqq \sum_{ij\mathbf{k}} U^{i\mathbf{k}\dagger}_{L'} \Sigma^{QSGW}_{ij\mathbf{k}} U^{j\mathbf{k}}_{L'} \,, \tag{4.28b}$$

where the sum of these two terms result in a static $\Sigma^{DC}_{LL'}$ to be employed in (4.24,4.25). A practical alternative for an approximated DC correction can be however found in the standard DC of (3.17) which is widely used in common LDA+DMFT implementations (such as the Wien2k-DMFT code of K.Haule [39]). The generalization of the Hartree and Fock terms are extracted according to

$$\varepsilon^{H\,DC}_{LL'} = U\left(n - \frac{1}{2}\right), \widetilde{\Sigma}^{DC}_{LL'} = J\left(\frac{n}{2} - \frac{1}{2}\right) , \tag{4.29}$$

where n is defined as the total occupation of the correlated subsystem (typically a parameter tuned with respect to the material under study).
The standard static approximation (4.29) of DC has been implemented and tested in the one-shot loop with encouraging results. The correction of eq.(4.28) instead has yet to be fully explored, even though it comes up as a natural choice when dealing directly with QSGW eigenvalues as in eq. (4.24). As mentioned already, in the full loop the dynamical DC of (4.26) would represent a better choice, but for the sake of an approximation these static corrections can otherwise be applied[1].
A reason of exploring the static corrections before implementing the dynamical DC comes from the necessity to optimize and test methods already in use in the community with a dual intent. In the first place to verify the reliability of the present implementation against similar calculations, and secondly to set up benchmarks against which we will compare the quality and the efficiency of the following methods and approximations to take.

[1] One can think of even another practical alternative for the full loop: taking the full dynamical $\Sigma^{GW}_{ij\mathbf{k}}(\omega)$ in place of $\Sigma^{QSGW}_{ij\mathbf{k}}$ in (4.28). The resulting dynamical term would stand as the most intuitive and feasible approximation for (4.26), accounting in principle for the same contributions (i.e. local Hartree + local GW diagrams).

4.4.3 Ensuring charge neutrality

A key step of the QSGW+DMFT implementation, either in the version of full or one-shot loop, is the conservation of the charge neutrality in every step of the calculation and in particular when updating the lattice Hamiltonian or the lattice Green's function with the DMFT insertion. The physical problem in both kinds of scheme is the following: a each stage of the loop an updated dynamical Hamiltonian sampled on a Matsubara mesh which reads

$$\bar{H}_{ij\mathbf{k}}(\omega_n) = \delta_{ij}\varepsilon_{i\mathbf{k}}^{QSGW} + \bar{\Sigma}_{ij\mathbf{k}}(\omega_n)\,, \tag{4.30}$$

has to be diagonalized for each frequency and k-point in order to extract some frequency-dependent eigenvalues from the static ones, this is expressed by the eigenvalue problem (for the right eigenvector C^{R}):

$$\sum_j \left[\delta_{ij}\varepsilon_{i\mathbf{k}}^{QSGW} + \bar{\Sigma}_{ij\mathbf{k}}(\omega_n)\right] C^{\mathrm{R}}_{jl\mathbf{k}}(\omega_n) = \varepsilon_{i\mathbf{k}}(\omega_n) C^{\mathrm{R}}_{il\mathbf{k}}(\omega_n)\,. \tag{4.31}$$

and similarly for the left eigenvector[1]. The corresponding electron count, extracted from these $\varepsilon_{i\mathbf{k}}(\omega_n)$, has to be kept constant to its original value, and this is accomplished by a small shift of the chemical potential μ. As customary in common electronic structure methods, a static correction potential V will be employed at each iteration to shift μ (whose value is instead fixed). We will outline the analytic procedure to ensure the conservation of charge neutrality.
In Solid State Physics the number of electrons N in a electronic system at equilibrium at temperature $T = (k_B\beta)^{-1}$ is given by

$$N = \sum_{\mathbf{k},i,\sigma} w_{\mathbf{k}} f_{i\mathbf{k}\sigma} = 2\sum_{\mathbf{k},i} w_{\mathbf{k}} f_{i\mathbf{k}}\,, \tag{4.32}$$

[1]When adding the non-hermitian function $\bar{\Sigma}$ to the Hermitian operator $H_{i\mathbf{k}}^{QSGW}$ we obtain a non-hermitian Hamiltonian $\bar{H}_{ij\mathbf{k}}$. Therefore eq.(4.31) is a non-hermitian eigenvalue problem for the right eigenvector only, the left is obtained by exchanging the order of operators.

where $w_{\mathbf{k}}$ is the k-point weight[1] and $f_{i\mathbf{k}\sigma} \coloneqq (e^{\beta(E_{i\mathbf{k}\sigma}-\mu)}+1)^{-1}$ is the Fermi-Dirac distribution, and where the last equality stands for a non-spin-polarized system. The single particle energies $E_{i\mathbf{k}\sigma}$ are assumed to be static and real. Therefore when handling complex and dynamical eigenvalues $\varepsilon_{i\mathbf{k}}(\omega_n)$ like in (4.31) we have to extend the electron number and the Fermi-Dirac distribution formulas. This can be done exploiting the relation between the Fermi-Dirac distribution and the Green's function (expressed in Matsubara frequencies representation):

$$f_{i\mathbf{k}} = \frac{1}{\beta}\sum_{n=-\infty}^{\infty} G_{i\mathbf{k}}(\omega_n) + \frac{1}{2} = \frac{1}{\beta}\sum_{n=-\infty}^{\infty} \frac{1}{i\omega_n + \mu - \varepsilon_{i\mathbf{k}}(\omega_n)} + \frac{1}{2}\,. \tag{4.33}$$

obtained as partial fraction decomposition (a Matsubara expansion in this case) in terms of the poles of the function, see [83] for more details. Given the following relations of parity satisfied by the eigenvalues:

$$\mathrm{Re}[\varepsilon_{i\mathbf{k}}(-\omega)] = \mathrm{Re}[\varepsilon_{i\mathbf{k}}(\omega)]\,, \quad \mathrm{Im}[\varepsilon_{i\mathbf{k}}(-\omega)] = -\,\mathrm{Im}[\varepsilon_{i\mathbf{k}}(\omega)]\,, \tag{4.34}$$

one can prove that only the real part of the expansion in (4.33) survives resulting in the real function $f_{i\mathbf{k}}$.

The practical numerical evaluation of expression (4.33) turns out not to be accurate even when very large frequency range is sampled. This is due to the fact that the analytic function $\mathrm{Re}[G(\omega)]$ is continuous in ω with a spike at $i\omega = 0$, therefore in the low energy range a very fine frequency sampling is required even though the $\omega_n = 0$ point is not typically included in the Matsubara set. Moreover, the closer $\varepsilon_{i\mathbf{k}}(\omega_n)$ is to μ, the sharper the spike is. This numerical can problem be overcome by subtracting and adding a trivial Green's function $G'(i\omega_n) = (i\omega_n - \xi')^{-1}$ crafted such as its energy levels ξ' are static and real. By means of this procedure

[1] This term is required just if a reduced k-point mesh is used (like in common implementations), otherwise it is equal to 1.

we obtain

$$\begin{aligned} f &= \frac{1}{\beta}\sum_{n=-\infty}^{\infty}\left(G(\omega_n)-G'(\omega_n)\right)+\left(\frac{1}{\beta}\sum_{n=-\infty}^{\infty}G'(\omega_n)+\frac{1}{2}\right) \\ &= \frac{1}{\beta}\sum_{n=-\infty}^{\infty}\left(\frac{1}{i\omega_n+\mu-\varepsilon(\omega_n)}-\frac{1}{i\omega_n-\xi'}\right)+f'\,, \end{aligned} \tag{4.35}$$

where we dropped the band and k-point indices to lighten the notation and the function f' is intended to indicate the standard Fermi-Dirac distribution (since the eigenvalues of $G'(\omega_n)$ are static and real). Relying again on (4.34), we can limit our study to the real part of the argument and the positive frequency points

$$f = \frac{2}{\beta}\sum_{n=0}^{\infty}\mathrm{Re}\left(\frac{1}{i\omega_n+\mu-\varepsilon(\omega_n)}-\frac{1}{i\omega_n-\xi'}\right)+f'\,, \tag{4.36}$$

and for a numerical evaluation of the above formula, a cut-off energy ω_M must be introduced: $\sum_n = \sum_{n=1}^{M}+\sum_{n=N+1}^{\infty}$. In order to evaluate the second term (high frequencies) the following assumptions are made: (i) we work in the low-temperature limit and (ii) we expect the eigenvalue to converge to a real constant in the high energy limit. This implies (i) that the interval $\Delta\omega = 2\pi/\beta$ tends to zero therefore the Matsubara frequencies collapse forming a continuous set along the imaginary axis: $\frac{2}{\beta}\sum_{n=M+1}^{\infty} = \frac{1}{\pi}\int_{\omega_M}^{\infty}d\omega$. Moreover, according to (ii) we take

$$\varepsilon(\omega) = \mathrm{Re}[\varepsilon(\omega_M)] = \varepsilon_M \;\forall\,\omega > \omega_M\,.$$

Under these two approximations the Fermi-Dirac distribution (4.36) reads

$$\begin{aligned} f = \frac{2}{\beta}\sum_{n=1}^{M}\mathrm{Re}\left(\frac{1}{i\omega_n+\mu-\varepsilon(\omega_n)}-\frac{1}{i\omega_n-\xi'}\right)+f'+ \\ -\frac{1}{\pi}\int_{\omega_M}^{\infty}\frac{\varepsilon_M-\mu}{\omega^2+(\varepsilon_M-\mu)^2}d\omega+\frac{1}{\pi}\int_{\omega_M}^{\infty}\frac{\xi'}{\omega^2+\xi'^2}d\omega\,. \end{aligned} \tag{4.37}$$

If $\varepsilon_M-\mu$ and ξ' are not zero, then both integrals can be computed analytically:

$$\int_a^{\infty}\frac{x}{\omega^2+x^2}d\omega = \arctan\left(\frac{x}{a}\right)\,. \tag{4.38}$$

By means of this expression we obtain

$$f = f' + \frac{2}{\beta}\sum_{n=1}^{M} \mathrm{Re}\left(\frac{1}{i\omega_n + \mu - \varepsilon(\omega_n)} - \frac{1}{i\omega_n - \xi'}\right) - \mathcal{B}(\varepsilon_M - \mu) + \mathcal{B}(\xi')\,, \quad (4.39)$$

where the function $\mathcal{B}$ has been introduced according to

$$\mathcal{B}(x) = \begin{cases} \frac{1}{\pi}\arctan\left(\frac{x}{\omega_M}\right) & \text{if} \quad x \neq 0\,, \\ 0 & \text{if} \quad x = 0\,. \end{cases} \quad (4.40)$$

Getting back to our original problem, we have to make sure that the electron count numerically extracted from the distribution (4.39) is kept constant at all stages of the calculation. Given a small shift V (a static correction) of our eigenvalues, we compute the electron count as a function of V and we adjust this correction in such a way to obtain our original total number of electrons.
The coefficients ξ' are set to a value which typically depends on the specific implementation and numerical procedure, in our formulation we set $\xi'_{i\mathbf{k}} = \epsilon_{i\mathbf{k}}(\omega_M) + V - \mu$ in such a way that the last two arctan terms in eq. (4.39) exactly cancel. By means of eq. (4.32) the electron number will be then given by the following expression

$$N(V) = \sum_{i\mathbf{k}\sigma} w_{\mathbf{k}} \left[f(\varepsilon_{i\mathbf{k}\sigma}(\omega_M) + V - \mu) + \right.$$
$$\left. + \frac{2}{\beta}\sum_{n=1}^{M} \mathrm{Re}\left(\frac{1}{i\omega_n + \mu - \varepsilon_{i\mathbf{k}\sigma}(\omega_n) - V} - \frac{1}{i\omega_n + \mu - \varepsilon_{i\mathbf{k}\sigma}(\omega_M) - V}\right)\right]\,, \quad (4.41)$$

the practical evaluation of which requires a diagonalization of the Hamiltonian at all frequencies (lower than ω_M) for each value of V. Calling N^0 the reference electron number, tuning the electron count to the correct value corresponds to find the root of $N(V) - N^0$. For this outcome, it is convenient to evaluate the

derivative of expression (4.41) with respect to V, one gets

$$\frac{dN(V)}{dV} = \sum_{i\mathbf{k}\sigma} w_{\mathbf{k}} \left[-\frac{\beta \exp\{\beta(\varepsilon_{i\mathbf{k}\sigma}(\omega_M) + V - \mu)\}}{(1 + \exp\{\beta(\varepsilon_{i\mathbf{k}\sigma}(\omega_M) + V - \mu)\})^2} + \right. \\ \left. + \frac{2}{\beta} \sum_{n=1}^{M} \mathrm{Re} \left(\frac{1}{(i\omega_n + \mu - \varepsilon_{i\mathbf{k}\sigma}(\omega_n) - V)^2} - \frac{1}{(\omega_n + \mu - \varepsilon_{i\mathbf{k}\sigma}(\omega_M) - V)^2} \right) \right] \tag{4.42}$$

where we used $f(x) = 1/(1 + e^{x\beta})$ for the Fermi function.

DMFT electronic density

Once a reliable algorithm has been developed, we can use the same scheme in order to evaluate the electronic density from the DMFT results and update the value computed at QSGW level (in step 3 of the full self-consistent loop) by means of a more consistent estimation.

Let us focus again on eq. (4.31), which is a non-hermitian eigenvalue problem in terms of the right eigenvector C^{R}, where the left and right eigenvectors are not complex conjugates of each other. Following the formulation of [39] we can define some non-hermitian DMFT eigenvectors from the set of eigenvectors C^{R} of (4.31) and the FP-LMTO quasi-particle eigenfunctions $\psi_{i\mathbf{k}}(\mathbf{r})$ of (4.4), this would result in a composite eigenfunction capturing both QSGW and DMFT physics:

$$\psi^{\mathrm{R}}_{i\mathbf{k}\omega}(\mathbf{r}) := \sum_j \psi_{j\mathbf{k}}(\mathbf{r}) C^{\mathrm{R}}_{ji\mathbf{k}}(\omega_n)\,, \tag{4.43}$$

and equivalently for the left eigenvector ψ^{R}, where the frequency dependence has been incorporated by means of an additional index. The DMFT electronic charge can be then defined as:

$$\rho^{\mathrm{DMFT}}(\mathbf{r}) := \sum_{\mathbf{k}in} \psi^{\mathrm{R}}_{i\mathbf{k}\omega}(\mathbf{r}) \left[\frac{1}{i\omega_n + \mu - \varepsilon_{i\mathbf{k}}(\omega_n)} + \frac{1}{2} \right] \psi^{\mathrm{L}}_{i\mathbf{k}\omega}(\mathbf{r})\,, \tag{4.44}$$

which has been extracted from the expression (4.33) of the Fermi-Dirac distribution function. From the analogy with the expression of the electronic charge we notice that we can use the same algorithm resulting in eq. (4.41) to evaluate the

DMFT electronic charge, with the insertion of the right and left DMFT eigenvectors as in eq. (4.44). Once the algorithm is refined this result can be considered a more reliable estimation of the total charge density after the DMFT loop.
In addition, exploiting the definition of the FP-LMTO eigenfunctions in (4.4) and the definition (4.44) we are then able to select the contribution to the charge density relative to a specific set orbitals (e.g. gaining the ability of singling out the degrees of freedom of a specific angular momentum).

Chapter 5

Practical implementation: overview of the codes

We will now present an outline of the programs of this implementation. Building an interface between the QSGW package and the CTQMC solver, where the DMFT main quantities of reference (in particular the hybridization function and local correlated Green's function) are extracted from the results of the QSGW converged calculation and translated into the language of DMFT by means of the projection and embedding operators, has been the main accomplishment of this work of thesis.

The first tangible result is a novel QSGW+DMFT implementation, in the preliminary version of the one-shot loop (see sec.4.3). This method has been tested, optimised and addressed to the study of different materials (see next chapter for an account of the corresponding results). As a prospective outcome to be evaluated in the long-term, a more advanced - in the form of the full self-consistent scheme - ab initio method - with the derivation of the Hubbard parameters from first principles - which is currently under development, will be completed holding the grounds from the present one. New promising features will be integrated (from a rigorous DC correction to the inclusion of ladder diagrams) as well as tools to improve the efficiency of the scheme (such as exploiting the symmetries of the problem and upgrading the parallelization of the main routines).

A simple flowchart with the key packages and routine involved in the one-shot

QSGW+DMFT loop is presented in Fig. 5.1.

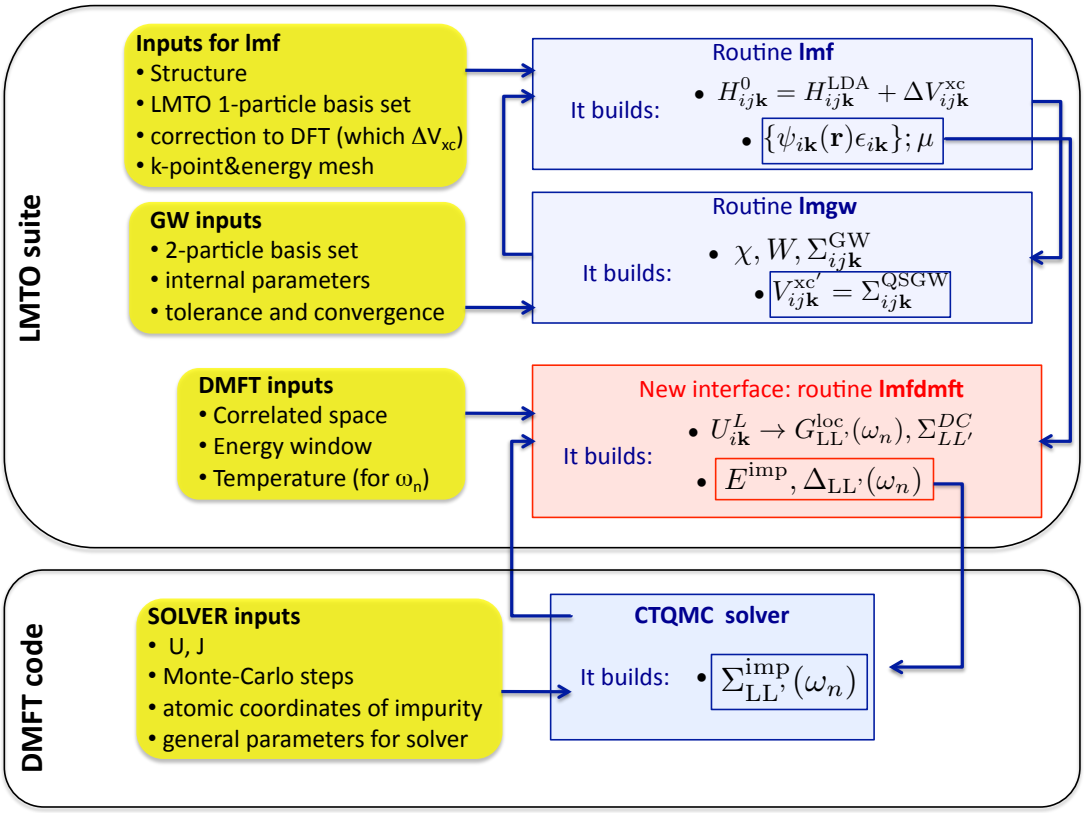

Figure 5.1: The flowchart of the main routines of the present QSGW+DMFT implementation. The new interface (lmfdmft routine) has been singled out in a red box. This interface connects the main LMTO suite package to the CTQMC solver of DMFT.

5.1 QSGW package

The QSGW calculation is implemented in the LMTO suite, a composite package (written by Mark van Schilfgaarde and collaborators) which is a collection of electronic structure codes based mostly on the local-density approximation (LDA) to density-functional theory (DFT) to solids. The specific DFT implementation

is an all-electron kind, where both core and valence electrons are accounted for (with different weights) at all stages of the calculation. A unique feature of the package is the basis set used, composed of atom centred functions (LMTO basis) rather than the more commonly used augmented plane wave basis, however with the augmentation carried out so to resemble the APW method. This has the advantage that basis sets are much smaller for a given level of accuracy, but it also requires somewhat more knowledge for the user to operate [99]. For more details on the augmented wave methods, see secs.2.1.4.

Another peculiar feature is the connection to implementation for GW calculations, in the all-electron framework. GW is implemented as an extension to the LDA, i.e. G and W are generated from the LDA. Therefore the package can be used for LDA-based GW calculations, but it also implements the Quasiparticle Self-consistent GW approximation (QSGW). QSGW may be thought of as an optimised form of the GW approximation, and being vastly superior to ordinary GW, it is much more demanding computationally. We refer again on section 2.3 for more details about the GW methods involved.

The LDA-based programs of the LMTO suite can be used to probe for a variety of physical properties, such as the energy bands, density-of-states (DOS), optical properties, magnetic exchange interactions [99].

The core of the QSGW+DMFT implementation inside the LMTO suite is the all-electron full-potential code called *lmf*, which is synchronised with the GW code through a driver called *lmf2gw*, based on lmf. We implemented a new driver called *lmfdmft*, also based on lmf, that coordinates with Haule's CTQMC package. The QSGW+DMFT scheme is based on three packages: CTQMC, QSGW, and the lmf-based family with their interfaces that must be linked together (presented in the next section).

5.1.1 Full-potential all-electron code lmf

The lmf driver is represented in the top block of Fig. 5.1 inside the main box of the LMTO suite. The full-potential package is somewhat different from conventional formulations of standard all-electron implementations in the LMTO basis in several respects.

1. The augmentation is done differently [76]. The charge density is represented in 3-fold manner: an interstitial density which extends everywhere in space, the true local density centred at each augmentation sphere, and a local representation of the interstitial density in the same form as the local density. With such a construction, the electronic structure converges much more rapidly with L than in conventional LAPW and LMTO implementations.
2. The envelope functions are smoothed generalizations of the conventional Hankel functions defined by the LMTO method. They are convolutions of Gaussian orbitals and Hankel functions, which adds flexibility to the basis function and improves the quality of the basis. They are a significantly better choice of basis than the customary LMTO basis set. However, the smoothing introduces complications because the augmentation of a smoothed Hankel function is less straightforward than of a normal Hankel [99]. In addition, there is also a capability to add APWs as additional envelope functions [60], which can increase the flexibility of the basis.

This package extends the linear method through the use of local orbitals. Augmented methods substitute radial solutions of the Schrödinger equation with combinations of partial waves of angular quantum number ℓ inside the augmentation region. Linear methods used a fixed radial function (more precisely, pair of functions), which has validity over only a certain energy window. With local orbitals, a third radial function is added to the basis, which greatly extends the energy window over which energy eigenvalues can be calculated [99].

The program lmf can generate: DOS and partial DOS within augmentation spheres, total energy, energy bands and charge density. An LDA+U functional (where the parameters U and J for selected orbitals are empirical) and the Spin-Orbit coupling are among the other capabilities of the package.

In addition, lmf is designed to work in coordination with a GW package by T. Kotani, lmf acts both as a driver for the GW package and also can be used in a self-consistent GW cycle. The GW calculation is implemented in a extra driver called *lmfgw*. As an option of the routine lmf additionally reads the static self-energy as generated by the QSGW implementation of the GW code. This enables lmf to do the same kinds of calculations as it performs with the LDA potential, but substituting the QSGW self-energy for the exchange-correlation potential.

5.1.2 GW driver lmgw

The GW driver package contains an executable lmfgwd, which acts to set up input needed by the GW package. Its structure is similar to lmf but its function is to supply eigenfunctions and eigenvalues, matrix elements of the LDA potential to the GW package. The executable lmfgwd works either with standard one-shot GW and QSGW. The GW codes that work with lmfgwd also have a feedback to lmf and lmfgwd, to implement QSGW. In the QSGW mode, a (static, hermitian) self-energy Σ is generated in a file which contains matrix elements of Σ in the basis used to generate it. When placed into file *sigm.ext* the full-potential program lmf and the GW driver lmfgwd read this potential and add it as an additional (static) potential to the LDA potential [99].
Independent from lmfgwd is lmgw (see centre-right block of Fig. 5.1), a multipurpose script that exercises the GW codes in many kinds of modes; in particular it can be used in one-shot or self-consistent GW calculations (including QSGW), depending on the flags used. In the one-shot GW loop, the QP energies are generated as the results of a one-shot perturbation theory over the LDA inputs (eigenfunctions and exchange-correlation potential). We now arrive at the QSGW implementation. Within the self-consistent loop, the convergence is checked by monitoring the RMS change of Σ the iterations are stopped when a certain tolerance is met. The self-energy Σ^{QSGW} is generated by the GW package on a mesh of points in the irreducible Brillouin zone (BZ). The quantity $\Delta V^{\mathrm{xc}} := \Sigma^{\mathrm{QSGW}} - V^{\mathrm{xc}}$ is stored in the file *sigm.ext*, it can be read by lmf and lmfgwd, and added to the LDA one-particle potential, so to cancel V^{xc}. When reading this file the self-energy is rotated to the entire BZ and then inverse Fourier (Bloch) transformed into a real-space form. It can be then computed at any k-point, so lmf can work in the just the same way in using a QSGW potential as it does an LDA potential. This is a crucial advantage of the present implementation. The drivers lmgw and lmf coordinate self-consistently until convergence and the corresponding QP eigenvalues and spectral functions for a specified list of k-points and QP levels.

5.1.3 Interface to DMFT: lmfdmft

As a novel implementation of the LMTO suite, we have built an interface between the QSGW driver and the CTQMC solver, capable of extracting the DMFT quantities of reference from the results of the QSGW loop, feed them to the impurity solver, and extract the result from the latter in order to reiterate the loop. This interface is built inside the lmf package and it aggregates several routines in the *lmfdmft* driver (see red centre block of Fig. 5.1).
The preliminary achievement of lmfdmft is the calculation of the projection operators within the FP-LMTO basis from the QP eigenvectors generated by the lmgw driver. In order to generate the projection matrices, an input file (called *indmfl.ext*) must be supplied with information about which correlated orbitals to select in the compound (e.g. $3d$ orbitals of Cu), the energy window for the band representation, the transformation matrices relative to the orbital basis chosen (e.g. spherical or cubic harmonics), the Hubbard parameters U, J entering the static approximation of the DC term, and finally the temperature $T = 1/\beta$, value that will be used to generate the mesh of Matsubara frequencies $i\omega_n \coloneqq i(2n+1)\pi/\beta$. Once the projection operators are calculated and orthonormalized, the local correlated quantities can be then generated, in particular the Green's function $G^{\mathrm{loc}}_{LL'}(\omega_n)$, the DC correction $\Sigma^{\mathrm{DC}}_{LL'}$ and the impurity level $E^{\mathrm{imp}}_{LL'}$. The lmfdmft driver coordinates with the CTQMC code which supplies the impurity self-energy $\Sigma^{\mathrm{imp}}_{LL'}(\omega_n)$ (scaled to the DC term) starting from the second iteration (null at the first iteration). Finally the hybridization function $\Delta_{LL'}(\omega_n)$ is produced and written to a file called *Delta.inp* which is sent to the CTQMC solver together with the file for the impurity level (*Eimp.inp*) and the other parameters (e.g. U, J, β).

5.2 CTQMC solver

The Continuous-Time Quantum Monte Carlo (CTQMC) solver is one of the main drivers belonging to the Wien2k-DMFT code mainly written by Kristjan Haule [39]. In this package the CTQMC coordinates with the other routines to implement a self-consistent LDA+DMFT loop, with the LDA part carried on

by the Wien2k code [13]. The accomplishment of this work of thesis, by means of the lmfdmft interface, was to isolate the CTQMC solver in order to work in connection with the LMTO suite in a QSGW+DMFT implementation.
The CTQMC method relies in expanding perturbatively the partition function Z of the Anderson Impurity Model (see appendix A for a definition of this quantity) in terms of powers of the hybridization function Δ while treating the interactions exactly. The corresponding diagrams are summed up by stochastic Metropolis-Hasting sampling [105]. This approach is extremely powerful at strong interactions (important for system of interests such as high-Tc cuprates), because the perturbation order actually decreases with increasing U. Moreover, this method allows insight to very low temperatures, providing new information unavailable by other methods [105].
In practice the CTQMC code is implemented in one single main routine which, due to the stochastic nature of the method, has been highly parallelized and requires a high number of steps to converge (depending on the case and the parameters used from 20 to 30 iterations). The code requires as an input the hybridization function and the impurity level (written respectively in the files Delta.inp and Eimp.inp) as well as two other input files: *PARAMS* and *actqmc.cix*. The file *PARAMS* stores parameters regarding the Monte-Carlo sampling, the number of iterations, the number of cores for the parallelization as well as physical quantities such as the temperature and the chemical potential of the full system. The file *actqmc.cix* is instead generated by the python script *atom_d.py* and has information about the impurity: atomic eigenvalues and eigenfunctions, and the Coulomb interaction U which is rotated the same harmonics basis of the hybridization function.
The Monte-Carlo sampling accurately accounts for the low frequency region of the self-energy, whereas it is known to be extremely noisy for the high-frequency regime. In order for the self-energy to approach its Hartree-Fock value in the high-energy limit, the high-frequency tails are analytically corrected and concatenated with the Monte-Carlo sampling according to boundary conditions on value and slope. The CTQMC code make use of the Hubbard I approximation for the tails.
The resulting impurity self-energy $\Sigma^{\mathrm{imp}}_{LL'}(\omega_n)$ is expressed in the same Matsubara

frequency mesh and correlated orbitals basis as the input hybridization function. The impurity self-energy is written to the file Sig.out. Inside the interface lmfdmft, this self-energy is then treated with a Gaussian broadening in order to reduce the Monte-Carlo noise and finally scaled with respect to the DC correction. At this point it can be used in the interface to correct the DMFT quantities and produce an updated hybridization function for a new iteration of the loop.

Part III

Application to materials and results

Chapter 6

Electronic Structure of La_2CuO_4

In what follows we will present an outline of the main results obtained within the present stage of the QSGW+DMFT implementation. It is worth stressing that the project of marrying QSGW and DMFT in a consistent manner is obviously a large-scale effort. The results presented in this work of thesis must be assessed as an early stage accomplishment, whereas the effort has been mostly addressed to the understanding and development of the method and to build the code architecture. We are confident that this achievement will lead the way to the complete refinement of the scheme in order to undertake the study of the most challenging materials.

The benchmark material that was first investigated is La_2CuO_4, a cuprate compound displaying high-temperature superconductivity [25, 66]. Cuprate high temperature superconductors have raised a growing interest [20] in the electronic-structure community in the past decades due to their peculiar phase-diagram and in particular the insulating-superconductor transition. The unusual properties of these materials are universally identified as a consequence of the strong correlations between electrons and many-body phenomena [38, 103, 104], since their behaviour is hard to explain by means of band-structure calculations inherent to independent-electron approximations (we will go back to this further on). Superconductivity is typically obtained by doping the cuprate, hence adding carriers to the parent compound [104]. The undoped parent materials are typically (it is the case of La_2CuO_4) charge-transfer (or Mott) insulators, exhibiting anti-ferromagnetic long-range order in the ground state [70]. Whether the su-

perconductivity is directly related to this magnetic ordering or rather to strong electronic correlations (as typically the case in Mott insulators) is still an object of debate [20]. It is commonly accepted that the physics of these materials (e.g. the superconducting state) is mainly "2-dimensional", i.e. largely determined by the hybridization of the Cu-$d_{x^2-y^2}$ states with the O-p_x, p_y states within the CuO_2 planes [25, 70].

Although its incomplete d band would classify La_2CuO_4 as metal, experimentally this cuprate emerges as an insulator [21, 32]. It has been therefore designated as a Mott insulator [3] or rather as a charge-transfer insulator [38]. LDA methods have failed to reproduce a gap for this material [19, 108] predicting a metallic state both in non spin-polarized and spin-polarized configuration. It was recently established [19] that more advanced methods such as scGW are unable to open a gap, at least in the non-magnetic state, whereas in the anti-ferromagnetic state the insulating gap is reproduced but quite overestimated.

By means of LDA+DMFT studies of this compound an insulating gap was found [103] both in the para-magnetic[1] and anti-ferromagnetic state where the size of the gap is only slightly increased when magnetic ordering is present, suggesting the magnetic long-range order is not the main responsible for the nature of charge-transfer insulator [38, 104], even if this claim is a subject of debate [20].

In this chapter we will show the results obtained for the total density of states, projected density of states and band-structure of this compound. In the first place these results will confirm the predictions in the literature just mentioned in order to verify the reliability of our implementation against similar calculations. Secondly, we will present a preliminary evidence that by means of a QSGW+DMFT scheme one is able to make the best of each theory.

6.1 DFT and QSGW electronic structure

The atomic structure of La_2CuO_4 for the non-magnetic (NM) and anti-ferromagnetic (AFM) phase respectively are represented in Figs.6.1,6.2.

[1] An important distinction is due. For what regards the LDA and QSGW methods we refer to a *non-magnetic* state, meaning that the spin degrees of freedom are neglected. On the other hand DMFT (and CPA) methods have the ability to configurationally average up- and down-states on one site, representing a true *para-magnetic* configuration.

(a) Unit cell

(b) Brillouin zone

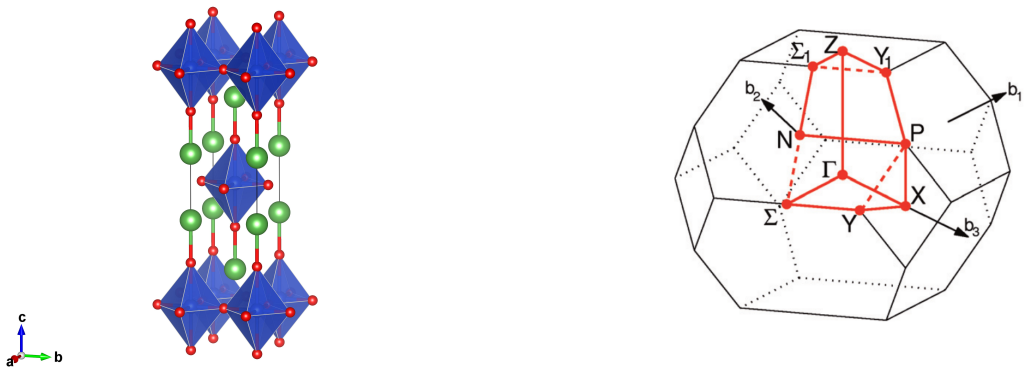

Figure 6.1: Left: body-centred tetragonal unit cell of the crystal structure of La_2CuO_4 in the NM phase (single cell). Lanthanum atoms are represented by green spheres, copper atoms by blue spheres in the blue octahedrons, and oxygen atoms by red spheres. Right: first Brillouin zone of body-centred tetragonal phase (image taken from [89]).

In order to describe the NM phase one can make use of a single unit cell, it has a body-centred tetragonal structure represented in Fig.6.1a with the following lattice vectors: $a_1 = (a, 0, 0)$, $a_2 = (0, a, 0)$, $a_3 = (0, 0, c)$ and lattice constants $a = 3.79$ $\mathring{A}$, $c = 13.13$ $\mathring{A}$. For the AFM ordering two categories of copper atoms must be introduced (with spin up and spin down configurations) and one needs to double the unit cell. By means of this procedure one obtains the single face-centred orthorhombic structure of Fig.6.2a. The AFM ordering induces a distortion in the position of the CuO_6 octahedra that get alternatively rotated along the x-direction. The lattice constants for the double cell become $a' = \sqrt{2}a = 5.35$ $\mathring{A}$, $c' = c = 13.13$ $\mathring{A}$.

The first Brillouin zone for the NM and AFM phase corresponding to the given atomic structure are represented in Fig.6.2b and 6.1b respectively. The k-points coordinates selected for the band-structure representation are singled out as well. In La_2CuO_4 Lanthanum favours the La^{+3} state and Oxygen the O^{-2} state and therefore Copper is in the state Cu^{+2} . The electronic configuration of Cu is $[Ar]3d^{10}4s^1$ and removal of 2 electrons gives an incomplete d shell with only 9

(a) Unit cell (b) Brillouin zone

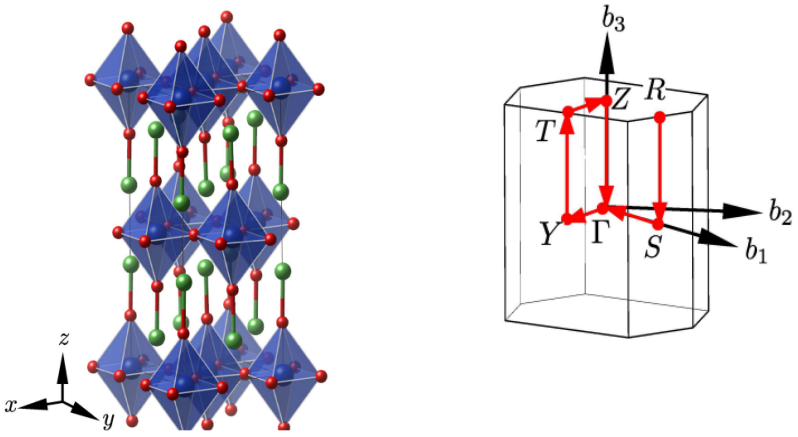

Figure 6.2: Left: single face-centred orthorhombic unit cell of the crystal structure of La_2CuO_4 in the AFM phase (double cell). The CuO_6 octahedra are alternatively tilted in the x-direction. Right: first Brillouin zone of the single face-centred orthorhombic phase (image taken from [19], since we have used the same atomic structure).

electrons.

Regarding the basis set the chosen values of the MT sphere radii R_{MT} for the FP-LMTO basis set are (in atomic units) 2.77 for La, 1.91 for Cu, 1.67 for O. The cut-off G_{MAX} is set to 9.2 Ry. This value controls the plane wave cutoff used to represent the Hankel functions of our basis set, it gives a measure of the quality of the representation. The smoothing radii R_{sm} of the Gaussians defining the basis is set by variational principle to minimize the total energy, it has one value for each element and each orbital ℓ. The following values are adopted: La (s,p,d,f components respectively): 1.85, 1.85, 1.70, 1.19 a.u.; Cu (s,p,d,f): 1.27, 1.27, 0.88, 1.27 a.u.; O (s,p,d,f): 0.86, 0.83, 1.115, 1.115 a.u. The radii R_{sm} determine the shape of the basis together with the Hankel energies E_{H}, controlling how "short range" is the basis. The values of E_{H} are also resolved in atom and ℓ components, a value of -0.3 Ry is chosen for all atoms and orbital components.

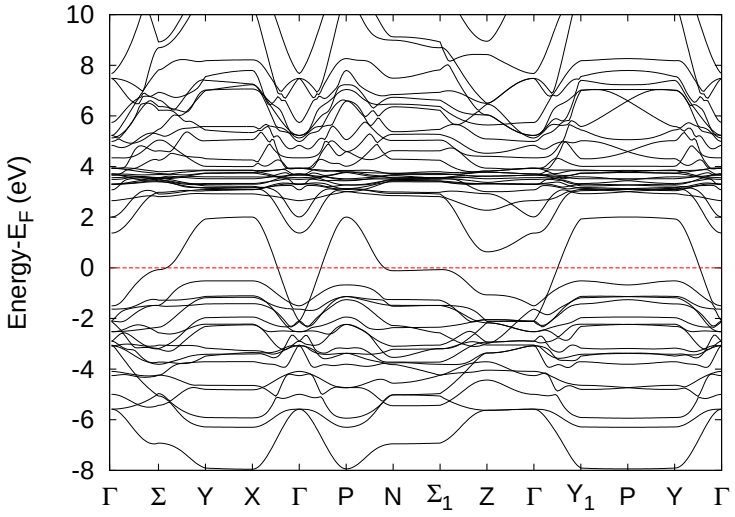

Figure 6.3: LDA electronic band-structure of non-magnetic La_2CuO_4 along the path of Fig.6.1b.

6.1.1 LDA study

We will now present the results of an LDA simulation of non-spin polarized La_2CuO_4. The Brillouin zone was sampled with a 8 8 8 k-point mesh, the path chosen for the band-structure representation is displayed in Fig.6.1b.

The electronic band-structure within LDA is represented in Fig.6.3. We notice a band crossing the Fermi level and a metallic solution as expected, the insulating state is not reproduced in DFT. The Lanthanum f states are packed around 3-4 eV above the Fermi level.

Consistent with the band-structure results are the total DOS and the projected DOS in LDA, which is resolved in angular momentum ℓ components. They are diplayed in Fig.6.4.

A metallic state is predicted also from the total DOS and the projected DOS at LDA level. In particular the structure around Fermi is of Cu-d and O-p character (these states are known to be hybridized) whereas a sharp La-f peak is observed at around 3 eV. Therefore, in addition to the wrong prediction of the metallic

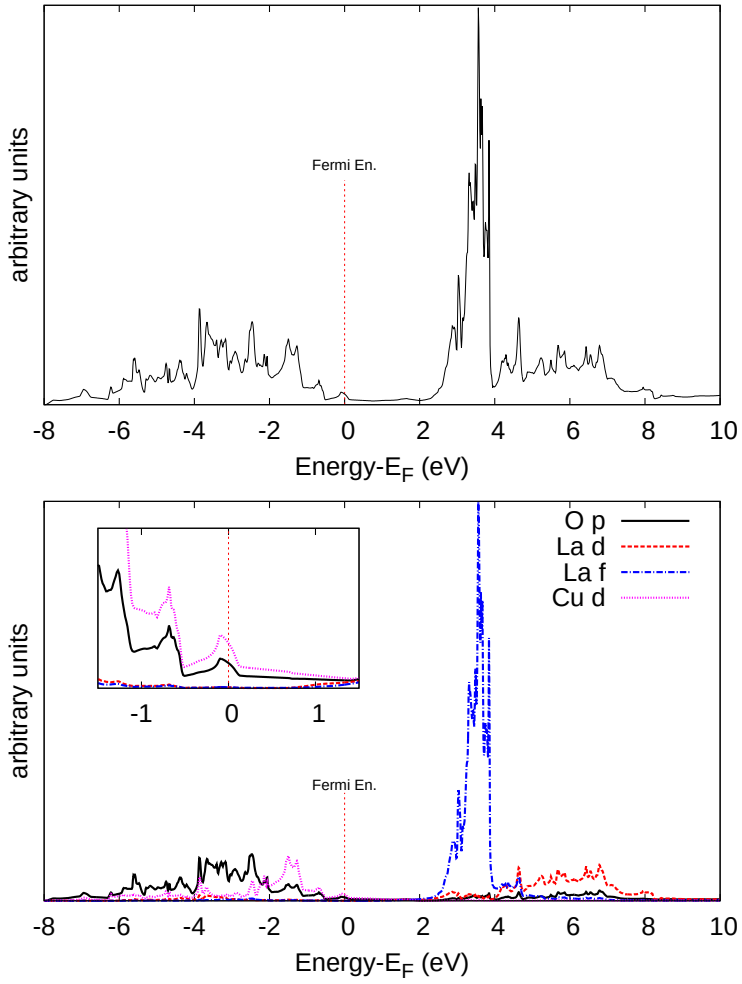

Figure 6.4: (Top panel) LDA total DOS and (bottom panel) LDA projected DOS of non-magnetic La_2CuO_4. The channels corresponding to different orbitals are specified in the top right corner. The gap region is zoomed in the top left corner.

state, in the LDA we notice the La-f state being much too low with respect to experiments [53], a typical feature since unoccupied $4f$ states are always too close to the Fermi level in the LDA.

6.1.2 QSGW study

6.1.2.1 Non-magnetic case

The GW calculation relies on a mixed basis which should span the Hilbert space by means of a product of eigenfunctions. It is required for example for the expansion of the Coulomb interaction v (and also the screened interaction W) because it connects the products as $\langle\Psi\Psi|v|\Psi\Psi\rangle$. The introduction of these basis products requires a cutoff for the $\mathbf{G}$ vector, one for the basis envelope functions (called $G_{\mathrm{B}}^{\mathrm{cut}}$) and one for the interstitial part of two-particle objects such as the screened coulomb interaction (called $G_{\mathrm{X}}^{\mathrm{cut}}$). These values are set in the file *GWinput* together with the spacing of the energy mesh used for real-axis integration of the polarizability, called dw. The values used for this GW calculation on non-magnetic La_2CuO_4 are $G_{\mathrm{B}}^{\mathrm{cut}} = 5, G_{\mathrm{X}}^{\mathrm{cut}} = 3.5, dw = 0.02$ Hartree.
A QSGW calculation using these parameters was carried on and converged after 8 runs setting a tolerance of $2\text{x}10^{-5}$. The corresponding total DOS and projected DOS are shown in Fig.6.5. Neither in this case a gap is opened. This is not surprising since the calculation is non-magnetic. The gap opens as a consequence of spin polarization. Whether local and disordered (para-magnetic) or ordered (anti-ferromagnetic), or somewhere in between, magnetism is essential.
We notice how the La-f peaks are pushed forward around 11 eV, significantly improving the LDA predictions[1]. This result is indeed much closer to the experimental value of 9 eV [53] and in line with the Matsubara QSGW calculation on La_2CuO_4 carried on recently by the group at Rutgers [19].
A small digression. There is a major difference before the GW method, based on V. Kutepov's algorithm called QPGW, on which the implementation of [19] is founded, and our QSGW implementation [61]. The key point of the QPGW

[1]The well-known better description of $4f$ states in QSGW compared to LDA originates from the effective dynamically screened exchange. In LDA the exchange term is captured by a potential that entirely depends on density by construction, not on the orbitals as in GW.

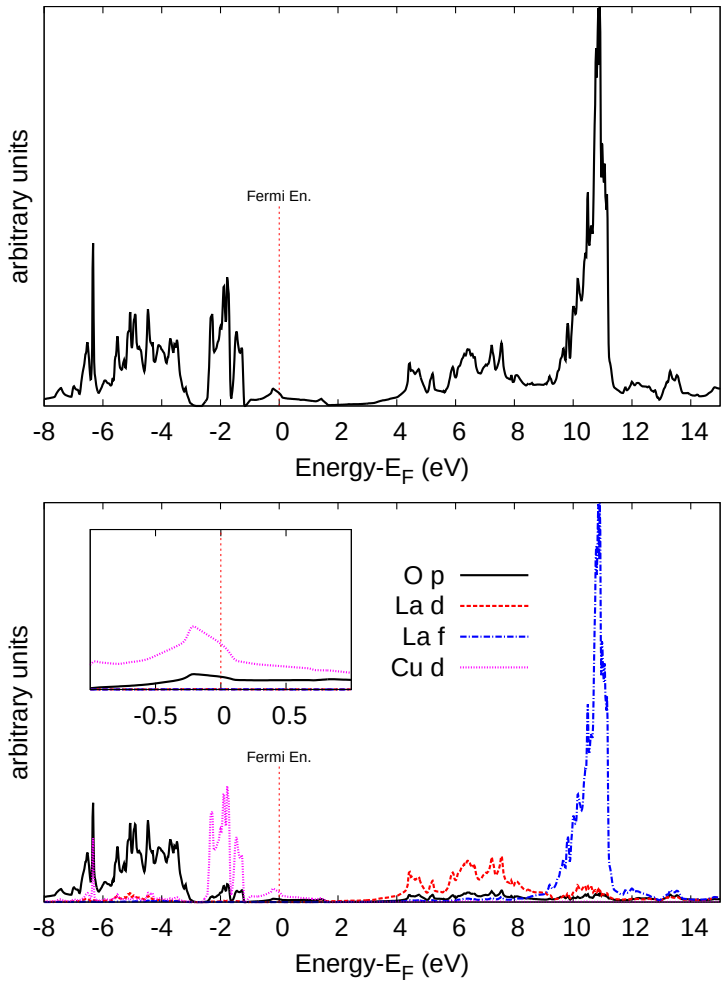

Figure 6.5: (Top panel) QSGW total DOS and (bottom panel) QSGW projected DOS of non-magnetic La_2CuO_4.

scheme is the construction of the static quasi-particle Hamiltonian $\hat{H}_{\mathrm{QP}}(\mathbf{k})$ from the dynamical self-energy $\hat{\Sigma}_{\mathrm{QP}}(\mathbf{k}, i\omega_n)$ defined on the Matsubara axis, and the Hartree Hamiltonian $\hat{H}_{\mathrm{H}}(\mathbf{k})$. The static Hamiltonian reads:

$$\hat{H}_{\mathrm{QP}}(\mathbf{k}) = \hat{Z}^{\frac{1}{2}}_{\mathrm{QP}}(\mathbf{k}) \left[\hat{H}_{\mathrm{H}}(\mathbf{k}) + \hat{\Sigma}_{\mathrm{QP}}(\mathbf{k}, i\omega_n = 0)\right] \hat{Z}^{\frac{1}{2}}_{\mathrm{QP}}(\mathbf{k}) \,,$$
$$\text{where} \quad \hat{Z}^{-1}_{\mathrm{QP}}(\mathbf{k}) \coloneqq 1 - \frac{\partial \hat{\Sigma}_{\mathrm{QP}}(\mathbf{k}, i\omega_n = 0)}{\partial i\omega_n} \,.$$

This algorithm results in taking the first order Taylor expansion of the dynamical self-energy over $i\omega_n = 0$ to evaluate the static counterpart, similarly to the procedure expressed by eq.(A1) of [93] in the approach of Held and co-workers. The QSGW algorithm, adopted in this work, makes use of a different expression for the static self-energy given by eq.(2.50), which is somewhat more accurate (as well as computationally more expensive). As a consequence the static QPGW self-energy is typically bigger than the QSGW one and therefore the gaps in QPGW are smaller than in QSGW.

6.1.2.2 Anti-ferromagnetic case

Another GW calculation for AFM phase of La_2CuO_4 was conducted starting from the double unit cell of Fig.6.2a. The following GWinput parameters are used in this case: $G^{\mathrm{cut}}_{\mathrm{B}} = 2.7, G^{\mathrm{cut}}_{\mathrm{X}} = 2.2, dw = 0.01$ Hartree. A QSGW calculation using these parameters was carried on and converged after 5 runs setting a tolerance of $2\mathrm{x}10^{-5}$.

The QSGW-based band-structure is obtained following the path along the first Brillouin zone represented in Fig.6.2b. It is displayed in Fig.6.6, the O-p states are coloured in blue, the minority Cu-d states in red, the majority Cu-d states in green, the La-f states in black. We notice a gap between the O-p bands (partially hybridized with the Cu-d states close to Fermi) and the Cu-d states at roughly 4 eV. This is in line with the past predictions of a charge-transfer insulator [104]. To be more precise, a pure "charge-transfer" insulator as defined by Sawatsky and Zaanen would mean that the valence band maximum would consist entirely of O-p character, as distinct from a "Mott insulator" in which it would consist of Cu-d character. From the colours in the figure, QSGW predicts La_2CuO_4 to be

intermediate between Mott and charge-transfer types.

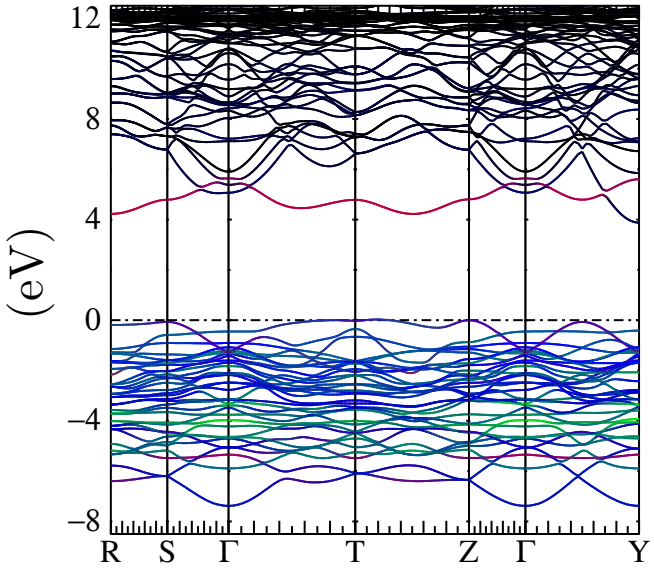

Figure 6.6: QSGW electronic band-structure of La_2CuO_4 in the AFM phase along the path of Fig.6.2b. the O-p states are coloured in blue, the minority Cu-d states in red, the majority Cu-d states in green, the La-f states in black.

The gap opening can be observed also from the total DOS and projected DOS resulting from the QSGW calculation on AFM La_2CuO_4. They are represented in Fig.6.7. There is a gap of about 4 eV, slightly bigger than the QPGW result of [19], and the reasons why the QSGW gaps are typically bigger than the QPGW ones have been explained. From a comparison with the non-magnetic result, we notice how the Cu-d peaks at -2 eV (in DMFT this is often referred as a Zhang-Rice peak which overlaps with the O-p states [104]) lose spectral weight in the AFM calculation and consequently some structure of Cu-d character is observed now at 4 eV. This gap is quite overestimated with respect the experimental value of 2 eV[21, 32], which is a typical feature of QSGW methods in the study of oxides even if usually not in this measure. The reasons of this big discrepancy regarding La_2CuO_4 are not trivial and two-fold. The first is related to the charge channel: the ladder diagrams missing from the RPA expansion result in an overestimated W and consequently too large splitting between occupied and unoccupied states.

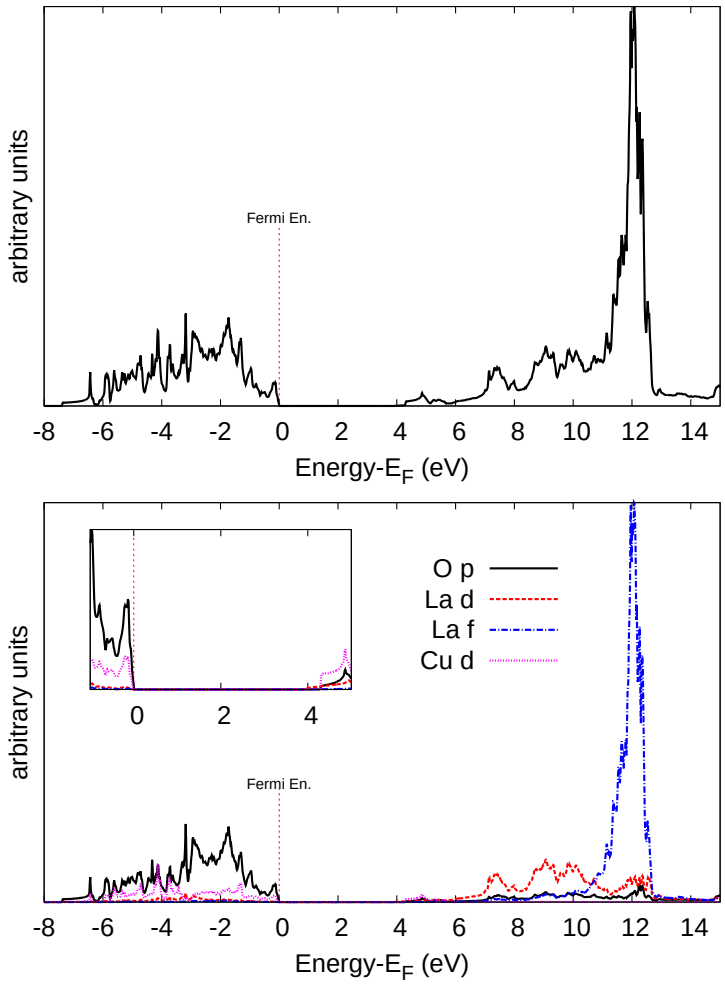

Figure 6.7: (Top panel) QSGW total DOS and (bottom panel) QSGW projected DOS of AFM La_2CuO_4.

Secondly, the discrepancy is affected by the missing magnetic diagrams from the exchange term in GW: this effect has proved to be extremely relevant when time-reversal symmetry is broken. This is the case of La_2CuO_4 where the Cu-d_m and Cu-d_{-m} states have different occupation numbers and potentials (since the potential is orbital dependent). We also notice how in the AFM phase the La-f peaks get shifted even more towards high-frequencies with respect to the non-magnetic case. They now lie around 12 eV, a little more distant to the experimental value of 9 eV. This feature, consequence to the missing ladder diagrams, was also found in [18].

6.2 Novel result: QSGW+DMFT loop

A DMFT loop was implemented starting from the QSGW converged results on non-magnetic La_2CuO_4, as a first example of a one shot QSGW+DMFT loop. In this case we can safely refer to the magnetic configuration of the material as para-magnetic (PM). This is because with the action of DMFT starting from a non-magnetic state we the gain ability to configurationally average and in particular to represent paramagnetism by configurational disorder at a single-site level. We will now present the parameter set for the DMFT implementation.
The projector is defined for the 3d electrons of Cu, assumed to be the correlated ones, within an energy window including 43 bands for each k-point on a 4 4 4 k-point mesh. This number of bands corresponds roughly to an interval of $\pm$10eV centred on the Fermi level, in order to include the entire Cu-3d spectra in our window (as well as some O-p states which are hybridized with the Cu-d ones).
The value of the inverse temperature β is 50 eV^{-1}, which determines also the Matsubara frequency mesh sampling (composed of 2000 points). The Hubbard parameters have been chosen from previous studies on the compound [82, 104]: $U = 11$ eV, $J = 0.7$ eV. The electron occupancy for the Cu-d orbitals is $n = 9$, therefore from (4.29) we get a value of the static DC correction of 90.7 eV. The DMFT loop converged after 13 iterations (i.e. after 13 runs of CTQMC). This convergence was estimated through the convergence of the values of the impurity level (see Fig.6.8).
Since we have not yet developed reliable analytic continuation method, we could

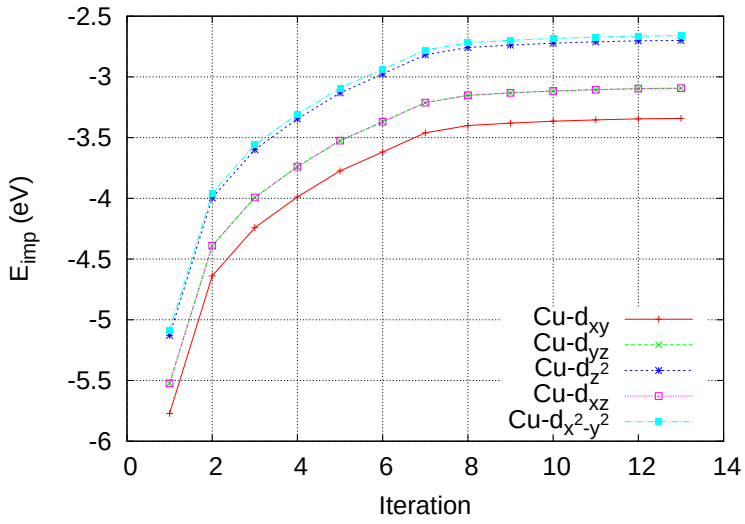

Figure 6.8: Convergence of the DMFT impurity level relative to Cu-d orbitals

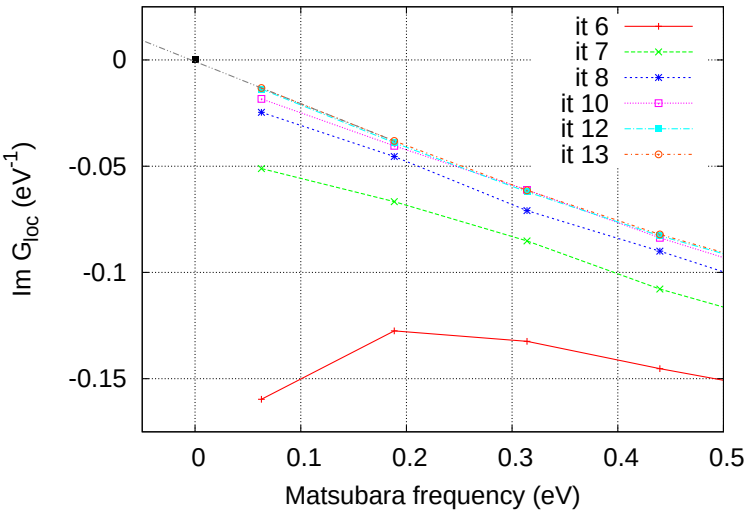

Figure 6.9: DMFT result: $\mathrm{Im}\, G^{\mathrm{loc}}_{LL'}$ as a function of Matsubara frequencies for the Cu-$d_{x^2-y^2}$ orbital for several iterations. The curve of the 13th iteration has been fitted in a grey line in order to estimate the convergence to 0.

not extract a reliable DOS on the real axis from the DMFT self-energy (the self-energy is defined for Matsubara imaginary frequencies). Nevertheless the opening of a gap, even in the PM phase, can be usually assessed in DMFT by evaluating the convergence to 0 of $\mathrm{Im}\, G^{\mathrm{loc}}_{LL'}$ (since this object directly gives the spectral function) where the LL' components range among the diagonal components ($LL' = LL\delta_{LL'}$) of the 5 m-resolved d-orbitals of Cu. In particular we focused the convergence to 0 of the component relative to the Cu-$d_{x^2-y^2}$ orbital, reckoned as responsible of the gap opening. This convergence is displayed in Fig.6.9.
We concluded that within a QSGW+DMFT approach the compound can be ascertained as an insulator even in the PM phase (as a consequence of the non-vanishing, but disordered and fluctuating magnetic moment). This result goes in the direction of asserting the correlated character of the insulating gap [38, 104]. Nevertheless it is not clear how much of the effect can be captured by a static (disordered) spin potential and how much the frequency dependence inside DMFT modifies the results, remembering how even a static potential such as the quasiparticlized GW self-energy is sufficient to open a gap at least for an ordered configuration (see Fig.6.7).
Further investigations on this material are demanded to address these issues as well as assess the quality of the QSGW+DMFT implementation.

Chapter 7

Importance of spin-fluctuations in study of Ni

Electronic structure calculations for transition metals such as Fe and Ni have been intensively exploited in the past decades thanks to the availability of experimental results of this prototypical systems [44, 102]. We focus in particular on Ni, an itinerant ferromagnet. If some aspects of ferro-magnetism in this material, in particular the magnetic moment M, are well described by conventional LDA calculations, a feature like the Hubbard-like satellite at about -6 eV appears to be a consequence of strongly correlated electrons. It is indeed only by means of more advanced methods such as LDA+DMFT [68] or GW+DMFT [12] that this satellite was found investigating Ni, whereas in LDA it is not present.
Regarding our study of this material however we took this aspect aside as we chose to focus on the predictions of the magnetic moment and the exchange splitting. As we will show, the LDA-derived magnetic moment agrees pretty well with the experimental value, while the exchange splitting is overestimated by a factor of two. If overall in transition metals exchange splitting and magnetic moment are usually well described by QSGW (see Fig. 7.4 later on), Ni is instead one element for which QSGW does not do better than LDA. Both the exchange splitting (by a factor of two), and the magnetic moment (by a factor of 1.5) of Ni are overestimated in QSGW. This discrepancy appears even more bizarre when looking at the QSGW-derived band-structure of Ni compared to ARPES data,

where the agreement with the experiments is excellent (at least regarding the minority channel).
What is missing in the QSGW (as well as LDA) is accounting for spin fluctuations, which are known to be important in itinerant magnets, whose main consequence is to reduce the average magnetic moment [80] (and thus the exchange splitting). By means of an *ad hoc* addition of magnetic contributions we will show in the first place how the LDA estimation of the magnetic moment is actually fortuitously good. Secondly, that correcting the QSGW result by means of a simple static correction provided by DMFT, which incorporates spin fluctuations, both the discrepancies for the values of exchange splitting and the magnetic moment will be eliminated.

7.1 DFT and QSGW electronic structure

Elementary Nickel is a ferromagnetic metal which crystallises in the face-centred lattice. The corresponding atomic cell is represented in Fig.7.1 together with the first Brillouin zone and the high-symmetry points. The lattice vectors are: $a_1 = (a, 0, 0)$, $a_2 = (0, a, 0)$, $a_3 = (0, 0, a)$ and lattice constant $a = 3.51$ $\mathring{A}$.
Some information about the basis. The MT sphere radii was chosen to be 2.23 a.u. The cut-off G_{MAX} is set to 9 Ry. The LMTO Hankel energies E_{H} are set to -0.3 Ry (this makes them short ranged enough to make it possible to interpolate the self-energy). The smoothing radii R_{sm} are determined automatically by minimizing the LDA total energy.

7.1.1 LSDA and LDA study

A LSDA and LDA calculation (respectively spin and non-spin polarized) has been carried on a $24 \times 24 \times 24$ k-point grid (centred in Γ) to compute the density. The corresponding total DOS and band-structure in both calculations are represented in Fig. 7.2. The LDA calculation has vanishing magnetic moment by construction, while the LSDA yields a magnetic moment $M = 0.62$ Bohr, and the exchange splitting at L given by ΔE_{x}= 0.60 eV. The first compares pretty well with the experimental value [44] $M = 0.57$ Bohr, while the second is overestimated by a

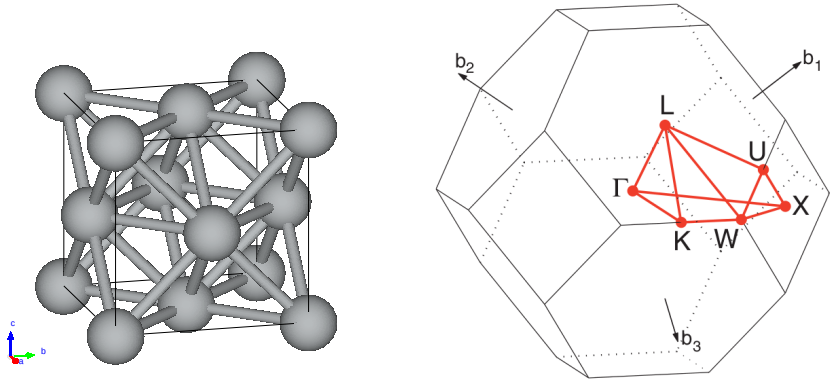

Figure 7.1: Left: face-centred crystal structure of ferromagnetic Ni. Right: first Brillouin zone with high-symmetry points (image taken from [89]).

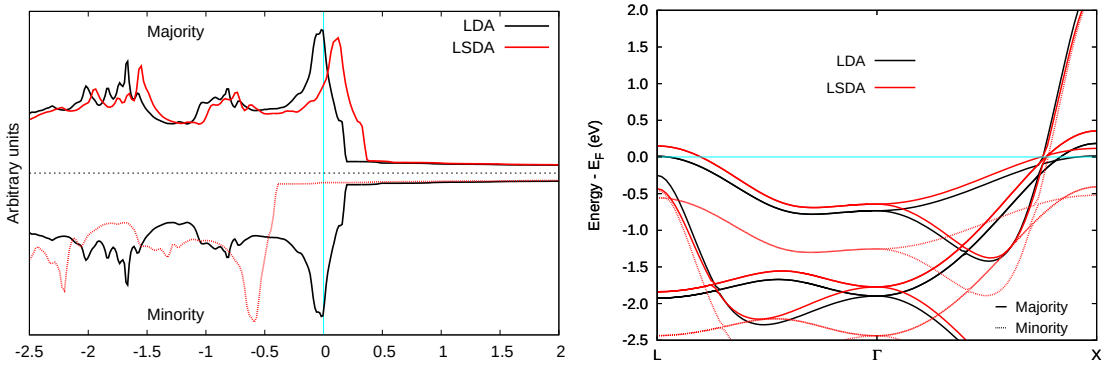

Figure 7.2: Density of states (left) and band structure (right) of Ni within LDA and LSDA.

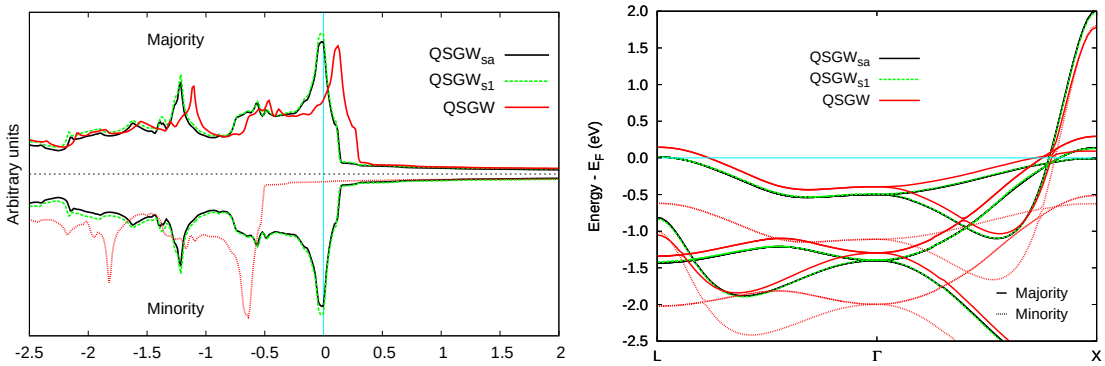

Figure 7.3: Density of states (left) and band structure (right) of Ni for QSGW, $\mathrm{QSGW_{s1}}$ and $\mathrm{QSGW_{sa}}$ calculations.

factor of two (experimental-ΔE_{x}= 0.31 eV).

7.1.2 QSGW study

For the GW calculation a coarser grid has been used ($12 \times 12 \times 12$). Values of the cutoff and the energy spacing used for this GW calculation are respectively $G_{\mathrm{B}}^{\mathrm{cut}} = 2.7, G_{\mathrm{X}}^{\mathrm{cut}} = 2.2, dw = 0.02$ Hartree.
Three different calculations have been carried out: the first is spin-polarized (QSGW), the second is non-magnetic, obtained neglecting the spin orientation ($\mathrm{QSGW_{s1}}$), the third is obtained after spin-averaging the QSGW results ($\mathrm{QSGW_{sa}}$). In the $\mathrm{QSGW_{sa}}$ in particular, only the charge component of the converged self-energy and the charge component of the consistent density have been kept. This is achieved by averaging out the spin components of the density $\rho_{\mathrm{sa}} = (\rho_{\uparrow} + \rho_{\downarrow})/2$ and the exchange-correlation potential $V_{\mathrm{sa}} = (V_{\uparrow}^{\mathrm{xc}} + V_{\downarrow}^{\mathrm{xc}})/2$. The overall resulting DOS and band-structures are displayed in Figure 7.3. The resulting magnetic moment and exchange splitting are respectively $M = 0.75$ Bohr and ΔE_{x}= 0.77 eV. Discrepancies with the experimental values for M and ΔE_{x}, that was anticipated, can be contextualized when looking at Fig. 7.4. Fig. 7.4(a) shows that in transition metals d bandwidth and exchange splitting seem to be very well described by QSGW, except that ΔE_{x} deviates strongly from experiment in Ni. Overall QSGW significantly improves not only on the LSDA, but also on fully self-consistent GW [11] because of loss of spectral weight in fully self-consistent

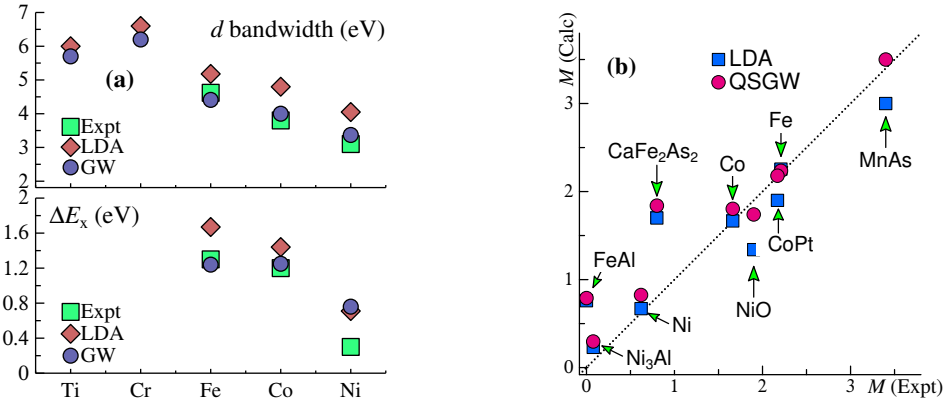

Figure 7.4: QSGW vs LDA: (a) d bandwidth (top panel) and exchange splitting ΔE_x (bottom panel) in the $3d$ elemental metals. (b): Magnetic moment of several compounds

G that is avoided in QSGW [61].

In order to summarize the previous results, Fig. 7.5 compares the QSGW and LSDA band-structure of Ni to ARPES data [44]. Agreement is excellent in the minority channel but not quite in the majority one, hence $\Delta E_{\rm x}$ comes out uniformly too large on the symmetry lines shown. Also the band near $-1\,$eV at L (consisting of s character there) is traditionally assumed to be a continuation of the d band denoted as white and green diamonds; but the calculations show that at it is a continuation of Ni s band. The corresponding LSDA band (light dotted lines) crosses L at roughly $E_F{-}0.45\,$eV; also the d bands are much wider. $\Delta E_{\rm x}$ is about twice too large in both QSGW and the LSDA, and for that reason spin wave frequencies are also too large [55].

Neither the LDA nor GW include spin fluctuations, which reduce the average moment and thus $\Delta E_{\rm x}$. Spin fluctuations $\langle M^2\rangle$ are important generally in itinerant magnets, and one important property they have is to reduce the average magnetic moment $\langle M\rangle$ [75, 90]. Fig. 7.4(b) shows this trend quite clearly: systems such as Fe, Co, and NiO are very well described by QSGW, but M is always overestimated in itinerant magnets such as FeAl, Ni_3Al, and Fe based superconductors such as $BaFe_2As_2$. Ni is also itinerant to some degree (unlike Fe, its average moment probably disappears as $T{\to}T_c$), and its moment should be overestimated. This is found to be the case for QSGW, as Fig. 7.4(b) shows.

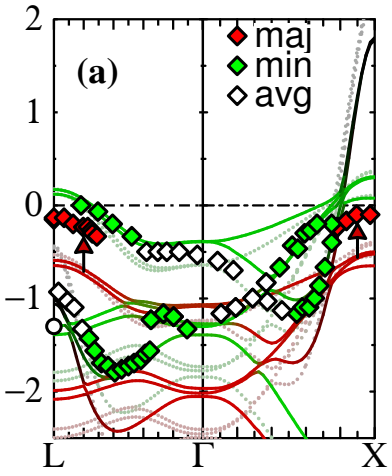

Figure 7.5: QSGW (solid lines) vs LSDA (light dotted lines) band-structure compared to ARPES measurements (read and green diamonds) [44] (the circle at −1.3 eV was taken from Ref. [24]). Red arrows highlight the discrepancy in the exchange splitting ΔE_{x} at near L and X.

7.2 Including spin-fluctuations: QSGW+DMFT

Local spin fluctuations are well captured by localised non perturbative approaches, such as DMFT, and we can reasonably expect that the addition of spin-flip diagrams to QSGW via, e.g. DMFT, would be sufficient to incorporate these effects. To verify this, we first assume that the predominant effect of spin fluctuations will result in an additional contribution to the static QSGW potential. This will be the case if the quasi-particle picture is a reasonable description of Ni, even if QSGW alone does not contain enough physics to yield an optimum quasi-particle approximation.

In order to corroborate this assumption, we first model spin fluctuations by carrying out the QSGW self-consistent cycle in the presence of a magnetic field B^{eff}, and tuning B^{eff} to reduce M. Our key finding is that when B^{eff} is tuned to make M agree with experiment, ΔE_x does also, reproducing ARPES spectra to high precision in the FL regime. Both QSGW and LSDA overestimate M for itinerant systems, but as shown in Fig. 7.4(b) the latter also underestimates it in local-moment systems. This is because it emphasises itinerancy too much, as manifested by its tendency to overestimate the d bandwidth. Ni is a case where the LDA's tendency to overestimate M (missing spin fluctuations) for small M and underestimate it for large M approximately cancel. As a consequence, in the LSDA treatment of Ni, the moment comes out fortuitously good. When spin fluctuations are folded in through B^{eff}, the LSDA moment becomes instead too

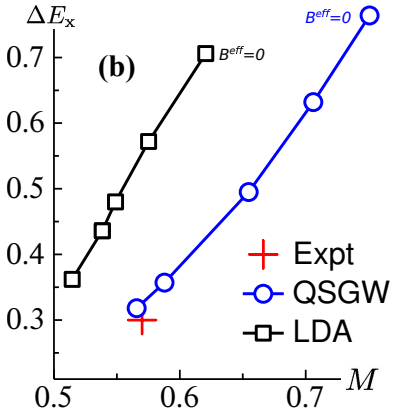

Figure 7.6: ΔE_x at the symmetry point L as a function of M, obtained by adding an external magnetic field to the QSGW or LDA potential.

small. This effect is displayed in Fig. 7.6.

Motivated by this result, one seeks for an *ab initio* foundation that incorporates spin fluctuations. We note that QSGW does an excellent job at handling the important diagrams (especially screening) in a parameter-free way, apart from the spin-flip contributions. On the other hand these latter are largely local, and they can be safely taken into account with DMFT.

A G_0W_0+DMFT study of ferromagnetic Ni was carried out[1] in [12]. Here we adopt our novel implementation of QSGW+DMFT with a specific prescription: we perform a DMFT calculation on the Ni d orbitals only with the intent of extracting a static correction to the QSGW calculation, claiming that we can afford to neglect the dynamical contributions carried by the local impurity self-energy. The bath degrees of freedom are computed with a spin-averaged exchange correlation potential from $\mathrm{QSGW_{sa}}$ (whose results are shown in Fig. 7.3) to which we add the static part of the spin-flip correction Σ^{sf} obtained from a complete DMFT loop. By means of this separation in the self-energy of charge contributions from spin-flip contributions we achieve to get rid of magnetic double counting problems. On the other hand, by taking just the static part of the impurity self-energy from DMFT, we avoid the need for an analytic continuation from Matsubara frequencies.

Let us present the parameters for the DMFT loop. The projectors are defined

[1] As we mentioned the main accomplishment of the work [12] was actually to reproduce at the GW+DMFT level the satellite structure at $\sim$-6 eV, already captured by Lichtenstein and co-workers in LDA+DMFT [68]. The investigation of this spectral feature is currently under study with our implementation.

for the Ni $3d$ orbitals, within an energy window from 5 bands below E_F and 3 bands above E_F, which correspond roughly to a window of $\sim\pm10$ eV over most of the symmetry points (apart from Γ where it is $\sim\pm12$ eV). We assume the energy window to be wide enough that U becomes nearly static [19]. In order preserve flexibility, the corresponding on-site Hubbard parameters were chosen to range among the values of U=8,10 eV and J=0.7,0.9 eV, close to the estimation calculated by constrained RPA [19]. The Matsubara frequency grid is defined over 2000 points with an inverse temperature $\beta = 50$ eV^{-1}. The nominal occupancy for Ni $3d$ orbitals is $n = 8$, therefore by means of (4.29) we get a value of the static DC correction of 72.2 eV.
The following steps are required to extract the static spin-flip component of the impurity self-energy:

- remove DC: $\Sigma^{\mathrm{loc}}_{LL'}(i\omega_n) = \Sigma^{\mathrm{imp}}_{LL'}(i\omega_n) - \Sigma^{\mathrm{DC}}$;
- extrapolate the static limit: $\mathrm{Re}\left[\Sigma^{\mathrm{loc}}_{LL'}(z)\right]\Big|_{z=0}$ by means of a polynomial fitting from the first Matsubara points;
- embed the static self-energy: $\Sigma^{\mathrm{loc}}_{ij\mathbf{k}} = U^{L\dagger}_{i\mathbf{k}}\,\mathrm{Re}\left[\Sigma^{\mathrm{loc}}_{LL'}(0)\right]U^{L'}_{j\mathbf{k}}$;
- symmetrise the resulting static correction: $\bar{\Sigma}^{\mathrm{loc}}_{ij\mathbf{k}} = (\Sigma^{\mathrm{loc}}_{ij\mathbf{k}} + \Sigma^{\mathrm{loc}}_{ji\mathbf{k}})/2$;
- subtract the charge contribution: $\Sigma^{\mathrm{sf}}_{ij\mathbf{k}} = \bar{\Sigma}^{\mathrm{loc}}_{ij\mathbf{k}} - (\bar{\Sigma}^{\mathrm{loc}}_{ij\mathbf{k}}\uparrow + \bar{\Sigma}^{\mathrm{loc}}_{ij\mathbf{k}}\downarrow)/2$ in such a way to obtain the spin-flip correction.

This object can be then added to the spin-averaged QSGW self-energy $\Sigma^{\mathrm{sa}}_{ij\mathbf{k}}$ (or the spin averaged exchange-correlation potential $V^{\mathrm{sa,xc}}_{ij\mathbf{k}}$ in LDA[1]) and the procedure can be reiterated until convergence to close the DMFT loop.
The results of this charge-magnetic one-shot QSGW+DMFT loop are represented in Fig. 7.7. We show in particular four independent calculations with the different combinations of U=8,10 eV and J=0.7,0.9 eV. All calculations converged within 15/20 iterations, the ones with lower J took longer to converge.
For completeness, we report also the results of a LDA+DMFT calculation carried out under the same procedure (but in this case starting from a non-magnetic LDA calculation rather than a spin-averaged one). For the LDA+DMFT loop,

[1] this entire procedure stands also in the case of a LDA+DMFT loop

the same DMFT parameters are used except that the Hubbard U is fixed to 10 eV whereas the Hund's coupling J takes the values 0.7 and 0.9 eV. The results are displayed in Fig. 7.8.

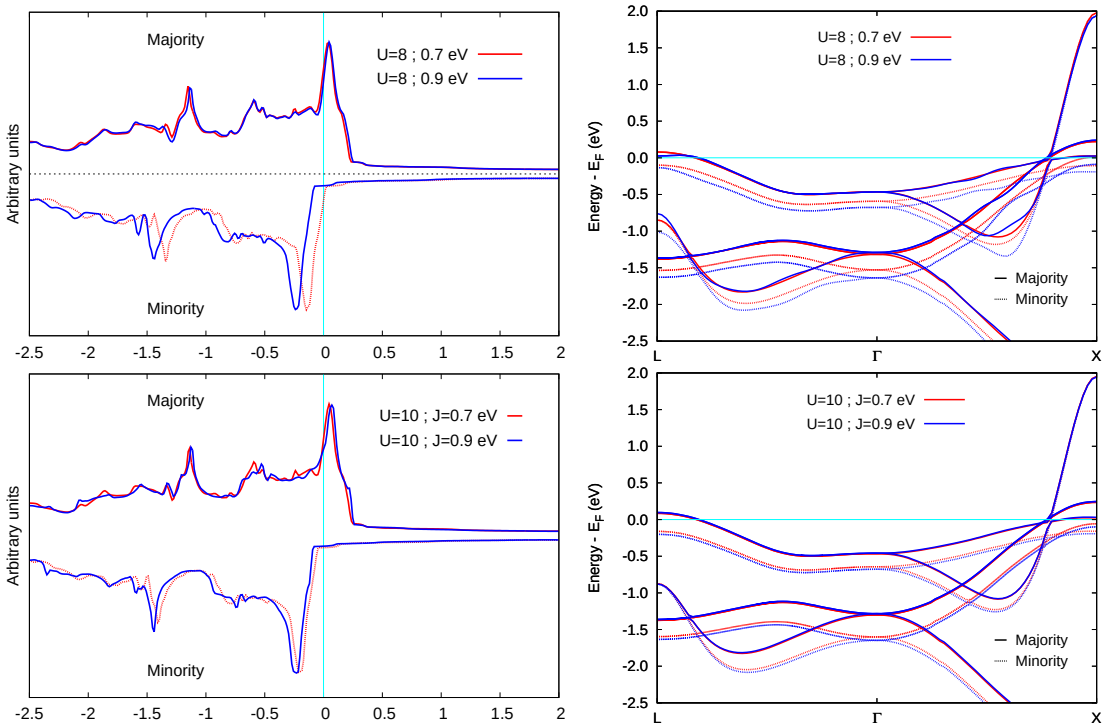

	$U=8$ eV		$U=10$ eV		
	J=0.7	J=0.9	J=0.7	J=0.9	Exp.[44]
M (Bohr)	0.48	0.54	0.52	0.57	0.57
ΔE_{x}(eV)	0.18	0.16	0.25	0.30	0.31

Figure 7.7: DOS and band-structure of the $\mathrm{QSGW_{sa}}$+$\mathrm{DMFT_{sf}}$ one-shot loop at the varying of U, J. The corresponding results on M and exchange splitting ΔE_{x} are compared to the experimental values [44].

We notice that by means of this static correction obtained with DMFT to the QSGW results (with the prescription we have outlined) we are able to extract values of the exchange splitting and the magnetic moment in excellent agreement with the experiments, especially in the calculation with U=10 eV, J=0.9 eV (see bottom table of Fig. 7.7). On the other hand within LDA+DMFT we do not achieve the same agreement, since when correcting the exchange splitting the magnetic moment deviates from its experimental value (see bottom table of

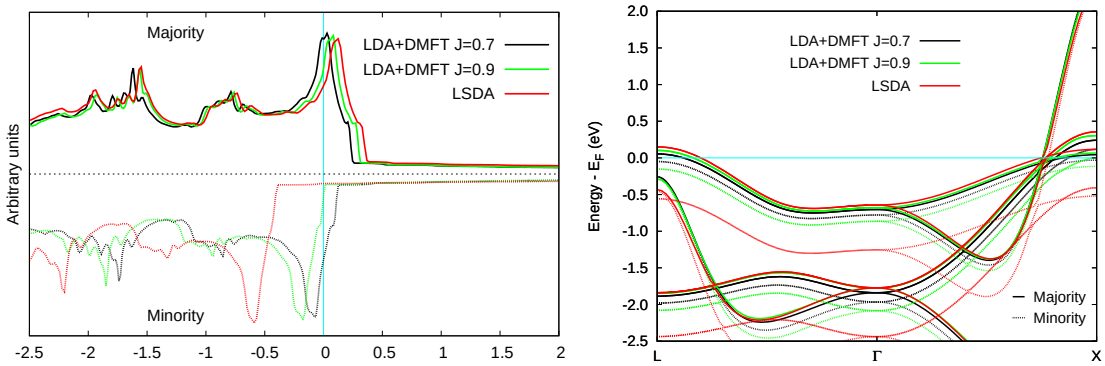

	LSDA	LDA+DMFT		Exp.[44]
		J=0.7	J=0.9	
M (Bohr)	0.62	0.25	0.48	0.57
ΔE_{x}(eV)	0.60	0.10	0.26	0.31

Figure 7.8: DOS and band-structure of the LDA+DMFT one-shot loop at the varying of J with U=10 eV.

Fig. 7.8). The natural conclusion for this result is that the LDA starting point is not accurate enough that a simple static DMFT correction guarantees reliable results. A dynamical DMFT contribution seems to be required in this case, in a full standard LDA+DMFT loop, like the calculation carried on in [68] has proved.
In Fig. 7.9 we compare the QSGW+DMFT band-structure computed with U=10 eV, J=0.9 eV of Fig. 7.7 to the ARPES data, with the intention of assessing the improvement with respect to the pure QSGW results showed in Fig. 7.5. A similar good trend was also found in the [68] (LDA+DMFT) and [12] (G_0W_0+DMFT) in comparison with the LDA benchmark.
Looking at Fig. 7.9 the agreement with both minority and majority channel is now excellent, and one can notice that the QSGW+DMFT results not only agree very well with the experimental values, but they are also almost indistinguishable from the semi-empirical QSGW+B^{eff} ones (obtained folding in an ad hoc magnetic field as presented in Fig. 7.6).
In conclusion, spin fluctuations are known to be important in itinerant magnets and in particular for Ni since they affect the average magnetic moment, and they are not included in QSGW. The spin fluctuations can be simulated artificially by the introduction of an ad hoc magnetic field B^{eff}: this eliminates discrepancies

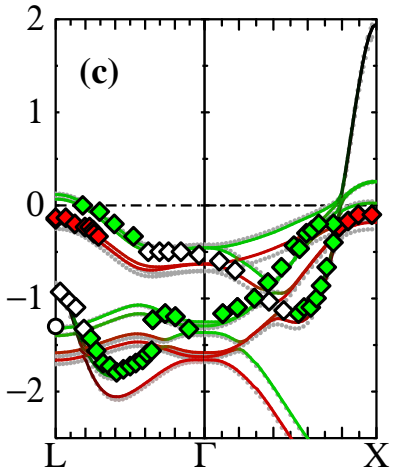

	LDA	QSGW	QSGW+B^{eff}	QSGW+DMFT	Exp.
M	0.62	0.75	0.57	0.57	0.57
ΔE_x	0.71	0.77	0.32	0.30	0.31

Figure 7.9: Solid lines: QSGW+DMFT band-structure with $U = 10$ eV, $J = 0.9$ eV. Light dotted lines: bands (almost indistinguishable from the QSGW+DMFT band-structure) generated by QSGW+B^{eff}, with B^{eff} corresponding to Fig. 7.6.

in both M and ΔE_{x}. However, in order to account for spin fluctuations in an *ab initio* framework, we built a novel QSGW+DMFT implementation with the self-energy in the charge channel carried by QSGW and the spin channel by DMFT, thus avoiding ambiguities in double-counting. The magnetic moment and band structure from a quasiparticlized Hamiltonian was essentially identical in the two cases showing that (at least for Ni) spin fluctuations are very well approximated by a static, constant field. Beside the fundamental relevance of this result, this conclusion is of particular interest also for technical reasons, especially when calculations on large magnetic systems are concerned.

Several aspect of this material have still to be addressed, from the ab initio derivation of spin waves starting from an accurate estimation of the exchange splitting [56] to the investigation at QSGW+DMFT level of spectral features like the Hubbard like satellite at -6 eV.

Part IV

Conclusions and outlook

Conclusions

The goal of this work of thesis was to present in a didactic and reproducible way the underlying steps towards the formulation and construction of an ab initio QSGW+DMFT implementation.
As lavishly mentioned throughout the manuscript, the full and optimised development of this scheme is a long-term accomplishment, of which my PhD project is just meant to be an intermediate stage, even though in retrospect very close to the final target.

Summary and deductions

This thesis started with a broad introduction on the theoretical framework of this method. This was the object of Part I. In order to prepare the grounds for a proper introduction of the fundamental models, a digression on the materials commonly under the investigation of electronic structure was necessary. This digression was also meant to draw a line between two substantially different classes of compounds calling for two fundamentally distinct strategies for modelling them. Belonging to the first class are weakly correlated materials, the majority of accessible compounds, whose physics is commonly understood and can be described and even predicted in terms of theories with a rather strong degree of approximation and simplicity (when obviously higher and higher accuracy requires more and more complexity). Different is the case of strongly correlated materials, together with their unusual and exotic properties open to many technological applications, and whose physical behaviour has still today some open questions and yet to be fully comprehended in full detail.
Density Functional Theory, doubtlessly the most recognized and successful (if

measured by the number of published papers), was presented, pointing out the genius and simplicity of its formulation, as well as its unavoidable limits of predictions, in particular regarding strong correlations. As a step forward the more advanced Green's functions methods were then introduced, first outlining the basic concepts - as the quasi-particles of Landau-Fermi theory and their limits of applications in terms of correlations - and quantities of reference - primarily the self-energy, connected to the Green's function via the Dyson equation. In the framework of Green's function method is Many-Body Perturbation Theory, whose principal example is the GW approximation (GWA), originally set as a shortcut of Hedin's equation. GWA-derived approaches are arguably the best available ab initio methods to electronic structure, meaning that no adjustable parameter has to be tailored for the specific material under study and in principle just the crystal structure is required to achieve a reasonable description of the physics of the compound. Two aspects can best summarize the embodying power of GW theory. The first is the inclusion of a dynamically screened Coulomb interaction W, which better than the bare interaction v accounts for the electrons dynamics. The second is that the self-energy is non-local in space, a unique feature with respect to the other models, and time (if we consider the full GW methods). A brief overview on GW approaches, with a specific focus of self-consistency, was intended to present the credits of the quasi-particle self-consistent GW (QSGW) method, which is based on a static (local in time) hermitian self-energy extracted from the GW one by means of a criterion of optimization. QSGW theory was able to overcome the limitations of the first GW implementations as well as the most advanced self-consistent methods suffering of a degree of inconsistency. Nevertheless even QSGW breaks down in presence of strong correlations. The main claim of this work is that GW theory, and in particular QSGW, is unquestionably the most rigorous and efficient method to treat weakly correlated materials, and by definition of a Green's function approach is naturally designed to get along with Dynamical Mean Field Theory.

Dynamical Mean Field Theory (DMFT), the object of chapter 3, is a non-perturbative method which better than any other has proved to capture the physics of strongly correlated materials, among which high-T_c superconductors and Mott insulators. The idea is simple: the full many-body problem of the

lattice is mapped to a single quantum *impurity*, treated calculating all orders at many-body level, while the rest of the system is accounted as a non-interacting *bath* coupled *self-consistently* to the impurity.
In order to exploit the principles of DMFT within a realistic ab initio electronic structure the self-consistent LDA+DMFT was developed and addressed successfully to the investigation of challenging materials. Despite its great advantages, it suffers from intrinsic limits and ambiguities, as we claimed in this work corroborated by serious motivations. It is to overcome these that our QSGW+DMFT scheme is proposed.
Part II of this work is devoted to an insight into the specific QSGW+DMFT method we have implemented, together with the open issues it still need to address and the improvements that are currently under development. An example of the latter is the determination of the double-counting correction, perhaps the most subtle point of such implementations and which is still an object open for debate. After a schematic overview of the programs building the architecture of the current scheme, part III was addressed to display the (preliminary) results of our novel method. We will try to summarize the main conclusions we drew on those.
La_2CuO_4 is a cuprate compound displaying high-temperature superconductivity, its unusual physical properties can be just captured in terms of advanced methods such as DMFT. The object of debate regarding this material regards the peculiar source of this correlated phenomena, in particular if mainly determined by magnetic ordering [20] or rather specifically by strong electronic correlations [19, 38]. We tried to address this question motivated by a recent simulation on La_2CuO_4 carried out by means of a similar approach to ours, a QPGW+DMFT scheme [19]. Our results can be summarized as follows. LDA is unable to reproduce La_2CuO_4 insulating gap (of charge-transfer character), regardless of the magnetic ordering superimposed. By means of QSGW instead, only when the anti-ferromagnetic (AFM) ordering is present a gap is opened and quite overestimated (~ 4 eV) with respect to the experimental value (~ 2 eV [21, 32]). Within the very preliminary result of a QSGW+DMFT loop we have a pretty clear evidence that a gap is opened also in the para-magnetic (PM) configuration. The natural conclusion is that a magnetic ordering, either in the configurational disordered state of the

PM DMFT calculation or in the superimposed AFM phase of the QSGW one (where the configurational average of up- and down- states on one site has never been attempted), is necessary in order to represent the Mott (or charge-transfer) insulating state. On the other hand the QSGW+DMFT result on PM La_2CuO_4, opening a gap, that according to [19] is very close to experiments, seems to elucidate the correlated character of this property. Further investigations are called for in order to give a definite answer to these technicalities.
The last chapter is dedicated to our investigation of the magnetic properties of ferro-magnetic (FM) Nickel, a transition metal which has been widely studied experimentally by means of ARPES measurements. Our study focused in particular on its magnetic moment M and the exchange splitting ΔE_{x}. Surprisingly, LDA describes M better than QSGW, while both overestimate ΔE_{x} equally. We tried to contextualize this result by showing that in transition metals d bandwidth and exchange splitting are very well described by QSGW, and the ΔE_{x} of Ni is a singular exception. Overall QSGW significantly improves both on the LSDA and also self-consistent GW [11] by avoiding the loss of spectral weight in fully self-consistent G. Our claim pivots on spin fluctuations. These effects, very important in itinerant magnets, have the main consequence to reduce the average magnetic moment [80] and the exchange splitting, and are completely absent in QSGW and LDA. They are instead accounted for in DMFT, and the DMFT can be introduced as a static, constant correction to our QSGW potential, claiming that the space non-locality and the diagrams included in QSGW are accurate enough to capture the physics of this material. The results offered a remarkable confirmation of this hypothesis, when both the discrepancies on exchange splitting and magnetic moment are cancelled by means of the static DMFT insertion and the agreement with experiments is extremely good.

Prospective developments

At the present stage, this novel implementation has the capabilities to address the study of a wide range of correlated materials that have been already investigated by means of advanced methods such as LDA+DMFT or GW+DMFT. This could offer a different perspective determined by the specifics of the methods and the

high level of accuracy (and a high computational cost) they bring, seeking for any improvement in the results they might be able to provide.
A refinement and optimization in our implementation is however planned for the immediate future, together with the investigation of new challenging features. Here are some:

- *Vertex corrections.* We plan to include vertex corrections in the GW self-energy as part of our implantation. This improvement is meant to correct misalignment of occupied, atomic-like or semicore states, such as the Cu $3d$ level in many compounds, and the Eu $4f$ state in EuO [71]. Our intention is to pursue the QSGW +DMFT scheme where the vertex on the localized state is calculated to all orders, to gain an understanding of the systematics of Γ of these states for a variety of materials systems where they appear: Cu, Ag, Au, $CuInSe_2$, CuO and EuO.

- *Improve over RPA screening.* Splitting between occupied and unoccupied levels is systematically overestimated by QSGW, an effect than increases with localisation. In NiO the fundamental gap is too large by 1 eV [26]; it can be $\sim$ 3 eV in $4f$ systems [18]. We believe this discrepancies would be cancelled through the inclusion of ladder diagrams in the screened coulomb interaction W.

- *Spin fluctuations.* The strategy of the last chapter can be extended to to the study of other itinerant magnets such as Ni3Al, Sc3In, FeAl, $BaFe2As_2$ all yield magnetic moments much larger than is experimentally observed, and magnetic susceptibility in materials such as Pd are overestimated. Our newly developed QSGW+DMFT approach is ideally suited to carry out a systematic study of these systems: the charge channels can be treated with QSGW diagrams and the spin channel with DMFT diagrams.

Appendix A: Effective action for the Anderson impurity model

We are dealing with a many-body system in which each site, seen as a function of imaginary time, undergoes transitions between the four possible quantum spin states by exchanging electrons with the rest of the lattice which can be described as a external bath; the dynamics of these processes is encoded in the Weiss function $\mathscr{G}_0(\tau - \tau')$.
In the Anderson Impurity Model the on-site is viewed as an "impurity orbital" and the bath as a "conduction band", the Hamiltonian of the system reads then

$$\hat{H} = \hat{H}_{\text{imp}} + \hat{H}_{\text{bath}} + \hat{H}_{\text{coup}}, \tag{1}$$

with

$$\hat{H}_{\text{imp}} = U\hat{n}_{0\downarrow}\hat{n}_{0\uparrow} + (\epsilon_0 - \mu)\sum_{\sigma}\hat{c}^{\dagger}_{\sigma}\hat{c}_{\sigma}; \tag{2a}$$

$$\hat{H}_{\text{bath}} = \sum_{i,\sigma}\tilde{\epsilon}_i\hat{a}^{\dagger}_{i\sigma}\hat{a}_{i\sigma}; \tag{2b}$$

$$\hat{H}_{\text{coup}} = \sum_{i,\sigma}V_i\left(\hat{a}^{\dagger}_{i\sigma}\hat{c}_{\sigma} + \hat{c}^{\dagger}_{\sigma}\hat{a}_{i\sigma}\right); \tag{2c}$$

where $\hat{c}^{\dagger}_{\sigma}, \hat{c}_{\sigma}$ are the operators describing the impurity orbital ($\hat{n}_{0\downarrow}, \hat{n}_{0\uparrow}$ the spin-dependent occupancies of the site) and $\hat{a}^{\dagger}_{i\sigma}, \hat{a}_{i\sigma}$ the ones describing the conduction

band, $\tilde{\epsilon}_i$ and V_i are the parameters[1] chosen in such a way that the impurity model Green function reproduces the original lattice Hubbard model one.

In order to obtain the expression of the effective action for the impurity model we need to introduce the Grassmann variables through which we will compute the functional integral in the partition function.

Grassmann Variables for fermions

Let c be a fermion annihilation operator, then $c|0\rangle = 0$, the fermion *coherent state* $|\eta\rangle$ is defined as a eigenstate of c:

$$c|\eta\rangle = \eta|\eta\rangle, \tag{3}$$

where the eigenvalue η is the so-called Grassmann number, it belongs to a specific algebra whose elements anticommute with each others but commute with ordinary numbers x_i:

$$\{\eta_1, \eta_2\} = 0;\ \{\eta^\dagger, \eta\} = 0; \tag{4a}$$

$$[\eta, x_i] = 0. \tag{4b}$$

The relation between the Fock space and the Grassmann states is given by

$$|\eta\rangle = (1 - \eta c^\dagger)|0\rangle, \tag{5}$$

constructed in such a way as to recover the definition of the coherent states:

$$c|\eta\rangle = c|0\rangle + \eta c c^\dagger|0\rangle = \eta|0\rangle = \eta(1 - \eta c^\dagger)|0\rangle = \eta|\eta\rangle, \tag{6}$$

[1] In particular the superscript over $\tilde{\epsilon}_i$ indicates that this is an effective parameter not to be confused with the single-particle energies of the original lattice model

where we used $\eta^2 = 0$ since we are dealing with fermion operators.
Moreover, knowing that

$$e^{\eta_1^\dagger \eta_2} = 1 + \eta_1^\dagger \eta_2 + \frac{1}{2!}(\eta_1^\dagger \eta_2)^2 + \cdots = 1 + \eta_1^\dagger \eta_2, \tag{7a}$$

$$e^{-\eta_1^\dagger \eta_2} = 1 - \eta_1^\dagger \eta_2, \tag{7b}$$

that also follows from $\eta^2 = 0$, the overlap between different Fock states is then given by

$$\langle \eta_1 | \eta_2 \rangle = \langle 0 | (1 - c\eta_1^\dagger)(1 - \eta_2 c^\dagger) | 0 \rangle = 1 + \eta_1^\dagger \eta_2 = e^{\eta_1^\dagger \eta_2}. \tag{8}$$

For what concerns the Grassmann integrals the following rules apply:

$$\int d\eta f(\eta + \xi) = \int d\eta f(\eta); \tag{9a}$$

$$\int d\eta = 0; \tag{9b}$$

$$\int d\eta \, \eta = 1. \tag{9c}$$

Completeness relations

It can be proved that the following completeness relation reads for fermion Grassmann variables:

$$\int d\eta^\dagger \int d\eta e^{-\eta^\dagger \eta} |\eta\rangle\langle\eta| = \int d\eta^\dagger \int d\eta (1 - \eta\eta^\dagger) |\eta\rangle\langle\eta| = \not{1}, \tag{10}$$

and similarly the trace of a generic operator O can be written as

$$\mathrm{Tr}[O] = \int d\eta^\dagger \int d\eta e^{-\eta^\dagger \eta} \langle -\eta | O | \eta \rangle. \tag{11}$$

Gaussian Grassmann integrals

Using (7b) with $\eta_1 = \eta, \ \eta_2 = a\eta$, a being a number, we find

$$\begin{aligned}\int d\eta^\dagger \int d\eta e^{-\eta^\dagger a\eta} &= \int d\eta^\dagger \int d\eta(1-\eta^\dagger a\eta) = -\int d\eta^\dagger \int d\eta\ \eta^\dagger a\eta \\ &= a\int d\eta^\dagger\eta^\dagger \int d\eta\ \eta = a = e^{\log(a)}, \end{aligned} \tag{12}$$

and for two Grassmann variables

$$\begin{aligned}&\int d\eta_1^\dagger \int d\eta_1 \int d\eta_2^\dagger \int d\eta_2 e^{-\eta_1^\dagger a_1\eta_1} e^{-\eta_2^\dagger a_2\eta_2} = \\ &\int d\eta_1^\dagger \int d\eta_1 e^{-\eta_1^\dagger a_1\eta_1} \int d\eta_2^\dagger \int d\eta_2 e^{-\eta_2^\dagger a_2\eta_2} = a_1a_2 = e^{\log(a_1)+\log(a_2)}. \end{aligned} \tag{13}$$

The quantity a_1a_2 can be seen as the determinant of a diagonal matrix with a_1 and a_2 on the diagonal, it is then easy to extend this calculation to many variables in matrix notation:

$$\prod_i \int d\eta_i^\dagger \int d\eta_i e^{-\boldsymbol{\eta}^\dagger \mathbf{A}\boldsymbol{\eta}} \equiv \int \mathcal{D}\eta^\dagger \int \mathcal{D}\eta e^{-\boldsymbol{\eta}^\dagger \mathbf{A}\boldsymbol{\eta}} = \det(A) = e^{\mathrm{Tr}(\log(A))}, \tag{14}$$

where we also defined the integration measure $\mathcal{D}\eta^\dagger\mathcal{D}\eta$.
In presence of coupling terms, i.e. linear expressions of the field operator (like in $\hat{H}_{\mathrm{coup}}$), we could deal with integrals like

$$\int d\eta^\dagger \int d\eta e^{-\eta^\dagger a\eta - \eta^\dagger J - J^\dagger\eta}$$

where the coupling term has been expressed in function of the Grassmann source fields $J, J^\dagger$; shifting the origin of integration like in (9*a*) one finds

$$\begin{aligned}\int d\eta^\dagger \int d\eta e^{-\eta^\dagger a\eta - \eta^\dagger J - J^\dagger\eta} &= \int d\eta^\dagger \int d\eta e^{-(\eta^\dagger + J^\dagger a^{-1})a(\eta + a^{-1}J) + J^\dagger a^{-1}J} \\ &= ae^{J^\dagger a^{-1}J}, \end{aligned} \tag{15}$$

and the generalization to many Grassmann variables in matrix notation reads

$$\begin{aligned}\int d\eta^\dagger \int d\eta e^{-\boldsymbol{\eta}^\dagger \boldsymbol{A}\boldsymbol{\eta}-\boldsymbol{\eta}^\dagger \boldsymbol{J}-\boldsymbol{J}^\dagger \boldsymbol{\eta}} &= \int d\eta^\dagger \int d\eta e^{-(\boldsymbol{\eta}^\dagger+\boldsymbol{J}^\dagger \boldsymbol{A}^{-1})\boldsymbol{A}(\boldsymbol{\eta}+\boldsymbol{A}^{-1}\boldsymbol{J})+\boldsymbol{J}^\dagger \boldsymbol{A}^{-1}\boldsymbol{J}} \\ &= \det(A) e^{\boldsymbol{J}^\dagger \boldsymbol{A}^{-1}\boldsymbol{J}}. \end{aligned} \tag{16}$$

Effective action in the Grassmann algebra

As is well known, the partition function is defined through the Hamiltonian of the system via

$$Z = \mathrm{Tr}(e^{-\beta H}). \tag{17}$$

Let's start with the Hamiltonian for a single spinless fermion state

$$\hat{H} = \epsilon\, c^\dagger c, \tag{18}$$

it is useful to express the exponential through the product

$$e^{-\beta H} = \lim_{N_\tau \to \infty} \prod_{i=1}^{N_\tau} e^{-\Delta\tau_i H}, \tag{19}$$

with $\tau = \beta/N_\tau$, and we will assume that in the limit $N_\tau \to \infty$ (i.e. $\Delta\tau \to 0$) the exponentials of sums of operators can be rewritten as a product of exponentials. To evaluate the trace in Z, we will use the definition (11) and insert the completeness relation (10) between each term of the product[1]

$$Z = \mathrm{Tr}\left[e^{-\Delta\tau H}\mathbb{1}_1 e^{-\Delta\tau H}\mathbb{1}_2 \cdots e^{-\Delta\tau H}\right] \tag{20}$$

[1] in case of time-dependent Hamiltonian the different terms of the product will depend on the time interval considered: $e^{-\Delta\tau H(\tau_n)} e^{-\Delta\tau H(\tau_{n+1})} \ldots$

where $\mathbb{1}_i \equiv \int d\eta_i^\dagger \int d\eta_i e^{-\eta_i^\dagger \eta_i} |\eta_i\rangle\langle\eta_i|$.
Provided that, following (11), $\eta_\beta = \eta_{N_\tau} = -\eta_0$ we find

$$\begin{aligned} Z &= \lim_{N_\tau\to\infty} \int \mathcal{D}\eta^\dagger \int \mathcal{D}\eta\, e^{-\eta_\beta^\dagger \eta_\beta} \langle \eta_\beta | e^{-\Delta\tau_{N_\tau} \epsilon c^\dagger c} | \eta_{N_{\tau-1}} \rangle e^{-\eta_{N_{\tau-1}}^\dagger \eta_{N_{\tau-1}}} \langle \eta_{N_{\tau-1}} | \\ &\quad \ldots |\eta_1\rangle e^{-\eta_1^\dagger \eta_1} \langle \eta_1 | e^{-\Delta\tau_1 \epsilon c^\dagger c} | \eta_0 \rangle \\ &= \lim_{N_\tau\to\infty} \int \mathcal{D}\eta^\dagger \int \mathcal{D}\eta\, e^{-\eta_\beta^\dagger \eta_\beta} \langle \eta_\beta | \eta_{N_{\tau-1}} \rangle e^{-\Delta\tau\epsilon\, \eta_\beta^\dagger \eta_{N_{\tau-1}}} e^{-\eta_{N_{\tau-1}}^\dagger \eta_{N_{\tau-1}}} \langle \eta_{N_{\tau-1}} | \\ &\quad \ldots |\eta_1\rangle e^{-\eta_1^\dagger \eta_1} \langle \eta_1 | \eta_0 \rangle e^{-\Delta\tau\epsilon\, \eta_1^\dagger \eta_0}. \end{aligned} \tag{21}$$

Using (8) to evaluate the overlap of fermion coherent states we can write as follows

$$e^{-\eta_1^\dagger \eta_1} \langle \eta_1 | \eta_0 \rangle = e^{-\eta_1^\dagger \eta_1 + \eta_1^\dagger \eta_0} = e^{-\eta_1^\dagger (\eta_1 - \eta_0)} = e^{-\eta_1^\dagger \frac{\partial}{\partial\tau} \eta_1 \Delta\tau} \tag{22}$$

and, in leading order in $\Delta\tau$, take the approximation $\eta_1^\dagger \eta_0 \Delta\tau \sim \eta_0^\dagger \eta_0 \Delta\tau$ (and similarly for the other terms).
Performing the time limit we obtain

$$\lim_{N_\tau\to\infty} \eta_{N_\tau}^\dagger (\frac{\partial}{\partial\tau} + \epsilon) \eta_{N_\tau} \Delta\tau + \cdots + \eta_0^\dagger (\frac{\partial}{\partial\tau} + \epsilon) \eta_0 \Delta\tau = \int_0^\beta d\tau \eta^\dagger(\tau) (\frac{\partial}{\partial\tau} + \epsilon) \eta(\tau), \tag{23}$$

and we can then rewrite the partition function as

$$Z = \int \mathcal{D}\eta^\dagger \int \mathcal{D}\eta\, e^{-S}, \tag{24}$$

where, in analogy with the Lagrangian formalism, we introduced the action of the system, which reads

$$S = \int_0^\beta d\tau\, \eta^\dagger(\tau) (\frac{\partial}{\partial\tau} + \epsilon) \eta(\tau). \tag{25}$$

So far we presented a general procedure to calculate the effective action of the system starting from the partition function in the Grassmann algebra formalism.

We are then now able to apply this method to the derivation of the effective action for the Anderson Impurity Model (AIM) Hamiltonian.

Anderson Impurity Model

The partition function for AIM Hamiltonian (1) reads

$$
\begin{aligned}
Z &= \int \mathcal{D}\psi^\dagger \int \mathcal{D}\psi \; e^{-S_{\text{imp}}(\psi,\psi^\dagger)} \int \mathcal{D}\eta^\dagger \int \mathcal{D}\eta \; e^{-S_{\text{bath}}(\eta,\eta^\dagger)} \; e^{-S_{\text{coup}}(\psi,\psi^\dagger,\eta,\eta^\dagger)} \\
&= \int \mathcal{D}\psi^\dagger \int \mathcal{D}\psi \exp\left[- \int d\tau \sum_\sigma \psi^\dagger_\sigma(\tau) \mathcal{G}_0^{-1}(\tau) \psi_\sigma(\tau) + U \psi^\dagger_\uparrow(\tau)\psi_\uparrow(\tau)\psi^\dagger_\downarrow(\tau)\psi_\downarrow(\tau) \right] \\
&\qquad \cdot \int \mathcal{D}\eta^\dagger \int \mathcal{D}\eta \exp\left[- \int d\tau \sum_{i,\sigma} \eta^\dagger_{i,\sigma}(\tau) \mathcal{G}^{-1}_{b,i}(\tau) \eta_{i,\sigma}(\tau) \right] \\
&\qquad \cdot \exp\left[- \int d\tau \sum_{i,\sigma} V_i \left(\eta^\dagger_{i,\sigma}(\tau)\psi_\sigma(\tau) + \psi^\dagger_\sigma(\tau)\eta_{i,\sigma}(\tau) \right) \right],
\end{aligned} \tag{26}
$$

where $\psi_\sigma(\tau)$ and $\eta_{i,\sigma}(\tau)$ are the Grassmann variables referred respectively to the impurity and the bath fermions, whereas the Green functions for both variables are defined as

$$
\begin{aligned}
\mathcal{G}_0^{-1}(\tau) &\equiv \frac{\partial}{\partial\tau} + \epsilon_0 - \mu \; ; \\
\mathcal{G}^{-1}_{b,i}(\tau) &\equiv \frac{\partial}{\partial\tau} + \tilde{\epsilon}_i \; .
\end{aligned} \tag{27}
$$

In order to solve the bath functional integral we can identify the source fields in the Gaussian Grassmann integral (15) as

$$
J_{\sigma,i}(\tau) = V_i \psi_\sigma(\tau), \tag{28}
$$

and then integrate on the bath degrees of freedom to obtain

$$\int \mathcal{D}\eta^\dagger \int \mathcal{D}\eta \ \exp\left[-\int d\tau \sum_{i,\sigma} \eta^\dagger_{i,\sigma}(\tau)\mathcal{G}^{-1}_{b,i}(\tau)\eta_{i,\sigma}(\tau) + \eta^\dagger_{i,\sigma}(\tau)J_{\sigma,i}(\tau) + J^\dagger_{\sigma,i}(\tau)\eta_{i,\sigma}(\tau)\right]$$
$$= \det(\mathcal{G}_b^{-1})e^{\mathbf{J}^\dagger(\mathcal{G}_b^{-1})^{-1}\mathbf{J}} = \exp[\mathrm{Tr}\log(\mathcal{G}_b^{-1})]e^{\mathbf{J}^\dagger\left(\mathcal{G}_b^{-1}\right)^{-1}\mathbf{J}}. \tag{29}$$

We can shift from time-dependency to frequency-dependency defining the Fourier transform according to

$$A(i\omega_n) \equiv \int_0^\beta d\tau e^{i\omega_n\tau}A(\tau), \tag{30a}$$
$$A(\tau) \equiv \frac{1}{\beta}\sum_n d\tau e^{-i\omega_n\tau}A(i\omega_n), \tag{30b}$$

where $\omega_n = \frac{(2n+1)\pi}{\beta}$ is the so called Matsubara frequency, which is discrete and imaginary.
The argument of the exponential of (29) as a function of Matsubara frequency reads

$$\mathbf{J}^\dagger\mathcal{G}_b(i\omega_n)\mathbf{J} \equiv \sum_i \mathbf{J}^\dagger\mathcal{G}_{b,i}(i\omega_n)\mathbf{J} = \sum_\sigma \psi^\dagger_\sigma(i\omega_n)\left(\sum_i \frac{-V_i^2}{i\omega_n - \tilde{\epsilon}_i}\right)\psi_\sigma(i\omega_n)$$
$$= -\sum_\sigma \psi^\dagger_\sigma(i\omega_n)\Delta(i\omega_n)\psi_\sigma(i\omega_n), \tag{31}$$

where we defined the Hybridization function according to

$$\Delta(i\omega_n) \equiv \sum_i \frac{V_i^2}{i\omega_n - \tilde{\epsilon}_i}\,, \tag{32}$$

equivalent to (3.9), which is meant as a proper definition of.
Referring to (26) for the definition of $S_{\rm imp}$ we find

$$\begin{aligned} Z &= \exp[\mathrm{Tr}\log(\mathcal{G}_b^{-1})]\int\mathcal{D}\psi^\dagger\int\mathcal{D}\psi\, e^{-S_{\rm imp}+\mathbf{J}^\dagger\left(\mathcal{G}_b^{-1}\right)^{-1}\mathbf{J}} \\ &= \exp[\mathrm{Tr}\log(\mathcal{G}_b^{-1})]\int\mathcal{D}\psi^\dagger\int\mathcal{D}\psi\, e^{-S_{\rm eff}}, \end{aligned} \tag{33}$$

where we introduced the effective action of the system as

$$S_{\rm eff} = -\sum_{n,\sigma}\psi_\sigma^\dagger(i\omega_n)\mathscr{G}_0(i\omega_n)\psi_\sigma(i\omega_n) + U\int_0^\beta d\tau\psi_\uparrow^\dagger(\tau)\psi_\uparrow(\tau)\psi_\downarrow^\dagger(\tau)\psi_\downarrow(\tau). \tag{34}$$

The function $\mathscr{G}_0(i\omega_n)$ appearing in the previous equation is just the Weiss dynamical mean-field which explicitely reads

$$\mathscr{G}_0^{-1}(i\omega_n) = i\omega_n + \mu - \epsilon_0 - \Delta(i\omega_n), \tag{35}$$

and is related to the local Green-function $G(\tau-\tau') = -\langle c(\tau)c^\dagger(\tau'\rangle_{S_{\rm eff}}$ via the self-consistency relation

$$\Sigma_{\rm imp}(i\omega_n) = \mathscr{G}_0^{-1}(i\omega_n) - G^{-1}(i\omega_n), \tag{36}$$

where $\Sigma_{\rm imp}(i\omega_n)$ is the local impurity model self-energy.

Appedix B: Derivation of the impurity level

We will now present a derivation of the impurity level in the full self-consistent QSGW+DMFT loop of sec. 4.2, and in the one-shot scheme of sec. 4.3. The definition undergoes the following statement: by definition the hybridization function has to vanish in the high-frequency limit, therefore the $E^{\text{imp}}_{LL'}$ changes to ensure this condition is satisfied: $\Delta_{LL'}(\omega \to \infty) = 0$.

The limit in the full-consistent cycle

After N iterations of the QSGW+DMFT loop, we require the validity of the DMFT self-consistent condition (4.17), that is we want the local Green's function

$$G^{\text{loc}}_{LL'}(\omega) = \sum_{i\mathbf{k}} U^{i\mathbf{k}}_{L} \frac{1}{i\omega + \mu - \varepsilon^{0}_{i\mathbf{k}}} U^{i\mathbf{k}\dagger}_{L'} \tag{37}$$

to coincide with the impurity Green's function

$$G^{\text{imp}}_{LL'}(\omega) = \left[i\omega - E^{\text{imp}} - \Sigma^{\text{imp}}(\omega) - \Delta(\omega)\right]^{-1}_{LL'} = \left[(G^{0,\text{imp}}_{LL'}(\omega))^{-1} - \Sigma^{\text{imp}}(\omega)\right]^{-1}_{LL'}. \tag{38}$$

where $G^{0,\text{imp}}_{LL'}(\omega)$ is non-interacting impurity Green's function of the first iteration. All the functions are defined on the imaginary axis (Matsubara frequencies), we will drop the index n in ω_n for convenience.

The local Green's function $G^{\text{loc}}_{LL'}(\omega)$ is the projection of the lattice Green's function $G_{i\mathbf{k}}(\omega)$ which is diagonal in the band components. It is obtained from the eigenvalues $\varepsilon^0_{i\mathbf{k}} = \varepsilon^H_{i\mathbf{k}} + \Sigma^0_{i\mathbf{k}}$ and the eigenstates $\psi^0_{i\mathbf{k}}(\mathbf{r})$ of the Hamiltonian $H^0_{ij\mathbf{k}}$. None of these quantities is energy-dependent as the Hamiltonian $H^0_{ij\mathbf{k}}$ is not, hence the energy-dependence is explicitly given by the factor $i\omega$. Since we are working in the full self-consistent scheme, the Hamiltonian comes from the quasiparticlization of the GW self-energy corrected with the impurity self-energy, but it could be obtained from a hybrid calculation, Hartree-Fock or even DFT.
Inverting eq. (38) to express the hybridization function $\Delta_{LL'}(\omega)$ we notice it depends on three quantities (which have non-zero real components): the impurity Green's function $G^{\text{imp}}_{LL'}(\omega)$: the impurity level $E^{\text{imp}}_{LL'}$, the impurity self-energy $\Sigma^{\text{imp}}_{LL'}(\omega)$. The sum of these elements has to vanish in the high-energy limit by definition of hybridization function. In the same limit $\Sigma^{\text{imp}}_{LL'}(\omega)$ is real, for this reason it is convenient to write $\Sigma^{\text{imp}}(\omega) = \Sigma^{\text{imp}}(\infty) + \tilde{\Sigma}^{\text{imp}}(\omega)$ as in sec. 4.2 with the latter matrix vanishing at $\omega = \infty$.
Let us take now the $\omega \to \infty$ limit of expression (37). Making a change of variable $z = 1/\omega$, the high-frequency limit coincides with $z \to 0^+$. For each $i\mathbf{k}$ pair, μ and $\varepsilon^0_{i\mathbf{k}}$ are constant functions of the frequency. Let $f_{i\mathbf{k}}(z) = \frac{1}{i/z + c_{i\mathbf{k}}} = \frac{z}{i + z c_{i\mathbf{k}}}$ with $c_{i\mathbf{k}} = \mu - \varepsilon^0_{i\mathbf{k}}$, then the expansion of $f_{i\mathbf{k}}(z)$ around small positive values of z reads

$$\begin{aligned} f_{i\mathbf{k}}(z) &= f(0) + z \left.\frac{df_{i\mathbf{k}}}{dz}\right|_0 + \frac{z^2}{2} \left.\frac{d^2 f_{i\mathbf{k}}}{dz^2}\right|_0 + \mathcal{O}(z^3) \\ &\approx 0 - iz + c_{i\mathbf{k}} z^2 + \mathcal{O}(z^3) \, . \end{aligned} \tag{39}$$

Using the fact that $z = 1/\omega$ and the definition of $c_{i\mathbf{k}}$, one finally gets the high-energy expansion of the local Green's function

$$\begin{aligned} G^{\text{loc}}_{LL'}(\omega) &\xrightarrow{\omega\to\infty} \sum_{i\mathbf{k}} U^{i\mathbf{k}}_L \left[-\frac{i}{\omega} + \frac{1}{\omega^2}(\mu - \varepsilon^0_{i\mathbf{k}}) \right] U^{i\mathbf{k}\dagger}_{L'} \\ &= -\frac{i}{\omega}\delta_{LL'} + \frac{\mu\delta_{LL'} - \sum_{i\mathbf{k}} U^{i\mathbf{k}}_L \varepsilon^0_{i\mathbf{k}} U^{i\mathbf{k}\dagger}_{L'}}{\omega^2} \, , \end{aligned} \tag{40}$$

where we used the fact that $\sum_{i\mathbf{k}} U_L^{i\mathbf{k}}\, c\, U_{L'}^{i\mathbf{k}\dagger} = \delta_{LL'}\, c$ for any complex number c. Let us now take the same limit for the right-hand side of equation (38). It is less straightforward since all the quantities in the expression are actually matrices. However one can make use of the exact Taylor expansion (geometric series)

$$(\mathbf{1}+\mathbf{A})^{-1} = \sum_{n=0}^{\infty}(-\mathbf{A})^n = \mathbf{1}-\mathbf{A}+\mathcal{O}(\mathbf{A}^2)\,. \tag{41}$$

Let us now rewrite the impurity Green's function

$$\begin{aligned} G^{\mathrm{imp}}_{LL'}(\omega) &= \left[i\omega - E^{\mathrm{imp}} - \Sigma^{\mathrm{imp}}(\omega) - \Delta(\omega)\right]^{-1}_{LL'} \\ &= \frac{1}{i\omega}\left[\mathbf{1} + \frac{iE^{\mathrm{imp}}}{\omega} + \frac{i\Sigma^{\mathrm{imp}}(\omega)}{\omega} + \frac{i\Delta(\omega)}{\omega}\right]^{-1}_{LL'}\,. \end{aligned} \tag{42}$$

Calling $\mathbf{A} = i\left(E^{\mathrm{imp}} + \Sigma^{\mathrm{imp}}(\omega) + \Delta(\omega)\right)/\omega$, then we can expand expression (42) using relation (41). In the high energy limit, the matrix $\mathbf{A}$ will be small enough for the expansion to be truncated at the first order. Moreover, we recall that $\Delta_{LL'}(\omega\to\infty) = 0$ and $\Sigma^{\mathrm{imp}}_{LL'}(\omega\to\infty) = \Sigma^{\mathrm{imp}}_{LL'}(\infty)$. The resulting high energy limit of the impurity Green's function reads

$$G^{\mathrm{imp}}_{LL'}(\omega) \xrightarrow{\omega\to\infty} -\frac{i}{\omega}\delta_{LL'} - \frac{E^{\mathrm{imp}}_{LL'} + \Sigma^{\mathrm{imp}}_{LL'}(\infty)}{\omega^2} \tag{43}$$

The self-consistent condition at high energy is obtained by equating expressions (40) and (43)

$$-\frac{i}{\omega}\delta_{LL'} + \frac{\mu\delta_{LL'} - \sum_{i\mathbf{k}} U_L^{i\mathbf{k}}\varepsilon^0_{i\mathbf{k}}U_{L'}^{i\mathbf{k}\dagger}}{\omega^2} = -\frac{i}{\omega}\delta_{LL'} - \frac{E^{\mathrm{imp}}_{LL'} + \Sigma^{\mathrm{imp}}_{LL'}(\infty)}{\omega^2}\,, \tag{44}$$

which leads to the following definition of the impurity level in the full self-consistent scheme (getting to the expression given in eq. (4.18)):

$$E^{\mathrm{imp}}_{LL'} = \sum_{i\mathbf{k}} U_L^{i\mathbf{k}}\varepsilon^0_{i\mathbf{k}}U_{L'}^{i\mathbf{k}\dagger} - \mu\delta_{LL'} - \Sigma^{\mathrm{imp}}_{LL'}(\infty)\,. \tag{45}$$

The limit in the one-shot scheme

In the one-shot QSGW+DMFT scheme, the local Green's function is extracted from a projection of the lattice Green's function given by (4.24):

$$G_{ij\mathbf{k}}(\omega_n) = \left(\left[i\omega_n + \mu - \varepsilon_{i\mathbf{k}}^{QSGW} \right] \delta_{ij} - \bar{\Sigma}_{ij\mathbf{k}}(\omega_n) \right)^{-1} . \tag{46}$$

So, when evaluating $G^{\text{imp}}_{LL'} = G^{\text{loc}}_{LL'}$ in the high-energy limit, new terms will appear with respect to definition (45).
The high-frequency limit of the local Green's function obtained projecting (46) reads as follows:

$$G^{\text{loc}}_{LL'}(\omega) \xrightarrow{\omega\to\infty} \sum_{ij\mathbf{k}} U_L^{i\mathbf{k}} \left[\frac{1}{i\omega} \left(\delta_{ij} - \frac{\mu\delta_{ij} - \delta_{ij}\varepsilon_{i\mathbf{k}}^{QSGW} - \bar{\Sigma}_{ij\mathbf{k}}(\infty)}{i\omega} \right) \right] U_{L'}^{j\mathbf{k}\dagger} \tag{47}$$

where in the last passage the geometric series (41) has been truncated at the first order. Working out all the expressions above, $G^{\text{loc}}_{LL'}(\infty)$ reads

$$G^{\text{loc}}_{LL'}(\infty) \approx -\frac{i}{\omega}\delta_{LL'} + \frac{\mu}{\omega^2}\delta_{LL'} - \frac{1}{\omega^2}\sum_{i\mathbf{k}} U_L^{i\mathbf{k}} \varepsilon_{i\mathbf{k}}^{QSGW} U_{L'}^{i\mathbf{k}\dagger} - \frac{1}{\omega^2}\sum_{ij\mathbf{k}} U_L^{i\mathbf{k}} \bar{\Sigma}_{ij\mathbf{k}}(\infty) U_{L'}^{j\mathbf{k}\dagger} \tag{48}$$

where we used $\sum_{i\mathbf{k}} U_L^{i\mathbf{k}} U_{L'}^{i\mathbf{k}\dagger} = \delta_{LL'}$. The $\bar{\Sigma}$ is a result of an embedding procedure (see eq. (4.13)) which is reported here:

$$\bar{\Sigma}_{ij\mathbf{k}}(\omega) = \sum_{MM'} U_M^{i\mathbf{k}\dagger} \left(\Sigma^{\text{imp}}_{MM'}(\omega) - \Sigma^{DC}_{MM'}(\omega) \right) U_{M'}^{j\mathbf{k}} . \tag{49}$$

This equation contains a DC term which is indicated as explicitly dynamical (differently from what we have done in sec. 4.2). This notation makes the derivation more general, anyway the same conclusion would be reached for a static DC correction.

At self-consistency, the quantity (48) is equal to (43), that is

$$\begin{aligned} -\frac{i}{\omega}\delta_{LL'} + \frac{\mu}{\omega^2}\delta_{LL'} - \frac{1}{\omega^2}\sum_{i\mathbf{k}} U_L^{i\mathbf{k}}\varepsilon_{i\mathbf{k}}^{QSGW}U_{L'}^{i\mathbf{k}\dagger} - \frac{1}{\omega^2}\sum_{ij\mathbf{k}} U_L^{i\mathbf{k}}\bar{\Sigma}_{ij\mathbf{k}}(\infty)U_{L'}^{j\mathbf{k}\dagger} = \\ = -\frac{i}{\omega}\delta_{LL'} - \frac{E_{LL'}^{\text{imp}} + \Sigma_{LL'}^{\text{imp}}(\infty)}{\omega^2}\,, \end{aligned} \tag{50}$$

which leads to the definition of $E_{LL'}^{\text{imp}}$

$$E_{LL'}^{\text{imp}} = \sum_{i\mathbf{k}} U_L^{i\mathbf{k}}\varepsilon_{i\mathbf{k}}^{QSGW}U_{L'}^{i\mathbf{k}\dagger} + \sum_{ij\mathbf{k}} U_L^{i\mathbf{k}}\bar{\Sigma}_{ij\mathbf{k}}(\infty)U_{L'}^{j\mathbf{k}\dagger} - \Sigma_{LL'}^{\text{imp}}(\infty) - \mu\delta_{LL'}\,. \tag{51}$$

We can simplify this expression even further by using the relation $\hat{P}\cdot\hat{E} = I$ between projection and embedding. It follows that

$$\begin{aligned} \sum_{ij\mathbf{k}} U_L^{i\mathbf{k}}\bar{\Sigma}_{ij\mathbf{k}}(\infty)U_{L'}^{j\mathbf{k}\dagger} &= \sum_{ijMM'\mathbf{k}} U_L^{i\mathbf{k}}U_M^{i\mathbf{k}\dagger}\left(\Sigma_{MM'}^{\text{imp}}(\infty) - \Sigma_{MM'}^{DC}(\infty)\right)U_{M'}^{j\mathbf{k}}U_{L'}^{j\mathbf{k}\dagger} \\ &= \sum_{MM'}\delta_{LM}\left(\Sigma_{MM'}^{\text{imp}}(\infty) - \Sigma_{MM'}^{DC}(\infty)\right)\delta_{M'L'} \\ &= \Sigma_{LL'}^{\text{imp}}(\infty) - \Sigma_{LL'}^{DC}(\infty) \end{aligned} \tag{52}$$

which inserted into (51) gives the following definition of the impurity level in the one-shot scheme:

$$E_{LL'}^{\text{imp}} = \sum_{i\mathbf{k}} U_L^{i\mathbf{k}}\varepsilon_{i\mathbf{k}}^{QSGW}U_{L'}^{i\mathbf{k}\dagger} - \Sigma_{LL'}^{DC}(\infty) - \mu\delta_{LL'} \tag{53}$$

which coincides with the expression given in eq. (4.25).

References

[1] O. K. Andersen. Linear methods in band theory. *Phys. Rev. B*, **12**:3060, 1975. 18

[2] P. W. Anderson. Localized magnetic states in metals. *Phys. Rev.*, **124**:41, 1961. 48

[3] P. W. Anderson. The Resonating Valence Bond State in La2CuO4 and Superconductivity. *Science*, **235**:1196, 1987. 102

[4] V I Anisimov, A I Poteryaev, M A Korotin, A O Anokhin, and G Kotliar. First-principles calculations of the electronic structure and spectra of strongly correlated systems: Dynamical Mean Field Theory. *Journal of Physics: Condensed Matter*, **9**:7359, 1997. 57

[5] V. I. Anisimov, J. Zaanen, and O. K. Andersen. Band theory and Mott insulators: Hubbard U instead of Stoner I. *Phys. Rev. B*, **44**:943, 1991. 55

[6] V.I. Anisimov, F. Aryasetiawan, and A.I. Lichtenstein. First-principles calculations of the electronic structure and spectra of strongly correlated systems: the lda+ u method. *Journal of Physics: Condensed Matter*, **9**[4]:767, 1997. 55

[7] F. Aryasetiawan and O. Gunnarsson. The GW method. *Reports on Progress in Physics*, **61**:237, 1998. 36, 40

[8] F. Aryasetiawan, L. Hedin, and K. Karlsson. Multiple plasmon satellites in na and al spectral functions from *Ab Initio* cumulant expansion. *Phys. Rev. Lett.*, **77**:2268, 1996. 39

[9] Ashcroft and Mermin. *Solid State Physics*. Hartcourt College Publishers, New York, 1976. 9

[10] Th. Ayral, P. Werner, and S. Biermann. Spectral properties of correlated materials: Local vertex and nonlocal two-particle correlations from combined *gw* and dynamical mean field theory. *Phys. Rev. Lett.*, **109**:226401, 2012. 5

[11] K. D. Belashchenko, V. P. Antropov, and N. E. Zein. Self-consistent local gw method: Application to 3*d* and 4*d* metals. *Phys. Rev. B*, **73**:073105, 2006. 4, 118, 130

[12] S. Biermann, F. Aryasetiawan, and A. Georges. First-Principles Approach to the Electronic Structure of Strongly Correlated Systems: Combining the *GW* Approximation and Dynamical Mean-Field Theory. *Phys. Rev. Lett.*, **90**:086402, 2003. 5, 60, 61, 82, 115, 121, 124

[13] P. Blaha, K. Schwarz, G. K. H. Madsen, D. Kvasnicka, and J. Luitz. *WIEN2K, An Augmented Plane Wave + Local Orbitals Program for Calculating Crystal Properties*. Karlheinz Schwarz, Techn. Universität Wien, Austria, 2001. 66, 98

[14] F. Bruneval, N. Vast, and L. Reining. Effect of self-consistency on quasiparticles in solids. *Phys. Rev. B*, **74**:045102, 2006. 40

[15] R. Bulla, T. A. Costi, and T. Pruschke. Numerical renormalization group method for quantum impurity systems. *Rev. Mod. Phys.*, **80**:395, 2008. 52

[16] M. Casula, A. Rubtsov, and S. Biermann. Dynamical screening effects in correlated materials: Plasmon satellites and spectral weight transfers from a green's function ansatz to extended dynamical mean field theory. *Phys. Rev. B*, **85**:035115, 2012. 76

[17] M. Casula, P. Werner, L. Vaugier, F. Aryasetiawan, T. Miyake, A. J. Millis, and S. Biermann. Low-energy models for correlated materials: Bandwidth renormalization from coulombic screening. *Phys. Rev. Lett.*, **109**:126408, 2012. 76

[18] A. N. Chantis, M. van Schilfgaarde, and Takao Kotani. Quasiparticle self-consistent GW method applied to localized $4f$ electron systems. *Phys. Rev. B*, **76**:165126, 2007. 112, 131

[19] S. Choi, A. Kutepov, K. Haule, M. van Schilfgaarde, and G. Kotliar. Matsubara QSGW+DMFT: application to Mott insulator La2CuO4. *arXiv:1504.07569*, 2015. 65, 76, 102, 104, 107, 110, 122, 129, 130

[20] A. Comanac, L. De' Medici, M. Capone, and A. J. Millis. Optical conductivity and the correlation strength of high-temperature copper-oxide superconductors. *Nat. Phys.*, **4**:287, 2008. 101, 102, 129

[21] S. L. Cooper, G. A. Thomas, A. J. Millis, P. E. Sulewski, J. Orenstein, D. H. Rapkine, S-W. Cheong, and P. L. Trevor. Optical studies of gap, exchange, and hopping energies in the insulating cuprates. *Phys. Rev. B*, **42**:10785, 1990. 102, 110, 129

[22] L. de' Medici, J. Mravlje, and A. Georges. Janus-faced influence of hund's rule coupling in strongly correlated materials. *Phys. Rev. Lett.*, **107**:256401, 2011. 12

[23] R. Del Sole, L. Reining, and R. W. Godby. GW Γ approximation for electron self-energies in semiconductors and insulators. *Phys. Rev. B*, **49**:8024, 1994. 39

[24] W. Eberhardt and E. W. Plummer. Angle-resolved photoemission determination of the band structure and multielectron excitations in ni. *Phys. Rev. B*, **21**:3245, 1980. 120

[25] V. J. Emery. Theory of high-T_c superconductivity in oxides. *Phys. Rev. Lett.*, **58**:2794, 1987. 101, 102

[26] S. V. Faleev, M. van Schilfgaarde, and T. Kotani. All-electron self-consistent *gw* approximation: Application to si, mno, and nio. *Phys. Rev. Lett.*, **93**:126406, 2004. 131

[27] Q. Feng. *Study of single impurity Anderson model and dynamical mean field theory based on equation-of-motion method.* PhD thesis, GoetheUniversit, Frankfurt, 2009. 48

[28] E. Fermi. Un metodo statistico per la determinazione di alcune prioprietà dell'atomo. *Rend. Accad. Naz. Linzei*, **6**:602, 1927. 13

[29] A. Georges. Strongly correlated electron materials : Dynamical mean field theory and electronic structure. *Lectures on the physics of highly correlated electron systems VI*, **715**, 2004. 11, 12, 47, 52

[30] A. Georges and G. Kotliar. Hubbard model in infinite dimensions. *Phys. Rev. B*, **45**:6479–6483, 1992. 45, 52

[31] A. Georges, G. Kotliar, W. Krauth, and M. J. Rozenberg. Dynamical mean-field theory of strongly correlated fermion systems and the limit of infinite dimensions. *Rev. Mod. Phys.*, **68**:13, 1996. 3, 45, 56

[32] J. M. Ginder, M. G. Roe, Y. Song, R. P. McCall, J. R. Gaines, E. Ehrenfreund, and A. J. Epstein. Photoexcitations in la_2cuo_4: 2-ev energy gap and long-lived defect states. *Phys. Rev. B*, **37**:7506, 1988. 102, 110, 129

[33] R. W. Godby, M. Schlüter, and L. J. Sham. Self-energy operators and exchange-correlation potentials in semiconductors. *Phys. Rev. B*, **37**:10159, 1988. 31

[34] J. E. Gubernatis, M. Jarrell, R. N. Silver, and D. S. Sivia. Quantum monte carlo simulations and maximum entropy: Dynamics from imaginary-time data. *Phys. Rev. B*, **44**:6011, 1991. 78

[35] E. Gull, A. J. Millis, A. I. Lichtenstein, A. N. Rubtsov, M. Troyer, and P. Werner. Continuous-time monte carlo methods for quantum impurity models. *Rev. Mod. Phys.*, **83**:349–404, 2011. 52

[36] K. Haule. Private communication. 65, 76

[37] K. Haule. Exact double counting in combining the dynamical mean field theory and the density functional theory. *Phys. Rev. Lett.*, **115**:196403, 2015. 59

[38] K. Haule, T. Birol, and G. Kotliar. Covalency in transition-metal oxides within all-electron dynamical mean-field theory. *Phys. Rev. B*, **90**:075136, 2014. 101, 102, 114, 129

[39] K. Haule, C.H. Yee, and K. Kim. Dynamical mean-field theory within the full-potential methods: Electronic structure of ceirin$_5$, cecoin$_5$, and cerhin$_5$. *Phys. Rev. B*, **81**:195107, 2010. 65, 66, 67, 69, 85, 90, 97

[40] L. Hedin. New method for calculating the one-particle Green's function with application to the electron-gas problem. *Phys. Rev.*, **139**:A796, 1965. 3, 33, 35, 40

[41] K. Held. Electronic structure calculations using Dynamical Mean Field Theory. *Advances in Physics*, **56**:829, 2007. 57

[42] K. Held, G. Keller, V. Eyert, D. Vollhardt, and V. I. Anisimov. Mott-Hubbard Metal-Insulator Transition in Paramagnetic V_2O_3: An $LDA + DMFT$(QMC) study. *Phys. Rev. Lett.*, **86**:5345, 2001. 57

[43] K. Held, C. Taranto, G. Rohringer, and A. Toschi. Hedin equations, gw, gw+dmft, and all that. *arXiv:1109.3972*, **56**, 2011. 37

[44] F. J. Himpsel, J. A. Knapp, and D. E. Eastman. Experimental energy-band dispersions and exchange splitting for ni. *Phys. Rev. B*, **19**:2919, 1979. 115, 116, 119, 120, 123, 124

[45] J. E. Hirsch and R. M. Fye. Monte carlo method for magnetic impurities in metals. *Phys. Rev. Lett.*, **56**:2521, 1986. 52

[46] P. Hohenberg and W. Kohn. Inhomogeneous electron gas. *Phys. Rev.*, **136**:B864, 1964. 14, 15

[47] B. Holm and U. von Barth. Fully self-consistent GW self-energy of the electron gas. *Phys. Rev. B*, **57**:2108, 1998. 3, 39

[48] J. Hubbard. Electron correlations in narrow energy bands. *Proceedings of the Royal Society of London A: Mathematical, Physical and Engineering Sciences*, **276**:238, 1963. 2, 47, 52

[49] M. S. Hybertsen and S. G. Louie. First-principles theory of quasiparticles: Calculation of band gaps in semiconductors and insulators. *Phys. Rev. Lett.*, **55**:1418, 1985. 38

[50] M. S. Hybertsen and S. G. Louie. Electron correlation in semiconductors and insulators: Band gaps and quasiparticle energies. *Phys. Rev. B*, **34**:5390, 1986. 40

[51] M. Imada, A. Fujimori, and Y. Tokura. Metal-insulator transitions. *Rev. Mod. Phys.*, **70**:1039, 1998. 21

[52] M. Imada and T. Miyake. Electronic structure calculation by first principles for strongly correlated electron systems. *Journal of the Physical Society of Japan*, **79**:112001, 2010. 20

[53] A. Ino. *Photoemission Study of the High-Temperature Superconductor* $La_{2x}Sr_xCuO_4$. PhD thesis, Tokyo University, 1999. 107

[54] S. Ismail-Beigi. Justifying quasiparticle self-consistent schemes via gradient optimization in Luttinger-Ward theory. *arXiv:1406.0772*, 2014. 43

[55] K. Karlsson and F. Aryasetiawan. Spin-wave excitation spectra of nickel and iron. *Phys. Rev. B*, **62**:3006, 2000. 119

[56] K. Karlsson and F. Aryasetiawan. Spin-wave excitation spectra of nickel and iron. *Phys. Rev. B*, **62**:3006, 2000. 125

[57] H. Keiter and J. C. Kimball. Diagrammatic Approach to the Anderson Model for Dilute Alloys. *Journal of Applied Physics*, **42**:1460, 1971. 52

[58] W. Kohn and L. J. Sham. Self-consistent equations including exchange and correlation effects. *Phys. Rev.*, **140**:A1133, 1965. 15, 17

[59] T. Kotani and M. van Schilfgaarde. All-electron GW approximation with the mixed basis expansion based on the full-potential LMTO method. *Solid State Communications*, **121**:461, 2002. 40

[60] T. Kotani and M. van Schilfgaarde. Fusion of the LAPW and LMTO methods: The augmented plane wave plus muffin-tin orbital method. *Phys. Rev. B*, **81**:125117, 2010. 20, 95

[61] T. Kotani, M. van Schilfgaarde, and S. V. Faleev. Quasiparticle self-consistent *GW* method: A basis for the independent-particle approximation. *Phys. Rev. B*, **76**:165106, 2007. 41, 68, 107, 119

[62] G. Kotliar, S. Y. Savrasov, K. Haule, V. S. Oudovenko, O. Parcollet, and C. A. Marianetti. Electronic structure calculations with dynamical mean-field theory. *Rev. Mod. Phys.*, **78**:865, 2006. 3, 45, 56, 57

[63] G. Kotliar and D. Vollhardt. Strongly correlated materials: Insights from Dynamical Mean-Field Theory. *Physics Today*, **57**:53, 2004. 54, 55

[64] R. Kuwahara and K. Ohno. Linearized self-consistent GW approach satisfying the Ward identity. *Phys. Rev. A*, **90**:032506, 2014. 39

[65] F. Lechermann, A. Georges, A. Poteryaev, S. Biermann, M. Posternak, A. Yamasaki, and O. K. Andersen. Dynamical mean-field theory using wannier functions: A flexible route to electronic structure calculations of strongly correlated materials. *Phys. Rev. B*, **74**:125120, 2006. 65

[66] A. J. Leggett. What DO we know about high Tc? *Nat. Phys.*, **2**:134, 2006. 101

[67] A. I. Lichtenstein and M. I. Katsnelson. ***ab initio*** calculations of quasiparticle band structure in correlated systems: LDA++ approach. *Phys. Rev. B*, **57**:6884, 1998. 56

[68] A. I. Lichtenstein, M. I. Katsnelson, and G. Kotliar. Finite-Temperature Magnetism of Transition Metals: An *ab initio* Dynamical Mean-Field Theory. *Phys. Rev. Lett.*, **87**:067205, 2001. 57, 58, 115, 121, 124

[69] A. I. Liechtenstein, V. I. Anisimov, and J. Zaanen. Density-functional theory and strong interactions: Orbital ordering in mott-hubbard insulators. *Phys. Rev. B*, **52**:R5467, 1995. 55

[70] C. Lubritto, K. Rosciszewski, and Oles A. M. The role of apical oxygen in the high-temperature superconductors. *Journal of Physics: Condensed Matter*, **8**:11053, 1996. 101, 102

[71] P. V. Lukashev, A. L. Wysocki, J. P. Velev, M. van Schilfgaarde, S. S. Jaswal, K. D. Belashchenko, and E. Y. Tsymbal. Spin filtering with euo: Insight from the complex band structure. *Phys. Rev. B*, **85**:224414, 2012. 131

[72] J. M. Luttinger and J. C. Ward. Ground-state energy of a many-fermion system. ii. *Phys. Rev.*, **118**:1417, 1960. 39

[73] R. M. Martin. *Electronic Structure : Basic Theory and Practical Methods*. Cambridge University Press, 2004. 10, 14, 21

[74] N. Marzari and D. Vanderbilt. Maximally localized generalized wannier functions for composite energy bands. *Phys. Rev. B*, **56**:12847, 1997. 65

[75] I.I. Mazin, D.J. Singh, and A. Aguayo. Density functional calculations near ferromagnetic quantum critical points. *arXiv:cond-mat/0401563*, 2004. 119

[76] M. Methfessel, M. van Schilfgaarde, and R.A.Casali. *Lecture Notes in Physics*, **535**. Springer-Verlag, Berlin, 2000. 66, 68, 95

[77] W. Metzner and D. Vollhardt. Correlated lattice fermions in $d = \infty$ dimensions. *Phys. Rev. Lett.*, **62**:324, 1989. 45, 51

[78] A. S. Mishchenko, N. V. Prokof'ev, A. Sakamoto, and B. V. Svistunov. Diagrammatic quantum Monte Carlo study of the Fröhlich polaron. *Phys. Rev. B*, **62**:6317, 2000. 78

[79] T. Miyake, F. Aryasetiawan, and M. Imada. *Ab initio* procedure for constructing effective models of correlated materials with entangled band structure. *Phys. Rev. B*, **80**:155134, 2009. 61

[80] T. Moriya. *Spin Fluctuations in Itinerant Electron Magnetisms*. Springer-Verlag, Berlin, 1985. 116, 130

[81] N. F. Mott. *Metal-insulator transitions*. Taylor and Francis, London, 1990. 12

[82] S. G. Ovchinnikov, A. A. Borisov, V. A Gavrichkov, and M. M. Korshunov. Prediction of the in-gap states above the top of the valence band in undoped insulating cuprates dueto the spin-polaron effect. *Journal of Physics: Condensed Matter*, **16**:L93, 2004. 112

[83] Taisuke Ozaki. Continued fraction representation of the fermi-dirac function for large-scale electronic structure calculations. *Phys. Rev. B*, **75**:035123, 2007. 87

[84] J. P. Perdew et al. Atoms, molecules, solids, and surfaces: Applications of the generalized gradient approximation for exchange and correlation. *Phys. Rev. B*, **46**:6671, 1992. 17

[85] E. Rrapaj, J. W. Holt, A. Bartl, S. Reddy, and A. Schwenk. Charged-current reactions in the supernova neutrino-sphere. *Phys. Rev. C*, **91**:035806, 2015. 31

[86] S. K. Sarker. A new functional integral formalism for strongly correlated fermi systems. *Journal of Physics C: Solid State Physics*, **21**:L667, 1988. 49

[87] W.D. Schöne and A. G. Eguiluz. Self-consistent calculations of quasiparticle states in metals and semiconductors. *Phys. Rev. Lett.*, **81**:1662, 1998. 39

[88] J. Schwinger. On the greens functions of quantized fields. I. *Proceedings of the National Academy of Sciences*, **37**:452, 1951. 26, 33

[89] W. Setyawan and S. Curtarolo. High-throughput electronic band structure calculations: Challenges and tools. *Computational Materials Science*, **49**:299, 2010. 103, 117

[90] M. Shimizu. Itinerant electron magnetism. *Rep. Prog. Phys.*, **44**:329, 1981. 119

[91] J. C. Slater. An augmented plane wave method for the periodic potential problem. *Phys. Rev.*, **92**:603, 1953. 18

[92] F. Sottile. Theoretical Spectroscopy: Developments and Applications. HDR Thesis. 30

[93] C. Taranto, M. Kaltak, N. Parragh, G. Sangiovanni, G. Kresse, A. Toschi, and K. Held. Comparing quasiparticle *gw*+dmft and lda+dmft for the test bed material $srvo_3$. *Phys. Rev. B*, **88**:165119, 2013. 109

[94] L. H. Thomas. The calculation of atomic fields. *Proceedings of the Cambridge Philosophical Society*, **23**:542, 1927. 13

[95] J. M. Tomczak, M. Casula, T. Miyake, F. Aryasetiawan, and S. Biermann. Combined gw and dynamical mean-field theory: Dynamical screening effects in transition metal oxides. *EPL (Europhysics Letters)*, **100**[6]:67001, 2012. 5

[96] J. M. Tomczak, M. van Schilfgaarde, and G. Kotliar. Many-body effects in iron pnictides and chalcogenides: Nonlocal versus dynamic origin of effective masses. *Phys. Rev. Lett.*, **109**:237010, 2012. 4

[97] R. Valenti. Introduction to the Density Functional Theory. `http://itp.uni-frankfurt.de/~valenti/WS09-10.html`. 19

[98] M. van Schilfgaarde, T. Kotani, and S. Faleev. Quasiparticle self-consistent *GW* theory. *Phys. Rev. Lett.*, **96**:226402, 2006. 4, 38, 41, 43, 44

[99] M. van Schilfgaarde et al. LMTO suite tutorial. http://www.lmsuite.org/. 94, 95, 96

[100] L. Vaugier, H. Jiang, and S. Biermann. Hubbard U and hund exchange J in transition metal oxides: Screening versus localization trends from constrained Random Phase Approximation. *Phys. Rev. B*, **86**:165105, 2012. 59

[101] U. von Barth and B. Holm. Self-consistent GW_0 results for the electron gas: Fixed screened potential w_0 within the random-phase approximation. *Phys. Rev. B*, **54**:8411, 1996. 39

[102] S. V. Vonsovsky. *Magnetism*, **2**. John Wiley, New York, 1974. 115

[103] X. Wang, M. J. Han, L. de' Medici, H. Park, C. A. Marianetti, and A. J. Millis. Covalency, double-counting, and the metal-insulator phase diagram in transition metal oxides. *Phys. Rev. B*, **86**:195136, 2012. 101, 102

[104] C. Weber, K. Haule, and G. Kotliar. Apical oxygens and correlation strength in electron- and hole-doped copper oxides. *Phys. Rev. B*, **82**:125107, 2010. 101, 102, 109, 110, 112, 114

[105] P. Werner, A. Comanac, L. de' Medici, M. Troyer, and A. J. Millis. Continuous-time solver for quantum impurity models. *Phys. Rev. Lett.*, **97**:076405, 2006. 3, 52, 98

[106] P. Werner and M.Casula. Dynamical screening in correlated electron systems from lattice models to realistic materials. *arXiv:1602.00584*, 2016. 76

[107] T. Yoshida, K. Tanaka, H. Yagi, A. Ino, H. Eisaki, A. Fujimori, and Z.X. Shen. Direct observation of the mass renormalization in $SrVo3$. *Phys. Rev. Lett.*, **95**:146404, 2005. 10

[108] J. Yu, A. J. Freeman, and J. H. Xu. Electronically driven instabilities and superconductivity in the layered $La_{2-x}Ba_xCuO_4$ perovskites. *Phys. Rev. Lett.*, **58**:1035, 1987. 102